AD-A131 290 OPTICAL MEANS OF MEASURING PARTICLE-SEA INTERACTIONS IN THE CARIBBEAN SEA..(U) UNIVERSITY OF SOUTH FLORIDA ST PETERSBURG MARINE SCIENCE INST.. K L CARDER ET AL. 1/2

UNCLASSIFIED APR 83 N00014-75-C-0539 F/G 8/3 NL

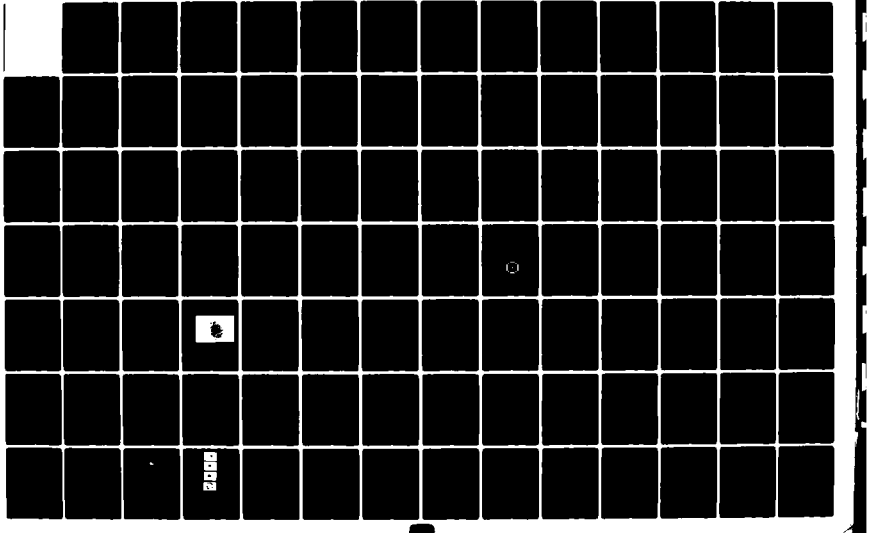

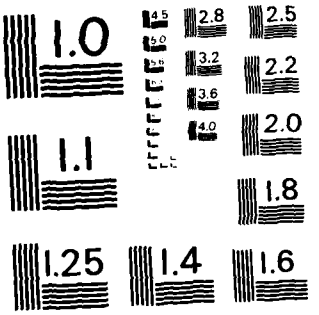

UNCLASSIFIED

SECURITY CLASSIFICATION OF THIS PAGE (When Data Entered)

| REPORT DOCUMENTATION PAGE | | READ INSTRUCTIONS BEFORE COMPLETING FORM |
|---|---|---|
| 1. REPORT NUMBER | 2. GOVT ACCESSION NO. AD-A131290 | 3. RECIPIENT'S CATALOG NUMBER |
| 4. TITLE (and Subtitle) Optical Means of Measuring Particle-Sea Interactions in the Caribbean Sea and Gulf of Mexico | | 5. TYPE OF REPORT & PERIOD COVERED Jan 79 - Mar 83 Final Report |
| | | 6. PERFORMING ORG. REPORT NUMBER |
| 7. AUTHOR(s) K. L. Carder R. G. Steward | | 8. CONTRACT OR GRANT NUMBER(s) N-0014-75-C-0539 |
| 9. PERFORMING ORGANIZATION NAME AND ADDRESS University of South Florida Dept. of Marine Science St. Petersburg, FL 33701 | | 10. PROGRAM ELEMENT, PROJECT, TASK AREA & WORK UNIT NUMBERS RR 031-03-01 |
| 11. CONTROLLING OFFICE NAME AND ADDRESS Office of Naval Research Code 422CB Arlington, VA 22217 | | 12. REPORT DATE APRIL 1983 |
| | | 13. NUMBER OF PAGES 100 |
| 14. MONITORING AGENCY NAME & ADDRESS(if different from Controlling Office) | | 15. SECURITY CLASS. (of this report) UNCLASSIFIED |
| | | 15a. DECLASSIFICATION/DOWNGRADING SCHEDULE |

16. DISTRIBUTION STATEMENT (of this Report)

17. DISTRIBUTION STATEMENT (of the abstract entered in Block 20, if different from Report)

APPROVED FOR PUBLIC RELEASE; DISTRIBUTION UNLIMITED

18. SUPPLEMENTARY NOTES

19. KEY WORDS (Continue on reverse side if necessary and identify by block number)

Optical Means
Particle-Sea Interactions
Measuring
Gulf of Mexico
Caribbean Sea

20. ABSTRACT (Continue on reverse side if necessary and identify by block number)

A holographic image analysis system has been developed to measure the position, velocity, size and shape of microscopic particles slowly settling in three-dimensional space. Images of particles recorded sequentially on individual holographic frames are reconstructed using an in-line, far field configuration. Image analysis is computer-controlled with two basic functions. First is the precision registration and XYZ positioning of the holographic frame so that accurate particle displacements between sequential frames can be measured. These displacements are compared to the elapsed time between the frames to get

DD FORM 1 JAN 73 1473 EDITION OF 1 NOV 65 IS OBSOLETE
S/N 0102-LF-014-6601

UNCLASSIFIED
SECURITY CLASSIFICATION OF THIS PAGE (When Data Entered)

particle settling velocity. Second, it scans a digitized video image of the reconstructed holographic image to measure size, shape, and area. A scanning algorithm has been developed to determine particle size (area, length, width) for classification by settling characteristics. An edge tracking algorithm has also been developed to facilitate particle identification by shape from frame to frame. A cataloging system was developed to provide for data entry, storage and retrieval.

(2)

Final Report

for

ONR Contract N00014-75-C-0539

entitled

# Optical Means of Measuring Particle-Sea Interactions in the Caribbean Sea and Gulf of Mexico

APR 1983

Prepared by

K. L. Carder

R. G. Steward

Department of Marine Science
University of South Florida
140 Seventh Avenue South
St. Petersburg, Florida 33701

A

Overview:

During the last contract period we have published two papers, we have one "in press," with a third ready for submittal and a fourth in the late-draft stages (see enclosures). The research culminating in these papers has been supported entirely or in part by ONR contract N00014-75-C-0539. We also have developed, modified, applied and documented a three-axis image-analysis system for analyzing holograms of dynamic particles. A description of the image-analysis hardware, algorithms for particle sizing and the accuracies attained can be found in Payne, Carder, and Steward (1983; see attachment). A description of the nine holographic image analysis subroutines for controlling a three-axis, 2-micron resolution positioning system, particle sizing, and performing data management functions is also provided along with program listings.

Synopsis of Results

The two papers published last summer resulted from earlier Navy contracted work. They are:

Fanning, K. A., K. L. Carder and P. R. Betzer, 1982. Sediment resuspension by coastal waters: a potential mechanism for nutrient re-cycling on the ocean's margins, Deep Sea Research 29(8A): 953-965.

Carder, K. L., R. G. Steward and P. R. Betzer, 1982. In situ holographic measurements of the sizes and settling rates of oceanic particulates, J. Geophysical Research 87(C8): 5681-5685.

In the first paper we demonstrated that very large light-attenuation coefficients (e.g., $C_p > 3.3\ m^{-1}$) measured near-bottom ($\sim$30m) during a

winter frontal passage over our three-day time series station south of Mobile Bay were accompanied by nutrient enrichments of as much as 10-fold over concentrations found in the overlying waters or between storms. We provided evidence that sediment resuspension may significantly accelerate nutrient recycling on continental margins.

The second paper documents the first in situ oceanic measurements of individual particle settling velocity parameters. They were obtained using a holographic technique in a vertically damped sediment trap/float array in the western Sargasso Sea. To our surprise there were significant numbers of large (15-45 μm) heavy minerals of Saharan dust origin. Such particles have been heretofore never reported in the aerosol literature so far (>5000 km) from the Sahara Desert. The holographically determined sizes, shapes, and Stokes-derived densities matched those determined by scanning electron microscopy analysis (SEM/EDXA) and particle compositions of samples collected in the sediment trap.

This research activity also led to three papers which are in various stages of publication:

Doyle, L. J., K. L. Carder, and R. G. Steward, The hydraulic equivalence of mica. J. Sedimentary Petrology, (in press).

Payne, P., K. L. Carder and R. G. Steward, A system to catalog and analyze holographic images of dynamic ocean particles, final draft to be submitted to Applied Optics.

Carder, K. L., R. G. Steward, P. R. Betzer, D. Johnson and J. Prospero, Chronology of an aeolian input event to the Sargasso Sea, to be submitted to J. Geophysical Research.

The first paper reports the findings of a laboratory experiment using the holographic microvelocimeter. The purpose of this experiment was to

determine the settling dynamics of sand- to silt-sized mica flakes. Mica has been classically considered to have a settling velocity relatively lower than other minerals of equivalent size and density. This was based upon the association of sand-sized mica and clay-sized minerals in various environments. Until our experiment, there had been no quantitative evidence to support this correlation. The holographic microvelocimeter provided the means of accurately viewing and measuring the settling behavior and velocities of individual mica flakes. These data established that mica is the hydraulic equivalent of quartz spheres between 4 to 12 times smaller in diameter.

This experiment was conducted using dual beam holography; i.e. simultaneous holograms were collected along the vertical and horizontal axes. These data showed that the mica flakes seldom settled in either the broadwise or edgewise orientation. Also the flakes usually maintained a stable orientation and rarely rotated further. The data allowed comparison between two different formulations of Stokes equations modified for shape and settling orientation. This comparison showed that for flakes where the diameter is approximately 50 times the thickness there was little difference between the two sets of shape modified equations. For thicker particles, the orientation factors in one set of equations allowed better accuracy in predicting the settling velocity.

The second paper (see Appendix) describes the image analysis hardware, algorithm concepts, and algorithm accuracies for a micro-computer controlled hologram positioning and particle analysis system. Particle size (area, perimeter), shape, settling velocities, and Stokes densities are measured/calculated with the system with accuracies of better than ±4% for high-contrast particle images and better than ±10%

for low-contrast holographic particle images with optical noise (speckle and particle diffraction patterns) superimposed. Techniques for improving signal extraction from the noisy images are also discussed.

The third paper discusses development of a three-week time series of Sahara-derived aerosol concentrations from the particle data collected by the holographic particle velocimeter trap data. In essence, a particle settling model (particle densities and shape parameters) consisting of eight particle classes (e.g., quartz, hematite, rutile, etc.), was calibrated by fitting the aerosol concentration data derived from taking the particles from the sediment trap (30 m depth) back in time, to aerosol concentration data collected by Joe Prospero on Virginia Key. This in effect was a natural sedimentation experiment with a 30-meter "settling tube." It produced Stokes particle densities for each mineral class. These matched almost precisely our holographically-derived densities (Carder, et al., 1982) for heavy minerals (e.g., 5.10 vs. 5.20 for "hematite," 4.10 and 4.16 vs. 4.20 for "goethite" and "rutile"), and for non-heavy minerals (e.g., from 2.55 to 2.72 versus 2.19 to 2.99). Since the non-heavy minerals included clays, quartz, and iron/titanium containing silicates, the variance of density values for these non-heavy mineral classes would be expected to be larger than for the dominant heavy mineral classes.

Thus success of this particle dynamics model for aeolian input will permit us to now look at fluxes of this component as a tracer through the ocean system (e.g., removal and repackaging by filter feeders) in future papers. With data collected over 5 days from traps at 30 m, 100 m and 300 m, development of aerosol time series for the Sargasso of up to 2 months should be possible. This would provide us the capability of

gathering time series data on aerosol inputs to the ocean in remote settings without the expense of maintaining a ship on station for long periods of time. The investigation of the temporal and spatial coherence of aeolian inputs to the sea might be useful future outgrowths of this line of research as well as to provide increased understanding of the real and "optical residence times" that Saharan and Gobi Desert dust have with respect to light propagation through various regions of the ocean. Our Sargasso Sea data indicate that Saharan dust particles smaller than about 5.0 μm diameter have a residence time in the upper 30 m of more than two weeks (8 weeks for 2.5 μm particles). Since during the summer, Saharan dust input events occur every 7 to 14 days, an optical signal may persist in the upper layers for days after an aerosol cloud has passed by. Whether or not this aeolian residue has a significant effect on interpretation of remotely sensed optical data or optical signal propagation awaits future study.

Other results apparent from the data of Carder *et al.* (in preparation) are as follows:

1. Aerosol size distributions and mineral types change significantly with the phase of the aerosol clouds:
    a. A disproportionately larger fraction of the particles are heavy minerals and "giant" particles ( 10 μm diameter) in the leading edge of the cloud than at the trailing edge. Aeolian particles in excess of 60 μm diameter were observed.
    b. Conversely, the trailing edge has a paucity of large, heavy particles.

c. A far larger fraction in summer dust clouds are heavy mineral particles than in winter, suggesting that the summer source, which is considerably north of the winter harmatan source, is a more titanium/hematite/goethite-rich region.

## IMAGE ANALYSIS SOFTWARE

The image analysis software developed in collaboration with Aztec Computer Engineering for this contract is composed of nine subroutines. The source code of each is listed in the Appendix. With this software the analysis of the holographic image is now semi-automated. The computer permits precise registration of the holograms, high resolution scanning of the video images to measure the particle area and perimeter, calculation of the particle fall distance between frames for velocity, and data base management. These software modules are described below.

1. MAIN The main routine controls the flow of the other modules through a menu, calculates particle settling velocity, and writes the data onto floppy disks.

2. HELP This is a help routine which can be entered at various places in the main routine to explain the program operation, operator inputs, and computer responses.

3. FMOVE Frame move is a routine to control the hologram positioning in three dimensions using the computer joystick and/or the keyboard.

4. STAGE This is the interface subroutine that interprets the output of the joystick and/or keyboard and moves the XYZ stage motors.

5. JSINP Joystick input is an interfacing subroutine which outputs a digital number from the computer joystick to be used in control of the XYZ stages or the video cursor.

6. PSCAN Particle scan is a routine that measures the area and perimeter of a video image. This algorithm operates by looking for video pixels of higher intensity than an operator selected threshold.

7. TVSCN Television scan is a subroutine of PSCAN which allows the operator to move the video cursor to the center of the video screen, particle center, and particle extremes. After setting the extremes of the particle, this routine sums up the area by counting all pixels greater than the selected threshold and sums up the perimeter from the number of the rows and columns of the scanned area.

8. TRACK This is the particle edge tracking routine which automatically tracks around the edge of the video image. This algorithm tests for an operator-selected video amplitude gradient that approximates the particle edge conditions.

9. TVTRK The television tracking routine is a subroutine of TRACK which moves the video cursor around a circle at each XY position on the particle edge. In moving around this circle, the video amplitude is tested to see if two adjacent perimeter points on the circle have difference in video amplitude which exceeds the selected gradient. If a complete circle is made, or if the gradient is exceeded then the routine returns the XY coordinates of the perimeter point to be used as the center of the next scan.

APPENDIX ONE

Holographic Image Analysis

System Software Listings

```
C.
C       MAIN PROGRAM FOR THE AZTEC HOLOGRAPHIC IMAGE ANALYSIS SYSTEM
C       REVISION 0.30, 5 SEP 1982
C
        LOGICAL ESC,AST,ANS,CHG,FILE(11),NAME(8),DATE(3),WORDS(46)
        INTEGER RMAX,FMAX,FRAME,PART,FR1,FR2
        INTEGER FRM(10),PRT(10),PX(10),PY(10),PZ(10),SEX(10),SEY(10)
        INTEGER SAREA(10),SPERIM(10),SWIDE(10),STALL(10)
        INTEGER TAREA(10),TPERIM(10),TLEN(10),TX(10,100),TY(10,100)
        INTEGER HLP,FX,FY,FZ,SX,SY,SA,SP,SW,SH,TA,TP,TL,TW(100),TH(100)
        DIMENSION TIME(10)
        EXTERNAL HELP,FMOVE,PSCAN,TRACK
        EXTERNAL JSINP,STAGE,TVSCN,TVTRK
        COMMON  ESC,AST,HLP,FX,FY,FZ,SX,SY,SA,SP,SW,SH,TA,TP,TL,TW,TH
C
C       DISPLAY TITLE AND OVERVIEW SCREEN (HLP=1)
C
100     ESC=27
        AST=42
        HLP=1
        CALL HELP
C
C       INITIALIZE SUBROUTINE PARAMETERS
C
        FX=0
        FY=0
        FZ=0
        SX=128
        SY=128
        SA=0
        SP=0
        SW=0
        SH=0
        TA=0
        TP=0
        TL=0
        DO 105 J=1,100
          TW(J)=0
          TH(J)=0
105       CONTINUE
C
C       SELECT TASK OR DISPLAY H,L,T,X SCREEN (HLP=2)
C
110     WRITE(1,1100)
1100    FORMAT(' SELECT (L)OAD OR (T)EST: ')
        READ(1,1110)ANS
1110    FORMAT(1A1)
        HLP=2
        IF(ANS.EQ.72)CALL HELP
        IF(ANS.EQ.76)GOTO 200
        IF(ANS.EQ.84)GOTO 120
        IF(ANS.EQ.88)GOTO 190
        GOTO 110
C
C       SELECT TASK OR DISPLAY H,F,P,T,X SCREEN (HLP=3)
C
120     WRITE(1,1120)
1120    FORMAT(' SELECT (F)MOVE,(P)SCAN OR (T)RACK: ')
        READ(1,1110)ANS
        HLP=3
        IF(ANS.EQ.72)CALL HELP
        IF(ANS.EQ.70)CALL FMOVE
        IF(ANS.EQ.80)CALL PSCAN
        IF(ANS.EQ.84)CALL TRACK
        IF(ANS.EQ.88)GOTO 190
        GOTO 110
C
C       SELECT TASK OR DISPLAY H,D,E,S,V,X SCREEN (HLP=4)
C
130     WRITE(1,1130)
1130    FORMAT(' SELECT (D)ISPLAY,(E)NTER,(S)AVE OR (V)ELOC: ')
        READ(1,1110)ANS
        HLP=4
        IF(ANS.EQ.72)CALL HELP
        IF(ANS.EQ.68)GOTO 400
        IF(ANS.EQ.69)GOTO 600
        IF(ANS.EQ.83)GOTO 800
        IF(ANS.EQ.86)GOTO 900
        IF(ANS.EQ.88)GOTO 190
        GOTO 130
```

```
C
C       SELECT TASK OR DISPLAY H,F,P,T,S,R,X SCREEN (HLP=5)
C
140     WRITE(1,1140)
1140    FORMAT(' SELECT (F)MOVE,(P)SCAN,(T)RACK,(S)TORE,(C)ONTINUE: ')
        READ(1,1110)ANS
        HLP=5
        IF(ANS.EQ.72)CALL HELP
        IF(ANS.EQ.70)CALL FMOVE
        IF(ANS.EQ.80)CALL PSCAN
        IF(ANS.EQ.84)CALL TRACK
        IF(ANS.EQ.83)GOTO 700
        IF(ANS.EQ.67)GOTO 130
        IF(ANS.EQ.88)GOTO 190
        GOTO 140
C
C       RESTART, EXIT OR CONTINUE
C
190     WRITE(1,1190)
1190    FORMAT(' (R)ESTART, (E)XIT, OR (C)ONTINUE: ')
        READ(1,1110)ANS
        HLP=1
        IF(ANS.EQ.72)CALL HELP
        IF(ANS.EQ.67)GOTO 130
        IF(ANS.EQ.82)GOTO 100
        IF(ANS.EQ.69)GOTO 1000
        GOTO 130
C
C       ENTER FILENAME
C
200     WRITE(1,1200)
1200    FORMAT('+ENTER FILENAME: ')
        READ(1,1210)(FILE(J),J=1,11)
1210    FORMAT(11A1)
210     WRITE(1,1220)
1220    FORMAT('+ENTER (O)LD OR (N)EW FILE: ')
        READ(1,1110)ANS
        IF(ANS.EQ.79)GOTO 300
        IF(ANS.EQ.78)GOTO 220
        GOTO 210
C
C       SETUP HEADER FOR NEW FILE OR CHANGE OLD HEADER
C
220     CHG=0
        RMAX=0
        FMAX=0
230     WRITE(1,1230)
1230    FORMAT('+ENTER NAME: ')
        READ(1,1235)(NAME(J),J=1,8)
1235    FORMAT(8A1)
        IF(CHG.EQ.1)GOTO 400
240     WRITE(1,1240)
1240    FORMAT('+ENTER DATE: ')
        READ(1,1235)(DATE(J),J=1,8)
        IF(CHG.EQ.1)GOTO 400
250     WRITE(1,1250)
1250    FORMAT('+ENTER COMMENTS: ')
        READ(1,1260)(WORDS(J),J=1,46)
1260    FORMAT(46A1)
        IF(CHG.EQ.1)GOTO 400
260     WRITE(1,1270)
1270    FORMAT('+ENTER FMAX: ')
        READ(1,1275)FMAX
1275    FORMAT(I8)
        WRITE(1,1280)
1280    FORMAT(' FRAME    TIME'/)
        DO 270 I=1,FMAX
          WRITE(1,1290)I
1290      FORMAT('+',I4,4X)
          READ(1,1300)TIME(I)
1300      FORMAT(F8.3)
270       CONTINUE
        GOTO 130
C
C       READ OLD DATA FROM DISK
C
300     CALL OPEN(6,FILE,1)
        READ(6,1310)RMAX,FMAX,(NAME(J),J=1,8),(DATE(J),J=1,8),
     1  (WORDS(J),J=1,46)
1310    FORMAT(2I8,2(8A1),46A1)
```

```
      IF(FMAX)370,370,310
310   DO 320 I=1,FMAX
        READ(6,1320)TIME(I)
1320    FORMAT(F8.3)
320     CONTINUE
      IF(RMAX)370,370,330
330   DO 360 I=1,RMAX
        READ(6,1330)FRM(I),PRT(I),PX(I),PY(I),PZ(I),
     1  SAREA(I),SPERIM(I),SEX(I),SEY(I),SWIDE(I),STALL(I),
     2  TAREA(I),TPERIM(I),TLEN(I)
1330    FORMAT(14I8)
        LEN=TLEN(I)
        IF(LEN)360,360,340
340     DO 350 J=1,LEN
          READ(6,1340)TX(I,J),TY(I,J)
1340      FORMAT(2I8)
350       CONTINUE
360     CONTINUE
370   ENDFILE 6
      GOTO 130
C
C     DISPLAY FILE HEADER AND CHANGE AS REQUIRED
C
400   WRITE(1,1400)ESC,AST,(FILE(J),J=1,11),(NAME(J),J=1,8),
     1(DATE(J),J=1,8),RMAX,FMAX,(WORDS(J),J=1,46)
1400  FORMAT(1X,2A1/' FILENAME: ',11A1,' NAME: ',8A1,  DATE: ',8A1/
     1' RMAX: ',I8,' FMAX: ',I8/' COMMENTS: ',46A1
     2/' FRAME    TIME')
      IF(FMAX)420,420,405
405   DO 410 I=1,FMAX
        WRITE(1,1410)I,TIME(I)
1410    FORMAT(I4,4X,F8.3)
410     CONTINUE
420   WRITE(1,1420)
1420  FORMAT(' CHANGE (N)AME,(D)ATE,(C)OMMENTS OR (F)RAME TIME? ')
      READ(1,1110)ANS
      CHG=1
      HLP=7
      IF(ANS.EQ.72)CALL HELP
      IF(ANS.EQ.78)GOTO 230
      IF(ANS.EQ.68)GOTO 240
      IF(ANS.EQ.67)GOTO 250
      IF(ANS.EQ.70)GOTO 422
      GOTO 430
422   WRITE(1,1424)
1424  FORMAT('+ENTER FRAME NO: ')
      READ(1,1275)I
      IF(I-FMAX)428,428,426
426   FMAX=FMAX+1
      TIME(I)=0
428   WRITE(1,1430)TIME(I)
1430  FORMAT('+OLD FRAME TIME: ',F8.3/' ENTER NEW FRAME TIME: ')
      READ(1,1300)TIME(I)
      GOTO 400
C
C     ENTER FRAME AND PARTICLE FOR DISPLAY
C
430   WRITE(1,1440)
1440  FORMAT('+ENTER FRAME NUMBER OR (CR) FOR ALL FRAMES: ')
      READ(1,1275)IFRM
      WRITE(1,1450)
1450  FORMAT('+ENTER PARTICLE NUMBER OR (CR) FOR ALL PARTICLES: ')
      READ(1,1275)IPRT
      IF(IFRM)432,440,432
432   IF(IPRT)540,510,540
440   IF(IPRT)480,450,480
C
C     DISPLAY ALL DATA IN FILE BY FRAME AND PARTICLE
C
450   WRITE(1,1460)ESC,AST,(FILE(J),J=1,11)
1460  FORMAT(1X,2A1/' FILENAME: ',11A1/
     1' ---FRAME-PARTCLE--X-AXIS--Y AXIS--Z AXIS',
     2'---SAREA--SPERIM---SWIDE---STALL')
      DO 470 I=1,FMAX
460     WRITE(1,1470)FRM(I),PRT(I),PX(I),PY(I),PZ(I),
     1  SAREA(I),SPERIM(I),SWIDE(I),STALL(I)
1470    FORMAT(9I8)
470     CONTINUE
      GOTO 130
C
```

```
C       DISPLAY PARTICLE DATA BY FRAME
C
480     WRITE(1,1480)ESC,AST,(FILE(J),J=1,11),IPRT
1480    FORMAT(1X,2A1/' FILENAME: ',11A1/' PARTICLE: ',I8/
     1  ' ---FRAME--X AXIS--Y AXIS--Z AXIS',
     2  '----SCNX----SCNY---SAREA--SPERIM---SWIDE---STALL')
        DO 500 I=1,RMAX
          IF(PRT(I)-IPRT)500,490,500
490       WRITE(1,1490)FRM(I),PX(I),PY(I),PZ(I),
     1    SEX(I),SEY(I),SAREA(I),SPERIM(I),SWIDE(I),STALL(I)
1490      FORMAT(10I8)
500       CONTINUE
        GOTO 130
C
C       DISPLAY FRAME DATA BY PARTICLE
C
510     WRITE(1,1500)ESC,AST,(FILE(J),J=1,11),IFRM
1500    FORMAT(1X,2A1/' FILENAME: ',11A1/' FRAME: ',I8/
     1  ' -PARTCLE--X AXIS--Y AXIS--Z AXIS',
     2  '---SAREA--SPERIM---SWIDE---STALL---TAREA--TPERIM')
        DO 530 I=1,RMAX
          IF(FRM(I)-IFRM)530,520,530
520       WRITE(1,1490)PRT(I),PX(I),PY(I),PZ(I),
     1    SAREA(I),SPERIM(I),SWIDE(I),STALL(I),
     2    TAREA(I),TPERIM(I)
530       CONTINUE
        GOTO 130
C
C       DISPLAY EDGE DATA FOR SELECTED PARTICLE AND FRAME
C
540     DO 560 I=1,RMAX
          IF(FRM(I)-IFRM)560,550,560
550       IF(PRT(I)-IPRT)560,570,560
560       CONTINUE
        GOTO 130
570     WRITE(1,1510)ESC,AST,(FILE(J),J=1,11),
     1  IFRM,IPRT,I,TAREA(I),TPERIM(I),TLEN(I)
1510    FORMAT(1X,2A1/
     1  ' FILENAME: ',11A1/' FRAME: ',I8/' PARTICLE: ',I8/
     2  ' RECORD: ',I8/' TAREA: ',I8/' TPERIM: ',I8/' TLEN: ',I8/
     3  ' ---POINT--X AXIS--Y AXIS')
        LEN=TLEN(I)
        IF(LEN)130,130,580
580     DO 590 J=1,LEN
          WRITE(1,1520)J,TX(I,J),TY(I,J)
1520      FORMAT(3I8)
590       CONTINUE
        GOTO 130
C
C       ENTER FRAME AND PARTICLE IDENTIFICATION
C
600     WRITE(1,1600)
1600    FORMAT('+ENTER FRAME NO: ')
        READ(1,1275)FRAME
        IF(FRAME)600,600,610
610     IF(FRAME-9)620,620,600
620     WRITE(1,1610)
1610    FORMAT('+ENTER PARTICLE NO: ')
        READ(1,1275)PART
        IF(PART)620,620,630
630     IF(PART-9)640,640,620
640     DO 650 I=1,RMAX
          IF(FRM(I)-FRAME)650,645,650
645       IF(PRT(I)-PART)650,660,650
650       CONTINUE
C
C       RESET FRAME AND PARTICLE DATA TO ZERO
C
        FX=0
        FY=0
        FZ=0
        SX=128
        SY=128
        SA=0
        SP=0
        SW=0
        SH=0
        TA=0
        TP=0
        TL=0
```

```
      DO 655 J=1,100
        TW(J)=0
        TH(J)=0
655     CONTINUE
      GOTO 140
C
C     RESET TO RECORD DATA
C
660   FX=PX(I)
      FY=PY(I)
      FZ=PZ(I)
      SX=SEX(I)
      SY=SEY(I)
      SA=SAREA(I)
      SP=SPERIM(I)
      SW=SWIDE(I)
      SH=STALL(I)
      TA=TAREA(I)
      TP=TPERIM(I)
      TL=TLEN(I)
      IF(TL)665,670,665
665   DO 670 J=1,TL
        TW(J)=TX(I,J)
        TH(J)=TY(I,J)
670     CONTINUE
      GOTO 140
C
C     SET RECORD DATA FOR SELECTED FRAME AND PARTICLE
C
700   IF(RMAX)730,730,710
710   DO 730 I=1,RMAX
        IF(FRM(I)-FRAME)730,720,730
720     IF(PRT(I)-PART)730,740,730
730     CONTINUE
      RMAX=RMAX+1
      I=RMAX
740   FRM(I)=FRAME
      PRT(I)=PART
      PX(I)=FX
      PY(I)=FY
      PZ(I)=FZ
      SEX(I)=SX
      SEY(I)=SY
      SAREA(I)=SA
      SPERIM(I)=SP
      SWIDE(I)=SW
      STALL(I)=SH
      TAREA(I)=TA
      TPERIM(I)=TP
      TLEN(I)=TL
      IF(TL)750,760,750
750   DO 760 J=1,TL
        TX(I,J)=TW(J)
        TY(I,J)=TH(J)
760     CONTINUE
      GOTO 130
C
C     SAVE DATA ON DISK
C
800   CALL OPEN(6,FILE,1)
      WRITE(6,1810)RMAX,FMAX,(NAME(J),J=1,8),(DATE(J),J=1,8),
     1 (WORDS(J),J=1,46)
1810  FORMAT(1X,2I8,2(8A1),46A1)
      IF(FMAX)860,860,810
810   DO 820 I=1,FMAX
        WRITE(6,1820)TIME(I)
1820    FORMAT(1X,F6.3)
820     CONTINUE
      IF(RMAX)860,860,830
830   DO 860 I=1,RMAX
        WRITE(6,1830)FRM(I),PRT(I),PX(I),PY(I),PZ(I),
     1  SAREA(I),SPERIM(I),SEX(I),SEY(I),SWIDE(I),STALL(I),
     2  TAREA(I),TPERIM(I),TLEN(I)
1830    FORMAT(1X,14I8)
        LEN=TLEN(I)
        IF(LEN)860,860,840
840     DO 850 J=1,LEN
          WRITE(6,1840)TX(I,J),TY(I,J)
1840      FORMAT(1X,2I8)
850       CONTINUE
```

```
860       CONTINUE
          ENDFILE 6
          GOTO 110
C
C         COMPUTE DRIFT VELOCITY FOR SELECTED PARTICLES AND FRAMES
C
900       WRITE(1,1900)ESC,AST
1900      FORMAT(1X,2A1,
     1    ' DRIFT VELOCITY AND AVERAGE PARTICLE SIZE COMPUTATION'/
     2    ' ENTER FIRST FRAME: ')
          READ(1,1910)FR1
1910      FORMAT(I8)
          WRITE(1,1920)
1920      FORMAT('+ENTER SECOND FRAME: ')
          READ(1,1910)FR2
          DT=TIME(FR2)-TIME(FR1)
          WRITE(1,1930)DT
1930      FORMAT('+TIME DIFFERENCE: ',F8.3//
     1    ' PARTICLE---X VEL---Y VEL---Z VEL',
     2    '----AREA---PERIM---WIDTH--HEIGHT')
          IF(DT)902,130,902
902       IF(RMAX)130,130,905
905       DO 950 I=1,RMAX
            IF(FRM(I)-FR1)950,910,950
910           DO 940 J=1,RMAX
              IF(FRM(J)-FR2)940,920,940
920           IF(PRT(I)-PRT(J))940,930,940
930           DX=PX(J)-PX(I)
              DY=PY(J)-PY(I)
              DZ=PZ(J)-PZ(I)
              XVEL=DX/DT
              YVEL=DY/DT
              ZVEL=DZ/DT
              AREA=(SAREA(I)+SAREA(J))/2
              PERIM=(SPERIM(I)+SPERIM(J))/2
              WIDTH=(SWIDE(I)+SWIDE(J))/2
              HEIGHT=(STALL(I)+STALL(J))/2
              WRITE(1,1940)PRT(I),XVEL,YVEL,ZVEL,
     1        AREA,PERIM,WIDTH,HEIGHT
1940          FORMAT(1X,I8,7F8.3)
940           CONTINUE
950         CONTINUE
          GOTO 130
C
C         EXIT FROM PROGRAM AND RETURN TO SYSTEM
C
1000      CONTINUE
          END
```

A.

```
C       SUBPROGRAM TO HELP OPERATOR USE THIS SYSTEM BY DISPLAYING
C       ADDITIONAL INFORMATION AND INSTRUCTIONS ON THE CRT WHEN
C       CALLED FROM DIFFERENT PARTS OF THE PROGRAM
C       REVISION 0.12, 28 AUG 1982
C
        SUBROUTINE HELP
C
        LOGICAL ESC,AST
        INTEGER HLP
        COMMON ESC,AST,HLP
C
        WRITE(1,1000)ESC,AST
1000    FORMAT(1X,2A1,'ADDITIONAL INFORMATION AND INSTRUCTIONS'//)
        GOTO(100,200,300,400,500,600,700,800),HLP
C
C       OVERVIEW SCREEN
C
100     WRITE(1,1010)ESC,AST
1010    FORMAT(1X,2A1/
     1  ' ------------HOLOGRAPHIC IMAGE ANALYSIS SYSTEM------------ '/
     2  '                        Written by'/
     3  '                AZTEC COMPUTER ENGINEERING'/
     4  '                 St. Petersburg, Florida'/
     5  '                    28 AUGUST 1982'/
     6  '-------------------------------------------------------'//)
110     WRITE(1,1020)
1020    FORMAT(' THE PROGRAM WILL PERFORM THE FOLLOWING FUNCTIONS:'/
     1  '  1. (H)ELP DISPLAYS MORE DETAIL AT ANY STEP IN THE PROGRAM'/
     2  '  2. (L)OADS EXISTING DATA FROM DISK TO MEMORY'/
     3  '  3. (D)ISPLAY PRINTS DATA BASE BY FRAME OR PARTICLE ON CRT'/
     4  '  4. (E)NTER ADDS NEW DATA OR CHANGES OLD DATA IN MEMORY'/
     5  '  5. (S)AVE WRITES COMPLETE DATA BASE FROM MEMORY TO DISK'/
     6  '  6. (F)RAME MOVES STAGE TO REFERENCE OR PARTICLE POSITION'/
     7  '  7. (P)ARTICLE SCANS IMAGE TO FIND PARTICLE SIZE'/
     8  '  7. (T)RACK TRACES IMAGE TO FIND PARTICLE SIZE AND EDGE'/
     9  '  8. (V)ELOCITY COMPUTES DRIFT VALUES FOR SELECTED PARTICLES'/
     A  ' 10. E(X)IT LEAVES PROGRAM AND RETURNS TO OPERATING SYSTEM'  )
        RETURN
C
C       LOAD AND TEST SCREEN
C
200     WRITE(1,1200)ESC,AST
1200    FORMAT(1X,2A1/
     1  ' THE FOLLOWING FUNCTIONS MAY BE INVOKED AT THIS LEVEL:'//
     2  '  1. (H)ELP DISPLAYS THIS SCREEN'//
     3  '  2. (L)OAD READS NEW DATA FROM DISK OVER OLD DATA IN MEMORY'//
     4  '  3. (T)EST ENABLES THE STAGE, TVSCAN AND TVTRACK FUNCTIONS'/
     5  '     TO BE TESTED BEFORE ANY DISK FILES ARE LOADED IN MEMORY'//
     6  '  4. E(X)IT RETURNS OPERATION TO CDOS'//
     7  '                    REMEMBER!!!'//
     8  '         SAVE OLD DATA BEFORE LOADING NEW DATA OR'/
     9  '             EXITING TO OPERATING SYSTEM!! '//)
        RETURN
C
C       FRAME, SCAN AND TRACK SCREEN
C
300     WRITE(1,1300)ESC,AST
1300    FORMAT(1X,2A1/
     1  ' THE FOLLOWING FUNCTIONS MAY BE TESTED AT THIS LEVEL:'//
     2  '  1. (F)RAME ENABLES XYZ STAGE TO BE TESTED WITH JOYSTICK'//
     3  '  2. (P)ARTICLE ENABLES IMAGE TO BE SCANNED WITH TV CURSOR'//
     4  '  3. (T)RACK ENABLES PARTICLE EDGE TO BE TRACED BY PROGRAM'//)
        RETURN
C
C       DISPLAY, ENTER, SAVE AND VELOCITY SCREEN
C
400     WRITE(1,1400)ESC,AST
1400    FORMAT(1X,2A1/
     1  ' THE FOLLOWING FUNCTIONS MAY BE INVOKED AT THIS LEVEL:'//
     2  '  1. (D)ISPLAY PRINTS POSITIONAL DATA BY FRAME OR PARTICLE'/
     3  '     AND EDGE DATA WHEN BOTH FRAME AND PARTICLE ARE ENTERED'//
     4  '  2. (E)NTER ENABLES FRAME AND PARTICLE DATA FROM XYZ STAGE,'/
     5  '     TV SCAN AND TRACK FUNCTIONS TO BE IDENTIFIED AND STORED'/
     6  '  3. (S)AVE WRITES ALL DATA IN MEMORY TO DISK UNDER FILENAME'//
     7  '  4. (V)ELOCITY COMPUTES DRIFT VALUES FOR SELECTED PARTICLES'//)
        RETURN
C
C       FRAME, SCAN, TRACK, SET AND RESET SCREEN
C
```

```
500     WRITE(1,1500)ESC,AST
1500    FORMAT(1X,2A1/
     1  ' THE FOLLOWING FUNCTIONS MAY BE INVOKED AT THIS LEVEL:'//
     2  '  1. (F)RAME ENABLES PARTICLE POSITION TO BE DETERMINED BY'/
     3  '     MOVING FRAME WITH THE XYZ STAGE UNDER JOYSTICK CONTROL'//
     4  '  2. (P)ARTICLE ENABLES PARTICLE SIZE TO BE DETERMINED BY'/
     5  '     SCANNING TV CURSOR OVER IMAGE UNDER JOYSTICK CONTROL'//
     6  '  3. (T)RACK ENABLES THE EDGE TO BE DETERMINED BY FOLLOWING'/
     7  '     THE PERIMETER USING THE JOYSTICK FOR INITIAL CONTROL'//
     8  '  4. (S)ET TEMPORARILY SAVES THESE VALUES FOR SELECTED FRAME'/
     9  '     AND PARTICLE'//
     A  '  5. (R)ESET RESTORES TO ORIGINAL FRAME AND PARTICLE VALUES'/)
        RETURN
C
C       ENTER, NEXT OR SAME SCREEN
C
600     WRITE(1,1600)ESC,AST
1600    FORMAT(1X,2A1/
     1  ' THE FOLLOWING FUNCTIONS MAY BE INVOKED AT THIS LEVEL:'//
     2  ' (E)NTER ENABLES A SPECIFIC FRAME OR PARTICLE TO BE SELECTED'//
     3  ' (N)EXT SELECTS THE NEXT FRAME OR PARTICLE IN SUCCESSION'//
     4  ' (S)AME ENABLES THE SAME FRAME OR PARTICLE TO BE REPEATED'//)
        RETURN
C
C       NAME, DATE AND COMMENTS SCREEN
C
700     WRITE(1,1700)ESC,AST
1700    FORMAT(1X,2A1/' NOTES ON ENTERING NAME, DATE AND COMMENTS:'//
     1  ' ANY EXISTING DATA NOT PROPERLY SAVED WILL BE DESTROYED!!'//
     2  ' FILE NAMES CAN BE A STRING AS GREAT AS 8 CHARACTERS BUT MUST'/
     3  ' START WITH A LETTER.  YOUR NAME AND DATE CAN BE AS GREAT'/
     4  ' AS 8 MIXED CHARACTERS WHILE COMMENTS CAN BE AS GREAT AS 32.'//
     5  '                    REMEMBER!!!'/
     6  '          SAVE OLD DATA BEFORE CREATING NEW FILES!!!!'/)
        RETURN
C
800     RETURN
        END

A.
```

```
C       FMOVE SUBROUTINE TO MOVE STAGE IN XYZ AXIS
C       REVISION 0.28, 2 APR 1983
C
C       A. MOVE STAGE TO (F)RAME REFERENCE (MOVE X,Y,Z TO 0,0,0)
C       B. MOVE STAGE TO (P)ARTICLE POSITION (MOVE X,Y,Z TO FX,FY,FZ)
C       C. ENTER COMMANDS FROM (J)OYSTICK
C              1. MOVE STAGE IN X AND Y AXIS
C              2. MOVE STAGE IN X AND Z AXIS
C              3. SET PARTICLE POSITION AND RETURN
C              4. RETURN
C       D. ENTER COMMANDS FROM (K)EYBOARD
C              1. INPUT (X),(Y),(Z) AXIS
C              2. (R)ESET FRAME REFERENCE (RESET X,Y,Z TO 0,0,0)
C              3. (S)ET PARTICLE POSITION (SET FX,FY,FZ TO X,Y,Z)
C              4. RETURN
C       E. RETURN
C
        SUBROUTINE FMOVE
C
        LOGICAL ESC,AST,ANS
        INTEGER XYZM,XOUT,YOUT,ZOUT,KJS,JSK,JSX,JSY,JSZ
        INTEGER HLP,FX,FY,FZ,SX,SY,SA,SP,SW,SH,TA,TP,TL,TW(100),TH(100)
        EXTERNAL JSINP,STAGE
        COMMON  ESC,AST,HLP,FX,FY,FZ,SX,SY,SA,SP,SW,SH,TA,TP,TL,TW,TH
C
C       ENTRY POINT
C
        XYZM=0
        CALL TVSCN(XYZM)
        XOUT=0
        YOUT=0
        ZOUT=0
        JSK=0
        JSX=0
        JSY=0
        KJS=0
C
C       SELECT MODE FOR MOVING STAGE
C
100     WRITE(1,1100)
1100    FORMAT('+MOVE TO (F)RAME REFERENCE,(P)ARTICLE POSITION,',
     1  '(J)OYSTICK OR (K)EYBOARD ENTRY: ')
        READ(1,1110)ANS
1110    FORMAT(1A1)
        HLP=11
        IF(ANS.EQ.72)CALL HELP
        IF(ANS.EQ.70)GOTO 200
        IF(ANS.EQ.80)GOTO 300
        IF(ANS.EQ.74)GOTO 400
        IF(ANS.EQ.75)GOTO 500
        GOTO 600
C
C       MOVE STAGE TO FRAME REFERENCE
C
200     XYZM=1
        XOUT=0
        YOUT=0
        ZOUT=0
        CALL STAGE(XYZM,XOUT,YOUT)
        WRITE(1,1200)
1200    FORMAT('+MOVE STAGE TO FRAME REFERENCE')
        GOTO 100
C
C       MOVE STAGE TO PARTICLE POSITION
C
300     XYZM=1
        XOUT=FX
        YOUT=FY
        ZOUT=FZ
        CALL STAGE(XYZM,XOUT,YOUT)
        WRITE(1,1300)
1300    FORMAT('+MOVE STAGE TO PARTICLE POSITION')
        GOTO 100
C
C       ENTER COMMANDS WITH JOYSTICK
C
400     WRITE(1,1400)ESC,AST
1400    FORMAT(1X,2A1,
     1  ' ------------------- JOYSTICK XYZ MODES ------------------'/
     2  '           1. MOVE STAGE RIGHT (X) OR UP (Y)'/
```

```
     3  '           2. MOVE STAGE RIGHT (X) OR FORWARD (Z)'/
     4  '           3. SET POSITION '/
     5  '           4. CONTINUE'/
     6  ' ----MODE-----JSX-----JSY-----JSZ----XOUT----YOUT----ZOUT'/)
        JSK=0
        JSX=0
        JSY=0
        JSZ=0
        KJS=0
410     WRITE(1,1410)KJS,JSX,JSY,JSZ,XOUT,YOUT,ZOUT
1410    FORMAT('+',7I8)
        CALL JSIMP(JSK,JSX,JSY)
        IF(JSK)430,430,420
420     IF(JSK-9)440,600,600
430     IF(KJS)410,410,450
440     KJS=JSK
450     GOTO(460,470,470,560,560,560,560,100),KJS
C
C       X AND Y AXIS
C
460     XYZM=1
        XOUT=XOUT+JSX/10
        YOUT=YOUT+JSY/10
        CALL STAGE(XYZM,XOUT,YOUT)
        GOTO 410
C
C       X AND Z AXIS
C
470     XYZM=1
        JSZ=JSY
        XOUT=XOUT+JSX/10
        ZOUT=ZOUT+JSZ/10
        CALL STAGE(XYZM,XOUT,YOUT)
        GOTO 410
C
C       ENTER COMMANDS FROM KEYBOARD
C
500     XYZM=1
        WRITE(1,1500)
1500    FORMAT('+ENTER (X),(Y),(Z) VALUES,(R)ESET REFERENCE OR',
     1  '(S)ET POSITION: ')
        READ(1,1110)ANS
        HLP=12
        IF(ANS.EQ.72)CALL HELP
        IF(ANS.EQ.88)GOTO 510
        IF(ANS.EQ.89)GOTO 520
        IF(ANS.EQ.90)GOTO 530
        IF(ANS.EQ.82)GOTO 550
        IF(ANS.EQ.83)GOTO 560
        GOTO 100
C
510     WRITE(1,1510)
1510    FORMAT('+X VALUE: ')
        READ(1,1520)XOUT
1520    FORMAT(I8)
        GOTO 540
520     WRITE(1,1530)
1530    FORMAT('+Y VALUE: ')
        READ(1,1520)YOUT
        GOTO 540
530     WRITE(1,1540)
1540    FORMAT('+Z VALUE: ')
        READ(1,1520)ZOUT
540     CALL STAGE(XYZM,XOUT,YOUT)
        GOTO 500
C
550     XYZM=0
        CALL STAGE(XYZM)
        GOTO 500
C
560     FX=XOUT
        FY=YOUT
        FZ=ZOUT
        GOTO 100
C
600     CONTINUE
        RETURN
        END
```

```
;       STAGE SUBROUTINE
;       REVISION 0.20, 27 JULY 1982
;
;       THIS ROUTINE MOVES THE XYZ STAGE TO THE DESIGNATED
;       POSITION AND RETURNS.
;
;       STAGE(XYZMEM[HL],XOUTCDE],YOUTCBC]),ZOUTCBC+2]
;
        ENTRY   STAGE
STAGE:  LD      A,(HL)          ;GET FLAG
        ADD     A,0             ;CHECK ZERO FLAG
        JP      NZ,START        ;START XFER IF FLAG OK
        LD      A,0             ;RESET A REG
        OUT     (84H),A         ;AND OUTPUT
        RET                     ;RETURN
;
START:  PUSH    BC              ;GET Y AXIS ADDRESS
        POP     HL              ;AND PUT IT IN HL REG
        INC     HL              ;INCREMENT ONCE
        INC     HL              ;TWICE
        PUSH    HL              ;SAVE Z AXIS ADDRESS
        PUSH    BC              ;SAVE Y AXIS ADDRESS
        PUSH    DE              ;SAVE X AXIS ADDRESS
        LD      A,208           ;INIT AXIS CODE
        LD      (ACODE),A       ;AND SAVE
        LD      A,3             ;INIT AXIS COUNT
        LD      (ACOUNT),A      ;AND SAVE
AXIS:   LD      A,5             ;INIT DIGIT COUNT
        LD      (DCOUNT),A      ;AND SAVE
        LD      C,192           ;INIT DIGIT CODE
        POP     HL              ;RECALL AXIS ADDRESS
        LD      E,(HL)          ;GET AXIS VALUE (LOW BYTE)
        INC     HL
        LD      D,(HL)          ;(HIGH BYTE)
        EX      DE,HL           ;MOVE VALUE TO HL
        LD      IX,DECADE       ;INIT DECADE ADDRESS
        LD      E,(IX)          ;LOAD HIGHEST DECADE (LOW BYTE)
        INC     IX
        LD      D,(IX)          ;(HIGH BYTE)
        INC     IX
        SBC     HL,DE           ;SUBTRACT HIGHEST DECADE FROM VALUE
        JP      P,NEG           ;JUMP IF VALUE IS NEGATIVE
        ADD     HL,DE           ;ADD BACK HIGHEST DECADE
        LD      B,0             ;LOAD POSITIVE FLAG
        JP      POS             ;VALUE IS POSITIVE
;
NEG:    LD      B,8             ;LOAD NEGATIVE FLAG INTO B REG
        EX      DE,HL           ;EXCHANGE REGS
        SBC     HL,DE           ;COMPLEMENT VALUE
POS:    XOR     A               ;RESET OUTPUT WORD TO ZERO
        OR      A               ;CLEAR CARRY
        LD      E,(IX)          ;LOAD NEXT DECADE (LOW BYTE)
        INC     IX
        LD      D,(IX)          ;(HIGH BYTE)
        INC     IX
LOOP:   INC     A               ;INCREMENT DIGIT VALUE
        SBC     HL,DE           ;SUBTRACT NEXT DECADE FROM VALUE
        JP      P,LOOP          ;DO AGAIN IF STILL POSITIVE
        OR      A               ;CLEAR CARRY
        ADC     HL,DE           ;TOO MUCH, ADD IT BACK
        DEC     A
        ADD     A,B             ;ADD SIGN TO OUTPUT WORD
        ADD     A,C             ;ADD DIGIT CODE TO OUTPUT WORD
        OUT     (84H),A         ;OUTPUT
        LD      A,(DCOUNT)      ;GET DIGIT COUNT
        DEC     A               ;AND DECREMENT
        JP      Z,OUTPUT        ;OUTPUT AXIS CODE IF DONE
;
        LD      (DCOUNT),A      ;SAVE DIGIT COUNT
        LD      B,0             ;RESET SIGN FLAG TO ZERO
        LD      A,C
        SUB     A,10H           ;DEC DIGIT CODE
        LD      C,A             ;SAVE
        JP      POS             ;DO AGAIN
;
OUTPUT: LD      A,(ACODE)       ;LOAD AXIS CODE
        OUT     (84H),A         ;OUTPUT
        ADD     A,10H           ;INC AXIS CODE
        LD      (ACODE),A       ;AND SAVE
```

```
        LD      A,(ACOUNT)      ;GET AXIS COUNT
        DEC     A               ;DEC IT
        LD      (ACOUNT),A      ;AND SAVE IT
        JP      NZ,AXIS         ;IF NOT ZERO DO AGAIN
        RET
;
;       STORAGE AREA
;
DECADE: DW      8000H,10000,1000,100,10,1
ACODE:  DS      2
ACOUNT: DS      2
DCOUNT: DS      2
;
        END
```

A.

```
TYPE JSINP.Z80
;       JOYSTICK SUBROUTINE
;       VERSION 0.21, 18 JULY 1982
;
;       THIS ROUTINE INPUTS UNIPOLAR DATA FROM THE MODE SWITCH, X AXIS
;       AND Y AXIS THEN RETURNS BIPOLAR VALUES TO CALLING PROGRAM
;
        ENTRY   JSINP
JSINP:  PUSH    BC              ;SAVE JSY ADDRESS
        PUSH    DE              ;SAVE JSX ADDRESS
        PUSH    HL              ;SAVE JSK ADDRESS
        IN      A,(18H)         ;INPUT JS SWITCH
        LD      B,A             ;MOVE IT TO B
        LD      A,255           ;LOAD A WITH 255
        SUB     B               ;SUB JS SWITCH
        POP     HL              ;GET JSK ADDRESS
        LD      (HL),A          ;STORE MODE
        LD      B,2             ;INIT AXIS COUNT
        LD      C,19H           ;INIT INPUT PORT
JSXY:   IN      A,(C)           ;INPUT JS VALUE
        LD      E,A             ;LOAD E WITH JS VALUE
        LD      D,0
        LD      HL,128          ;LOAD HL WITH 128
        SBC     HL,DE           ;SUBTRACT JS VALUE FROM 128
        JP      P,JSOUT         ;JUMP IF POSITIVE VALUE
        EX      DE,HL           ;FIND NEGATIVE VALUE
        LD      DE,255
        SBC     HL,DE
        EX      DE,HL
JSOUT:  POP     HL              ;GET X OR Y AXIS ADDRESS
        LD      (HL),E          ;LOAD BIPOLAR VALUE FOR RETURN
        INC     HL
        LD      (HL),D
        DEC     B               ;MOVE TO NEXT AXIS
        JP      Z,RETURN        ;RETURN IF DONE
        INC     C               ;MUST BE Y AXIS
        JP      JSXY
RETURN: RET
        END
```

```
C       PSCAN SUBROUTINE TO INPUT PARTICLE SCAN DATA
C       REVISION 0.28, 7 APR 1983
C
        SUBROUTINE PSCAN
C
        LOGICAL ESC,AST,ANSWER
        INTEGER KJS,JSK,JSX,JSY,THRESH,VIDEO
        INTEGER XOUT,YOUT,LOUT,TOUT,VINP,AINP,PINP
        INTEGER HLP,FX,FY,FZ,SX,SY,SA,SP,SW,SH,TA,TP,TL,TW(100),TH(100)
        COMMON  ESC,AST,HLP,FX,FY,FZ,SX,SY,SA,SP,SW,SH,TA,TP,TL,TW,TH
C
C       ZERO CURSOR ON TV MONITOR
C
        JSK=0
        JSX=0
        JSY=0
        KJS=0
        LR=0
        IPRINT=0
        MR=10
        NR=10
        SX=128
        SY=128
        SW=1
        SH=1
        XOUT=128
        YOUT=128
        LOUT=130
        TOUT=0
        VINP=0
        AINP=0
        PINP=0
        VIDEO=0
        THRESH=0
        CALL TVSCN(TOUT)
C
C       DISPLAY JOYSTICK SELECTIONS
C
5       WRITE(1,1000)ESC,AST
1000    FORMAT(1X,2A1,
     1  ' -------- JOYSTICK PARTICLE SCAN MODES ---------'/
     2  '       1. MOVE CURSOR WITH JOYSTICK'/
     3  '       2. MOVE CURSOR TO EXTREMES OF PARTICLE'/
     4  '       3. MOVE CENTER OF CURSOR SCAN'/
     5  '       4. ENTER COMMANDS WITH KEYBOARD'/
     A  ' --JSMODE--X CNTR--Y CNTR---WIDTH--HEIGHT---VIDEO'/)
C
C       FIND PARTICLE CENTER, SIZE AND SHAPE
C
        KJS=5
10      CALL JSINP(JSK,JSX,JSY)
        IF(JSK)20,20,30
20      IF(KJS)10,10,50
30      IF(JSK-9)40,900,900
40      KJS=JSK
        LR=0
50      GOTO(100,200,200,300,700,300,300,400),KJS
C
C       MOVE CURSOR WITH JOYSTICK
C
100     IF(LR)110,110,120
110     XOUT=SX
        YOUT=SY
120     LR=1
        XOUT=XOUT+JSX/MR
        YOUT=YOUT-JSY/MR
        LOUT=YOUT+1
        TOUT=1
        CALL TVSCN(XOUT,VINP)
        VIDEO=VINP
        GOTO 700
C
C       FIND PARTICLE SCAN SIZE
C
200     SW=SW+JSX/NR
        IF(SW)210,210,220
210     SW=1
220     SH=SH+JSY/NR
        IF(SH)230,230,240
```

```
220     SH=1
240     XOUT=SX-SW
        YOUT=SY-SH
        LOUT=SY+SH
        TOUT=1
        CALL TVSCN(XOUT,VINP)
        XOUT=SX
        CALL TVSCN(XOUT,VINP)
        XOUT=SX+SW
        CALL TVSCN(XOUT,VINP)
        GOTO 700
C
C       FIND PARTICLE SCAN CENTER
C
300     SX=SX+JSX/NR
        SY=SY-JSY/NR
        YOUT=SY-SH
        LOUT=SY+SH
        TOUT=1
        XOUT=SX-SW
        CALL TVSCN(XOUT,VINP)
        XOUT=SX
        CALL TVSCN(XOUT,VINP)
        XOUT=SX+SW
        CALL TVSCN(XOUT,VINP)
        GOTO 700
C
C       ENTER COMMANDS WITH KEYBOARD
C
400     WRITE(1,1400)
1400    FORMAT(1X,
     1  '/ ---------- KEYBOARD COMMANDS ----------'/
     2  '/        1. ENTER THRESHOLD AND SCAN IMAGE'/
     3  '/        2. REPEAT SCAN WITH SAME THRESHOLD'/
     4  '/        3. JOYSTICK CONTROL WITH DISPLAY'/
     5  '/        4. JOYSTICK CONTROL WITHOUT DISPLAY'/
     6  '/        5. SET VALUES AND RETURN'/)
        WRITE(1,1410)
1410    FORMAT(1X,'ENTER SELECTION: ')
        READ(1,1420)ISEL
1420    FORMAT(I4)
        KJS=0
        JKS=0
        IF(ISEL)400,400,410
410     IF(ISEL-6)420,420,400
420     GOTO(500,550,600,650,700),ISEL
C
C       ENTER THRESHOLD
C
500     WRITE(1,1500)
1500    FORMAT(' ENTER THRESHOLD: ')
        READ(1,1420)THRESH
        IF(THRESH)500,500,510
510     IF(THRESH-255)800,800,500
550     IF(THRESH)500,500,800
C
C       SET/RESET PRINT FLAG
C
600     IPRINT=0
        GOTO 5
C
650     IPRINT=1
        GOTO 5
C
C       PRINT PARAMETERS IF FLAG IS SET
C
700     IF(IPRINT)710,710,10
710     WRITE(1,1710)KJS,SX,SY,SW,SH,VIDEO
1710    FORMAT('+',6I8)
        IF(KJS-5)10,720,10
720     XOUT=128
        LOUT=130
        TOUT=0
        CALL TVSCN(XOUT)
        GOTO 10
C
750     WRITE(1,1750)
1750    FORMAT(1X,
     1  '/ -NB MODE---X CTR---Y CTR----AREA---PERIM--THRESH'/)
```

```
      WRITE(1,1760)ISEL,SX,SY,SA,SP,THRESH
1760  FORMAT(6I8)
      GOTO 400
C
C     SCAN PARTICLE FOR SIZE AND SHAPE
C
800   XOUT=SX-SW
      YOUT=SY-SH
      LOUT=SY+SH
      XLIM=SX+SW
      TOUT=THRESH
      SA=0
      SP=0
      LASTA=0
810   CALL TVSCN(XOUT,VINP)
      SA=SA+(AINP*0.79)
      SP=SP+PINP+(IABS(LASTA-AINP)*0.79)
      LASTA=AINP
820   XOUT=XOUT+1
      IF(XOUT-XLIM)810,830,830
830   KJS=0
      GOTO 750
C
C     RETURN TO CALLING PROGRAM
C
900   CONTINUE
      RETURN
      END
```

A.

```
C       TRACK.FOR SUBPROGRAM
C       REVISION 0.34, 7 FEB 83
C
C       THIS PROGRAM PROVIDES FOR AUTO TRACKING A VIDEO IMAGE,
C       SAVING THE EDGE COORDINATES OF THE VIDEO IMAGE,
C       COMPUTING THE PERIMETER AND AREA OF THE IMAGE AND
C       DISPLAYING THE PROCESSED PERIMETER ON TOP OF THE IMAGE.
C
        SUBROUTINE TRACK
C
        LOGICAL ESC,AST
        INTEGER JSK,JSX,JSY
        INTEGER XOUT,YOUT,LOUT,TOUT,VINP,AINP,PINP
        INTEGER SCAMP,SCART,START,AW,DW,DH,DX(64),DY(64)
        INTEGER NSCAN,TOLER,POINT,XSCAN(32),YSCAN(32)
        INTEGER AREA,PERIM,PTSIZE,VIDEO
        INTEGER HLP,FX,FY,FZ,SX,SY,SA,SP,SW,SH,TA,TP,TL,TW(100),TH(100)
        COMMON  ESC,AST,HLP,FX,FY,FZ,SX,SY,SA,SP,SW,SH,TA,TP,TL,TW,TH
C
C       DISPLAY JOYSTICK SELECTIONS
C
10      WRITE(1,11)
11      FORMAT(' ENTER FY/FX: ')
        READ(1,12)FH
12      FORMAT(F8.3)
        KJS=1
        JSK=0
        JSX=0
        JSY=0
        XOUT=128
        YOUT=128
        VIDEO=0
        TL=0
        PTSIZE=TL
        PERIM=0
        AREA=0
20      WRITE(1,1000)ESC,AST
1000    FORMAT(1X,2A1,
     1  '  ------------JOYSTICK CONTROL MODES------------'/
     2  '        1. MOVE CURSOR TO SCREEN CENTER'/
     3  '        2. MOVE CURSOR TO PARTICLE EDGE'/
     4  '        3. AUTO TRACK AROUND PARTICLE EDGE'/
     5  '        4. DISPLAY DIGITIZED EDGE OVER PARTICLE'/
     6  '     3+4. RETURN TO OPERATING SYSTEM'/
     7  ' --X POSN--Y POSN---VIDEO--PTSIZE----AREA---PERIM'/)
        GOTO 100
30      WRITE(1,1010)XOUT,YOUT,VIDEO,PTSIZE,AREA,PERIM
1010    FORMAT('+',6I8)
40      CALL JSINP(JSK,JSX,JSY)
        IF(JSK)50,50,60
50      IF(KJS)40,40,80
60      IF(JSK-9)70,500,500
70      KJS=JSK
80      GOTO(100,200,200,300,300,300,300,400),KJS
C
C       ZERO CURSOR ON SCREEN
C
100     XOUT=128
        YOUT=128
        LOUT=130
        TOUT=0
        VINP=0
        AINP=0
        PINP=0
        CALL TVSCN(XOUT,VINP)
        VIDEO=VINP
        X1=128
        Y1=128
        KJS=1
        GOTO 30
C
C       MOVE CURSOR TO PARTICLE EDGE WITH JOYSTICK
C
200     X1=X1+JSX/10
        Y1=Y1-JSY/10
        IF(X1-254)210,210,30
210     IF(Y1-254)220,220,30
```

```
220     IF(X1-2)30,30,230
230     IF(Y1-2)30,30,240
240     XOUT=X1
        YOUT=Y1
        LOUT=YOUT+2
        TOUT=0
        CALL TVSCN(XOUT,VINP)
        VIDEO=VINP
        GOTO 30
C
C       AUTO TRACK IMAGE EDGE
C
300     WRITE(1,1300)
1300    FORMAT(' ENTER NUMBER OF SCAN POINTS: ')
        READ(1,1310)NSCAN
1310    FORMAT(I8)
        IF(NSCAN-32)310,310,300
310     WRITE(1,1320)
1320    FORMAT(' ENTER SCAN AMPLITUDE: ')
        READ(1,1310)SCAMP
        IF(SCAMP-16)320,320,310
320     WRITE(1,1330)
1330    FORMAT(' ENTER SCAN LEAD START: ')
        READ(1,1310)SCART
        IF(SCART-NSCAN/2)330,330,320
330     WRITE(1,1340)
1340    FORMAT(' ENTER VIDEO TOLERANCE: ')
        READ(1,1310)TOLER
        POINT=NSCAN/4
        TW(0)=XOUT
        TH(0)=YOUT
        TAREA=0
        TERIM=0
        JMP=0
        DA=6.28318/NSCAN
        DO 340 I=1,NSCAN
          DX(I)=SCAMP*COS(I*DA)
          DY(I)=SCAMP*SIN(I*DA)
          INS=I+NSCAN
          DX(INS)=DX(I)
          DY(INS)=DY(I)
340       CONTINUE
        DO 370 J=1,100
          START=POINT-SCART
          IF(START)344,346,346
344       START=NSCAN+POINT-SCART
346       DO 350 I=1,NSCAN
            IST=I+START
            XSCAN(I)=TW(J-1)-DX(IST)
            YSCAN(I)=TH(J-1)+DY(IST)
350         CONTINUE
          CALL TVTRK(NSCAN,XSCAN(1),YSCAN(1))
          CALL JSINP(JSK,JSX,JSY)
          IF(JSK)360,360,60
360       TW(J)=XSCAN(POINT)
          TH(J)=YSCAN(POINT)
          POINT=POINT+START
          IF(POINT-NSCAN)362,362,361
361       POINT=POINT-NSCAN
362       IF(J-2)370,365,363
363       IF(IABS(TW(J)-TW(1))+IABS(TH(J)-TH(1))-SCAMP+1)364,365,365
364       TW(J)=TW(1)
          TH(J)=TH(1)
          JMP=1
365       DH=TH(J-1)-TH(J)
          DW=TW(J-1)-TW(J)
          AW=TW(J-1)+TW(J)-256
          TAREA=TAREA+AW*DH/2
          TERIM=TERIM+SQRT(DW**2+(FH*DH)**2)
          IF(JMP-1)370,380,330
370       CONTINUE
380     PTSIZE=J
        AREA=INT(FH*TAREA)
        PERIM=INT(TERIM)
        WRITE(1,1370)PTSIZE,PERIM,AREA
1370    FORMAT('  NUMBER    PERIM     AREA'/3I8/
     1  '     POINT   X AXIS   Y AXIS')
        DO 390 J=1,PTSIZE
          WRITE(1,1380)J,TW(J),TH(J)
1380      FORMAT(3I8)
```

```
350       CONTINUE
          GOTO 20
C
C         DISPLAY DIGITIZED PERIMETER OVER IMAGE
C
400       TOUT=1
          DO 450 I=1,PTSIZE
C            RND=RAN(1.0)
C            J=INT(PTSIZE*RND)
             J=I
             XOUT=TW(J)
             YOUT=TH(J)
             LOUT=YOUT+2
             CALL TVSCN(XOUT,VINP)
             CALL JSINP(JSK,JSX,JSY)
             IF(JSK)450,450,60
450       CONTINUE
          GOTO 400
C
C          RETURN TO CALLING PROGRAM
C
500       CONTINUE
          TL=PTSIZE
          TP=PERIM
          TA=AREA
          RETURN
          END

A.
```

```
;       TVTRK.Z80 SUBROUTINE
;       REVISION 0.22, 4 AUGUST 1982
;
;       THIS ROUTINE MOVES THE CURSOR TO EACH X AND Y
;       POSITION AROUND A POINT ON THE PARTICLE EDGE
;       UNTIL A CIRCLE IS COMPLETED OR THE VIDEO EXCEEDS
;       THE PREVIOUS VIDEO BY A CERTAIN TOLERANCE.
;       THE POINT AT WHICH THIS OCCURS IS THEN RETURNED.
;
;       PARAMETER ASSIGNMENT
;
;       TVTRK(NSCANCHL],XSCANCDE],YSCANCBC])
;       YSCAN ARRAY WILL START AT BC AND BE PUT IN IY.
;       XSCAN ARRAY WILL START AT DE AND BE PUT IN IX.
;       NSCAN ADDRESS IS IN HL REG, VALUE PUT IN E REG.
;       TOLER IS AT HL+2, VALUE PUT IN C.
;       EDGE POINT WILL BE PUT IN HL+4 LOCATION FOR RETURN.
;
;       SUBROUTINE INITIALIZATION
;
        ENTRY   TVTRK
TVTRK:  PUSH    BC              ;STORE YSCAN ADDRESS IN IY
        POP     IY
        PUSH    DE              ;STORE XSCAN ADDRESS IN IX
        POP     IX
        LD      E,(HL)          ;STORE NSCAN VALUE IN E
        INC     HL
        INC     HL
        LD      C,(HL)          ;STORE VIDEO TOLERANCE IN C
        INC     HL
        INC     HL
        PUSH    HL              ;SAVE POINT ADDRESS ON STACK
        LD      D,0             ;INIT POINT IN D
        LD      B,0             ;INIT FOR WHITE TO BLACK EDGE
;
;       OUTPUT NEXT SCAN POINT
;
SCOUT:  INC     D               ;SETUP FOR NEXT POINT
        LD      A,10            ;LOAD X CONTROL
        OUT     74H,A           ;OUTPUT X CONTROL
        LD      A,(IX)          ;LOAD X VALUE
        OUT     64H,A           ;OUTPUT X VALUE
        LD      A,4             ;LOAD Y CONTROL
        OUT     74H,A           ;OUTPUT Y CONTROL
        LD      A,(IY)          ;LOAD Y VALUE
        OUT     64H,A           ;OUTPUT Y VALUE
        INC     IX              ;SETUP FOR NEXT POSITION
        INC     IX
        INC     IY
        INC     IY
STAT:   IN      A,64H           ;INPUT STATUS
        BIT     0,A             ;CHECK STATUS BIT
        JP      Z,STAT          ;KEEP CHECKING UNTIL STATUS IS OK
        IN      A,74H           ;INPUT VIDEO
        CP      B               ;COMPARE VIDEO WITH PREVIOUS THRESHOLD
        JP      C,FOUT          ;EDGE IS FOUND IF VIDEO IS LESS
        CP      C               ;COMPARE WITH TOLER
        JP      C,NEXT          ;NEXT POINT IF LESS
        SUB     A,C             ;SUBTRACT TOLER FROM VIDEO IF MORE
        LD      B,A             ;AND STORE AS NEXT THRESHOLD
NEXT:   DEC     E               ;DEC NSCAN
        JP      NZ,SCOUT        ;REPEAT IF NOT ZERO
;
;       RETURN EDGE POINT
;
FOUT:   LD      A,D             ;LOAD EDGE POINT
        POP     HL
        LD      (HL),A          ;AND RETURN
        RET
        END

A.
```

```
;       VIDEO INTERFACE SUBROUTINE
;       REVISION 0.21, 4 AUGUST 1982
;
;       THIS ROUTINE MOVES THE CURSOR TO THE CENTER OF THE
;       TV SCREEN, PARTICLE CENTER OR THE PARTICLE EXTREMES
;       AND SCANS THE PARTICLE TO FIND THE AREA AND PERIMETER.
;
;       SUBROUTINE PARAMETERS
;
;       TVSCN(XINP[HL],VOUT[DE])
;       YINP IS AT HL+2
;       LINP IS AT HL+4
;       TINP IS AT HL+6
;       AOUT IS AT DE+2
;       POUT IS AT DE+4
;
;       DATA BASE
;
XINP:   DB      1       ;X VALUE
YINP:   DB      1       ;Y VALUE
LINP:   DB      1       ;Y LIMIT
TINP:   DB      1       ;THRESHOLD
VOUT:   DB      1       ;VIDEO
AOUT:   DB      1       ;AREA
POUT:   DB      1       ;PERIMETER
;
        ENTRY   TVSCN
TVSCN:  LD      A,(HL)          ;BRING IN FIRST PARAMETER
        ADD     A,0             ;SET FLAGS
        JP      Z,CNTR          ;IF ZERO GO CENTER TV CURSOR
        PUSH    DE              ;SAVE OUTPUT ADDRESS
        LD      A,(HL)          ;STORE X VALUE
        LD      (XINP),A
        INC     HL
        INC     HL
        LD      A,(HL)          ;STORE Y VALUE
        LD      (YINP),A
        INC     HL
        INC     HL
        LD      A,(HL)          ;STORE Y LIMIT
        LD      (LINP),A
        INC     HL
        INC     HL
        LD      A,(HL)          ;STORE THRESHOLD
        LD      (TINP),A
        LD      HL,00           ;RESET HL
        LD      DE,00           ;RESET DE
        LD      BC,00           ;RESET BC
;
;       OUTPUT POSITION
;
START:  LD      A,10            ;LOAD X CONTROL
        OUT     74H,A           ;OUTPUT X CONTROL
        LD      A,(XINP)        ;LOAD X VALUE
        OUT     64H,A           ;OUTPUT X VALUE
        LD      A,4             ;LOAD Y CONTROL
        OUT     74H,A           ;OUTPUT Y CONTROL
        LD      A,(YINP)        ;LOAD Y VALUE
        LD      E,A             ;INTO E
;
;       INPUT VIDEO
;
NEXTY:  LD      A,E             ;LOAD Y VALUE
        OUT     64H,A           ;AND OUTPUT
STAT:   IN      A,64H           ;INPUT STATUS
        BIT     0,A             ;CHECK STATUS BIT
        JP      Z,STAT          ;JUMP TO INPUT IF NOT SET
        LD      H,0             ;RESET PRES PIXEL
        IN      A,74H           ;INPUT VIDEO
        LD      B,A             ;SAVE VIDEO
        LD      A,(TINP)        ;RECALL THRESH
        CP      B               ;COMPARE THRESH WITH VIDEO
        JP      NC,PERIM        ;GO IF MORE THAN VIDEO
        LD      H,1             ;SET PRESENT PIXEL
        INC     C               ;INCREMENT AREA
PERIM:  LD      A,H             ;LOAD A WITH PRES PIX
        CP      L               ;COMPARE PRES TO PREV
        JP      Z,CONT          ;CONTINUE IF SAME
```

```
        INC     D               ;INCREMENT PERIM
CONT:   LD      L,H             ;LOAD PREV WITH PRES
        LD      A,(LINP)        ;LOAD Y LIMIT
        INC     E               ;DECREMENT Y VALUE
        CP      E               ;COMPARE Y VALUE TO LIMIT
        JP      NZ,NEXTY        ;DO AGAIN IF NOT ZERO
;
;       RETURN PARAMETERS
;
        POP     HL              ;RECALL OUTPUT ADDRESS
        LD      (HL),B          ;STORE VIDEO
        INC     HL
        INC     HL
        LD      (HL),C          ;STORE AREA
        INC     HL
        INC     HL
        LD      (HL),D          ;STORE PERIMETER
        RET
;
;       CENTER TV CURSOR
;
CNTR:   LD      A,10
        OUT     74H,A
        LD      A,128
        OUT     64H,A
        LD      A,4
        OUT     74H,A
        LD      A,128
        OUT     64H,A
        RET
;
        END

A.
```

APPENDIX TWO

Holographic Image Analysis

Hardware - Software

Publication Draft

# "A System to Catalog and Analyze Holographic Images of Dynamic Ocean Particles"

Prepared by

Paul R. Payne, Aztec Computer Engineering

Kendall L. Carder, University of South Florida

Robert G. Steward, University of South Florida

St. Petersburg, Florida

## ABSTRACT

A holographic image analysis system has been developed to measure the position, velocity, size and shape of microscopic particles slowly settling in three-dimensional space. Images of particles recorded sequentially on individual holographic frames are reconstructed using an in-line, far field configuration. Image analysis is computer-controlled with two basic functions. First is the precision registration and XYZ positioning of the holographic frame so that accurate particle displacements between sequential frames can be measured. These displacements are compared to the elapsed time between the frames to get particle settling velocity. Second, it scans a digitized video image of the reconstructed holographic image to measure size, shape, and area. A scanning algorithm has been developed to determine particle size (area, length, width) for classification by settling characteristics. An edge tracking algorithm has also been developed to facilitate particle identification by shape from frame to frame. A cataloging system was developed to provide for data entry, storage and retrieval.

# I. INTRODUCTION

Measurement of size, shape and density are critical factors in the study of particle dynamics and settling characteristics of marine hydrosols. Micrographic holography has been widely used in aerosol studies (1) and holographic movie cameras have been developed for studying zooplankton feeding behavior in ocean waters (2). The size and settling behavior of aggregates resulting from mixing riverine water with seawater has been holographically determined in the laboratory (3) and effect of particle shape on the settling velocities of primary hydrosols (unaggregated) has also been investigated holographically (4), (5).

Carder et al. (6) have developed an in situ holographic micro-velocimeter for the study of microscopic particles suspended in sea water. This device records the image of each particle in three-dimensional space on a series of successive holograms with respect to time. Horizontal and vertical dimensions and cross sectional area have been used to determine particle density using Stokes' Theorem (3). Edge coordinates are useful for particle identification (e.g., Zernike moments) and analysis of shape on particle rotation and settling speed (4). During these studies, a great number of samples must be analyzed in order to provide sufficient statistics for determining particle population characteristics of shape and size as well as settling velocity, trajectory, orientation and oscillations. Such measurements can be facilitated by use of a computer-controlled image analysis system to improve the accuracy and reduce the number of man-hours in analyzing holographic particle data.

## II. PROBLEM DEFINITION

A measurement technique was needed to determine the position, size, shape, orientation and velocity of microscopic particles moving in three-dimensional space. The marine particles of interest in the study (6) cited above typically ranged from 5 to 250 microns in diameter, which necessitated the use of microscopic techniques for any detailed size or shape analysis. Since oceanic particle densities may vary from about 1.03 to 5.2 g/ml and typical settling velocities may range from less than .0001 to 1.0 cm/s, a variety of frame or sample periods from less than one second to as much as one minute may be necessary in order to provide short-term velocity measurement accuracy. In addition, the duration or exposure time for the position measurement should be less than 1/500 sec. in order to maintain sufficient positional accuracy and prevent hologram "smearing." Therefore, a relatively high speed, microscopic technique was developed (6) to record the images of multiple particles as they settled in three-dimensional space. In order to deal with the enormous data volume generated in applying these techniques (more than 50 particles per hologram), an automated method for reconstructing and analyzing the particle data has been developed. Edge coordinates are recorded when needed for particle identification and for analysis of the particle shape effects on particle rotation.

## III. SYSTEM DESCRIPTION

A functional block diagram of the holographic image analysis system is shown in Figure 1. The major components and functions are: 1) a laser to reconstruct the holographic image, 2) a mechanical stage to position the hologram in three-dimensional space, 3) a magnification lens and rear

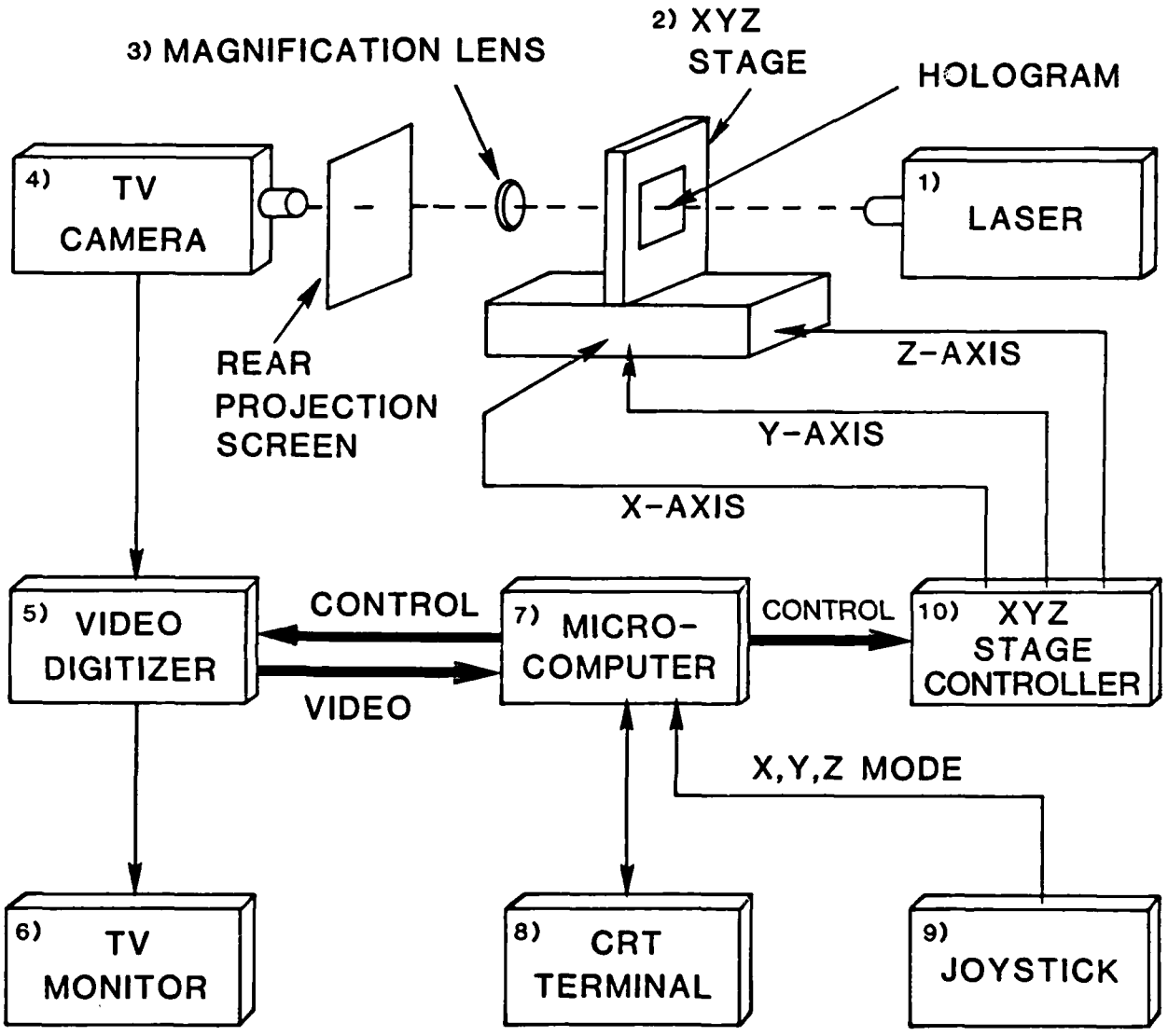


FIGURE 1 HOLOGRAPHIC IMAGE ANALYSIS SYSTEM BLOCK DIAGRAM

projection screen on which to reconstruct the particle image, 4) a television camera to view the images, 5) a video digitizer to convert the image into digital data, 6) a television monitor to display the particle image, 7) a microcomputer with disk storage for processing and storing input data from the video digitizer and controlling the position of the mechanical stage, 8) an interactive terminal to enable operator control of the system, 9) a joystick for manual control of the frame position and 10) the XYZ drive controller to move the holographic frame in the laser beam. Table 1 presents a list of the equipment which comprises the system.

Table 1. HOLOGRAPHIC IMAGE ANALYSIS SYSTEM EQUIPMENT

| Item | Description | Manufacturer | Model |
|---|---|---|---|
| 1 | Laser, 15 mW, He-Ne | Spectraphysics | 124B |
| 2 | XYZ axis table | Aerotech, XY: | ATS-303 |
| | | Z: | ATS-416 |
| 3 | 28mm or 50mm lens | Nikon | |
| 4 | Television camera, high resolution | Dage | 650 |
| 5 | Video digitizer | Colorado Video | 270A |
| 6 | Television monitor | Panasonic | WV 5300 |
| 7 | Micro-computer, Z-80, dual disk | Cromemco | Z-2D |
| 8 | CRT terminal | Soroc | IQ 120 |
| 9 | Joystick | Cromemco | |
| 10 | XYZ drive controller | Aerotech | EC-2 |

The system performs the following functions: 1) determines the position of a particle with respect to a three-dimensional frame reference, 2) determines the width, height, cross sectional area and perimeter of a particle using a scanning algorithm, 3) determines the

cross-sectional area, perimeter and edge coordinates of the particle using a tracking algorithm, 4) provides for particle identification from frame-to-frame by displaying the particle position and edge points (shape) from the previous holographic frame on the current frame and 5) computes the velocity, average diameter and particle density from the recorded data for each particle.

## IV. TECHNICAL DISCUSSION

Successive holograms of settling particles were recorded in situ on negative holographic transparency film using the particle velocimeter described in reference (6). The film was processed using standard photographic techniques and mounted on individual frames. Each holographic frame was positioned in a laser beam to reconstruct a two-dimensional profile of each particle in the direct transmission mode. The image of each particle was successively focused on the rear projection screen by moving the holographic frame in the Z axis. The projected scene was viewed with a television camera and converted into a digitized video signal. The holographic frame was then moved in the X and Y axes to bring the focused image of each particle into the center of a TV monitor. The position of the frame and the size, shape and orientation of each particle was analyzed and recorded by the computer. As images of the same particles in subsequent frames were catalogued, a matrix of settling velocity and lateral motion characteristics was generated for each particle. The statistical distribution of settling velocity with respect to particle size, shape and orientation provided an accurate determination of particle density and ultimately permitted a general particle classification (e.g., organic, mineral, heavy mineral), based largely upon density.

## A. PARTICLE POSITION AND VELOCITY

Particle settling velocity using the system described in Figure 1 was determined by measuring the position of each particle in three-dimensional space at two or more different sample times. A typical particle configuration is shown in Figure 2. Prior to cataloging any particle images from a frame, an accurate and repeatable reference is established for a point common to all frames. The reference point in a frame is centered on the television monitor by moving the frame in the X, Y and Z axes under computer control with a joystick. The image of each particle in the frame is then subsequently moved to the center of the monitor with the joystick and its position recorded. Size and orientation parameters are determined using the particle scanning and edge tracking algorithms described below. Once recorded, the particle data from a previous frame can be retrieved and the XYZ stage driven to that position under computer control to enhance location and identification of that particle on a subsequent frame. When the entry of data for all frames has been completed, the distance each particle has travelled between successive frames is determined and the individual velocities calculated as shown:

$$Vt = (Vx^2 + Vy^2 + Vz^2)^{1/2} \qquad (1)$$

where

$$Vx = dx/dt$$

$$Vy = dy/dt$$

$$Vz = dz/dt.$$

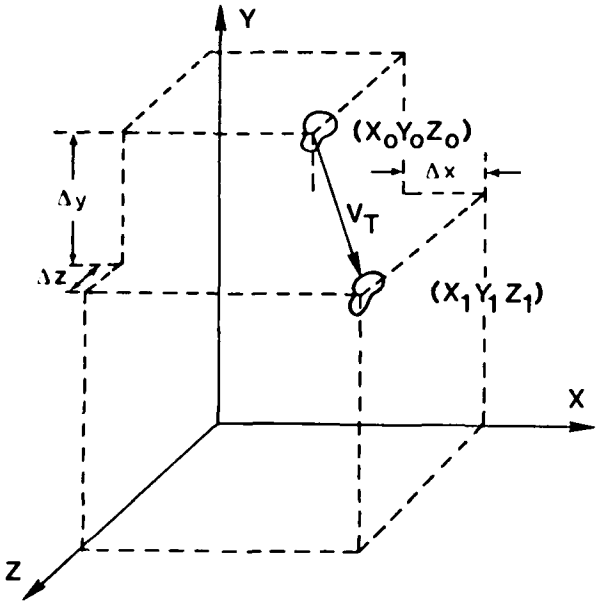


FIGURE 2 PARTICLE MOVING IN THREE DIMENSIONAL SPACE

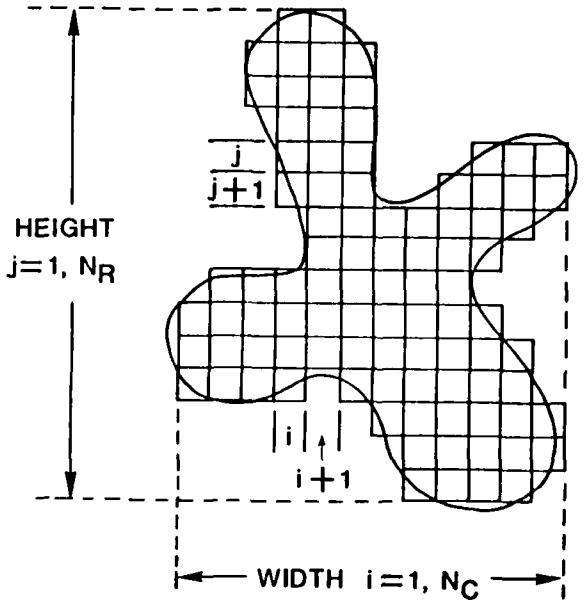


FIGURE 3 SCANNING ALGORITHM PROCESSES PIXELS ABOVE THRESHOLD FOR AREA AND PERIMETER

## B. PARTICLE AREA AND PERIMETER

Determination of the projected cross-sectional area of a particle can be derived from the reconstructed image by counting the number of pixels inside the particle boundary. In a similar manner, the perimeter of the particle can be derived from the number of pixels along the edge. One of the major problems with a "noisy" image is detection of the pixels which represent the edge. Yakimovsky discussed an edge detection technique (7) based on maximizing the likelihood ratio with a simple single-pass, region-growing algorithm. This ratio is a comparison of the intensities of neighboring pixels within the same object to neighboring pixels from two different objects. The boundary decision is based on comparing the ratio with a pre-defined threshold and accumulating those neighborhoods which are considered to be within a single object into one contiguous region. McKee and Aggarwal have developed a multi-pass technique (8) which processes a full video frame of data to obtain edge coordinates of very complex shapes. However, this method would be far more complex and time-consuming than necessary for determination of area and perimeter in most of our applications. Also, it is rare for more than one particle image to be found in a given focal plane.

Therefore, we have chosen to use a simplified edge detection technique based upon a comparison of the pixel intensity with a threshold adjusted for the average intensity between the particle and background (SCAN technique) and a simplified edge-tracking method (TRACK technique). Pixels at each transition across the threshold are accumulated as the edge of the particle, while pixels above the threshold are accumulated as its area.

## C. PARTICLE AREA SCAN TECHNIQUE

The particle scanning algorithm developed for this system is based on a simplified single-pass edge detection process. The surface area and edge perimeter of each particle are determined by comparing the video intensity of each pixel with a selected threshold value. The technique consists of processing a series of vertical scans which horizontally cover the image as depicted in Figure 3. The horizontal (equatorial) and vertical (polar) axes of the particle are determined by manually adjusting a vertically scanning cursor to the edges of the particle when the algorithm is first executed for each measurement. This limits the region under investigation to the immediate environment of the particle and eliminates the generally out-of-focus neighboring particles from consideration.

Beginning on the left side, the particle is scanned from top to bottom in synchronism with the television raster. The video intensity (0-255) of each pixel is compared with a threshold value corresponding to the intensity at the particle edge. If the pixel intensity is greater than the threshold, the pixel area is assigned a unit value and the column area is incremented. Otherwise, its value is zero. If the pixel area value is different from that of the last pixel, the horizontal perimeter is incremented. When the vertical scan is complete, the difference between areas of the current and previous columns is added to the vertical perimeter. The scan is then incremented to the right and the process repeated until the entire particle has been scanned. The selected scan consists of $N_r$ rows vertically and $N_c$ columns horizontally. The total area of the particle is the sum of all column areas scaled as shown in Eq. (2). Since the shape of each pixel is not square, the vertical component

must be scaled to provide an accurate measurement of the area and perimeter. Or simply,

If $V_{p(i,j)} > V_t$ then $A_{p(i,j)} = 1$

If $V_{p(i,j)} < V_t$ then $A_{p(i,j)} = 0$

$$\text{Area} = F_x * F_y * \sum_{i=1}^{N_c} \left( \sum_{j=1}^{N_r} A_p(i,j) \right) \tag{2}$$

where i and j are the pixel column and row,

$V_p$ is the video amplitude of pixel (i,j),

$V_t$ is the preselected video threshold,

$N_c$ is the number of scanned columns,

$N_r$ is the number of scanned rows,

$F_x$ is the horizontal scale factor and

$F_y$ is the vertical scale factor.

The error introduced by the quantization of area should converge toward zero and become negligible as the size of the particle increases.

The vertical component of the perimeter ($P_v$), is the difference between the number of pixels above the threshold in one column compared to the number in the previous column. The horizontal component ($P_h$), is the sum of all transitions across the threshold occurring in each column. The horizontal and vertical components are scaled by $F_x$ and $F_y$, respectively, and combined to form the particle perimeter as shown in Eq. (3). If $V_p(i,j)$ is not equal to $V_p(i,j+1)$ then the incremental horizontal component ($H_p(i,j) = 1$, otherwise $H_p(i,j) = 0$.

$$\text{Perimeter} = ( F_x * P_h ) + ( F_y * P_v ) \tag{3}$$

where $$P_h = \sum_{i=1}^{N_c} \left( \sum_{j=1}^{N_r} H_p(i,j) \right)$$

and $$P_v = \sum_{i=1}^{N_c} \left( \sum_{j=1}^{N_r} A_p(i,j) - \sum_{j=1}^{N_r} A_p(i-1,j) \right).$$

The major error in this method is highly dependent on the orientation of any edge segment with respect to the scanning axis. Although straight edges orthogonal to the scan will yield good measurements of perimeter, those same straight edges oriented diagonally to the scan axis can degrade the perimeter measurement by as much as 30% [1-SQRT (1/2)]. Therefore, a different method of determining perimeter which will be insensitive to particle orientation was required. Also, variations in the pixel intensity around the particle perimeter with respect to the threshold level increase measurement uncertainty. A dynamic threshold which can adapt to varying particle and background video intensities will improve this condition. Such a technique is implemented in an edge-tracking routine described below that provides data for determination of particle shape and orientation.

## D. PARTICLE SHAPE AND ORIENTATION

Boundary definition using direction and curvature chains have been described by Eccles et al. (9). These techniques generally describe an image boundary in terms of a one-dimensional list of angles starting from an origin on the image edge and incrementing uniformly around the boundary. Freeman has described another method for determining shape by defining critical points around the boundary (10). These points include

discontinuities in curvature, points of inflection, curvature maxima, intersections and points of tangency. Fourier transforms have been used as digital filters to smooth the digitized boundaries of planar objects. Pavlidis discusses several algorithms using Fourier transform coefficients to define detailed shape characteristics (11). Teague has developed similar shape analysis techniques using Zernike moments (12).

We have chosen a boundary chain technique to determine particle shape and orientation which is similar to the method described by Eccles (9). The edge-tracking algorithm, described below, determines the boundary between the particle and background by examining a small region of pixels along the particle edge. Edge detection is based on the intensity gradient between neighboring pixels rather than the simple threshold technique used in the particle scanning algorithm described above. As each new point along the the particle edge is determined, the tracking pattern is then centered on that point and the new neighborhood is explored. This process continues until the particle has been fully circumnavigated. A more detailed discussion is given below.

## E. PARTICLE EDGE-TRACKING TECHNIQUE

The particle edge-tracking algorithm provides the capability to classify particle size, shape and orientation for applications dealing with particle settling dynamics. The edge tracking algorithm scans across the particle edge in a series of small circular patterns where i is one of the $N_p$ scans around the particle edge and j is one of the $N_s$ points in a scan as shown in Figure 4. The point j in the scan for which the pixel intensity V(i,j) exceeds the previous pixel intensity V(i,j-1) by a threshold value $V_t$, is defined as the edge for the current scan pattern

FIGURE 4: TRACKING ALGORITHM

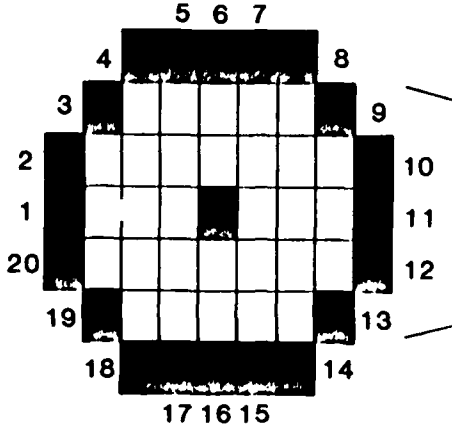


ENLARGED SCAN PATTERN

WHERE $N_s = 20$

FIGURE REPRESENTS $\frac{\Delta x}{\Delta y} = 0.75$

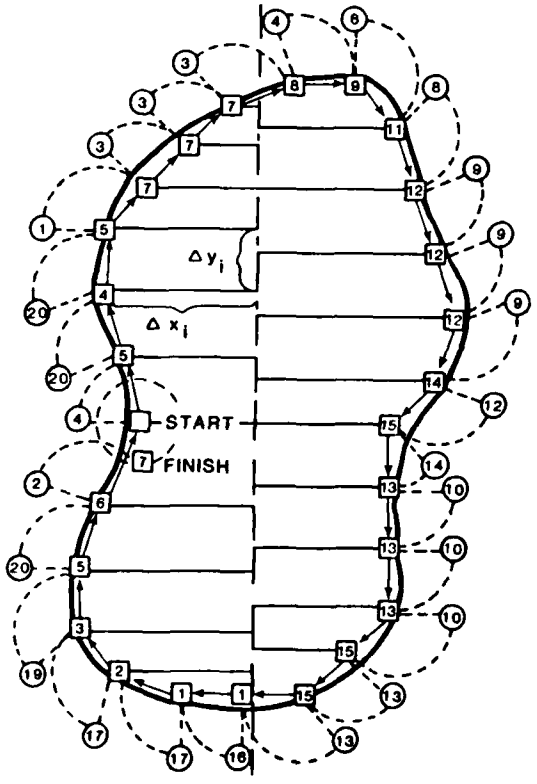


SCAN START NUMBER

SCAN END NUMBER AND ORIGIN OF NEXT SCAN PATTERN

TRACKED EDGE

PARTICLE EDGE

FOR PARTICLE WITH $N_p = 27$ PERIMETER POINTS

i and is used as the center of the next scan pattern (i+1). This process continues until the scan returns to the neighborhood of the starting point. The scan radius $R_s$, number of points per scan $N_s$, and threshold value $V_t$, can be manually selected, depending upon the particle size and shape.

The perimeter of each particle is measured by accumulating the radial distance of each threshold transition around the particle edge until the circumnavigation of the particle is complete. Since the shape of each pixel is not square, both vertical and horizontal components must be scaled accordingly, by $F_y$ and $F_x$, respectively, to provide an accurate measurement of the distance around the particle. The algorithm for this function is:

$$\text{Perimeter} = \sum_{i=1}^{N_p} \left[ \left( F_y * T_y \right)^2 + \left( F_x * T_x \right)^2 \right]^{1/2} \qquad (4)$$

where $T_y = R_s \sin$

$T_x = R_s \cos$

$R_s$ = scan radius

$N_p$ = number of threshold transition points along edge.

The area of each particle is determined by accumulating the trapezoidal area defined by each new transition as shown in Figure 4. The distance $x_i$ between the particle edge and a vertical reference line at the center of the screen is determined for each transition point and multiplied by the vertical distance $dy_i$ between two successive edges. The entire area of the particle is determined by successively adding or

subtracting each incremental area depending on the vertical direction until the particle has been completely encircled as described by:

$$\text{Area} = \left( 1/2 \sum_{i=1}^{N_p} \left( x_i + x_{i+1} \right) * dy_i * F_y / F_x \right) \qquad (5)$$

Particle identification from frame-to-frame is achieved by displaying the edge pixels of a selected particle on the next frame and comparing it to the shapes of the new particles for correlation.

## E. ALGORITHM ERROR ANALYSIS

The inherent error in the tracking process consists of radial and angular components, as shown in Figures 5 and 6, respectively. These errors are functions of the number of scan points ($N_s$), and the scan radius ($R_s$), as shown in:

$$\text{Radial error} = R_s * \left( 1 - \cos \left( 2 \pi / N_s \right) \right) / 2$$

$$\text{Angular error} = +/- \; 2 \pi / N_s \qquad (6)$$

These errors on average will produce a small positive error (e.g., 2.5% for $N_s = 20$) in determining the perimeter of a smooth boundary as shown in Eq. (7). However, the algorithm may also exhibit a negative "corner truncation" error for figures with sharp corners because of truncation produced by the discrete scan process. The difference between the actual and measured area for large, smooth particles should be small but may become negative for particles with sharp corners, Eq. (8).

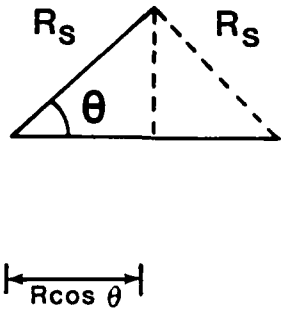


FIGURE 5 RADIAL ERROR DUE TO $\Delta\theta$ AFFECTING PERIMETER ACCURACY

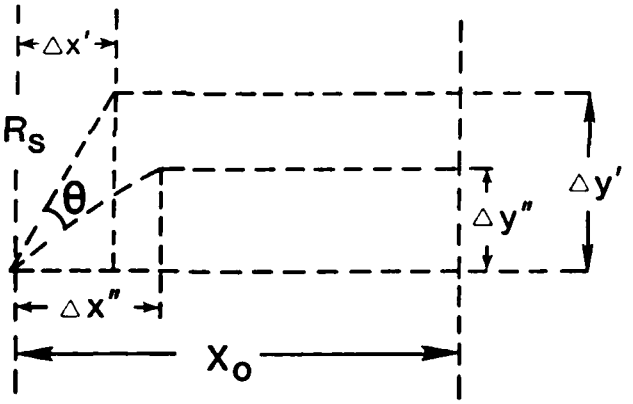


FIGURE 6 ANGULAR ERROR AFFECTING AREA ACCURACY

$$\text{Perim error} = + N_p * R_s ( 1 - \cos 2\pi / N_s ) \quad (7)$$

$$\text{Area error} = +/- ( N_p * R_s * \sin 2\pi / N_s ) / 2 \quad (8)$$

Area and perimeter measurements will also vary as a function of the video intensity threshold value for the scan mode and as a function of the video intensity gradient threshold value for the tracking mode. The video amplitude across the edge of an image with varying contrasts is shown in Figure 7. The effects due to variation of the threshold values on measurements of a high-contrast, white-on-black square (2 cm/side) are summarized in Table 2. In generating these data the video threshold intensity for the scan mode was set at values from 23% to 74% of the intensity difference between the square and the background, whereas the intensity gradient threshold (intensity difference/pixel) for the tracking algorithm was varied from 8% to 32% of the total intensity difference between the square and the background. This particular application used a negative threshold gradient (i.e., a bright-to-dark transition).

Table 2. Effects of variation of video threshold intensity (scan) and intensity gradient (track). Variation is represented by ± one standard deviation as well as the total range of deviation.

| AREA (PIXELS) | | PERIMETER (PIXELS) | |
|---|---|---|---|
| Scan | Track | Scan | Track |
| 2165.6 ± 4.0% | 2058.1 ± 1.3% | 185.6 ± 4.7% | 180.4 ± 1.7% |
| 11% Range | 4% Range | 15% Range | 5.5% Range |

The range of threshold effects is smaller for the tracking mode than the scanning mode because the maximum video intensity gradient, generally

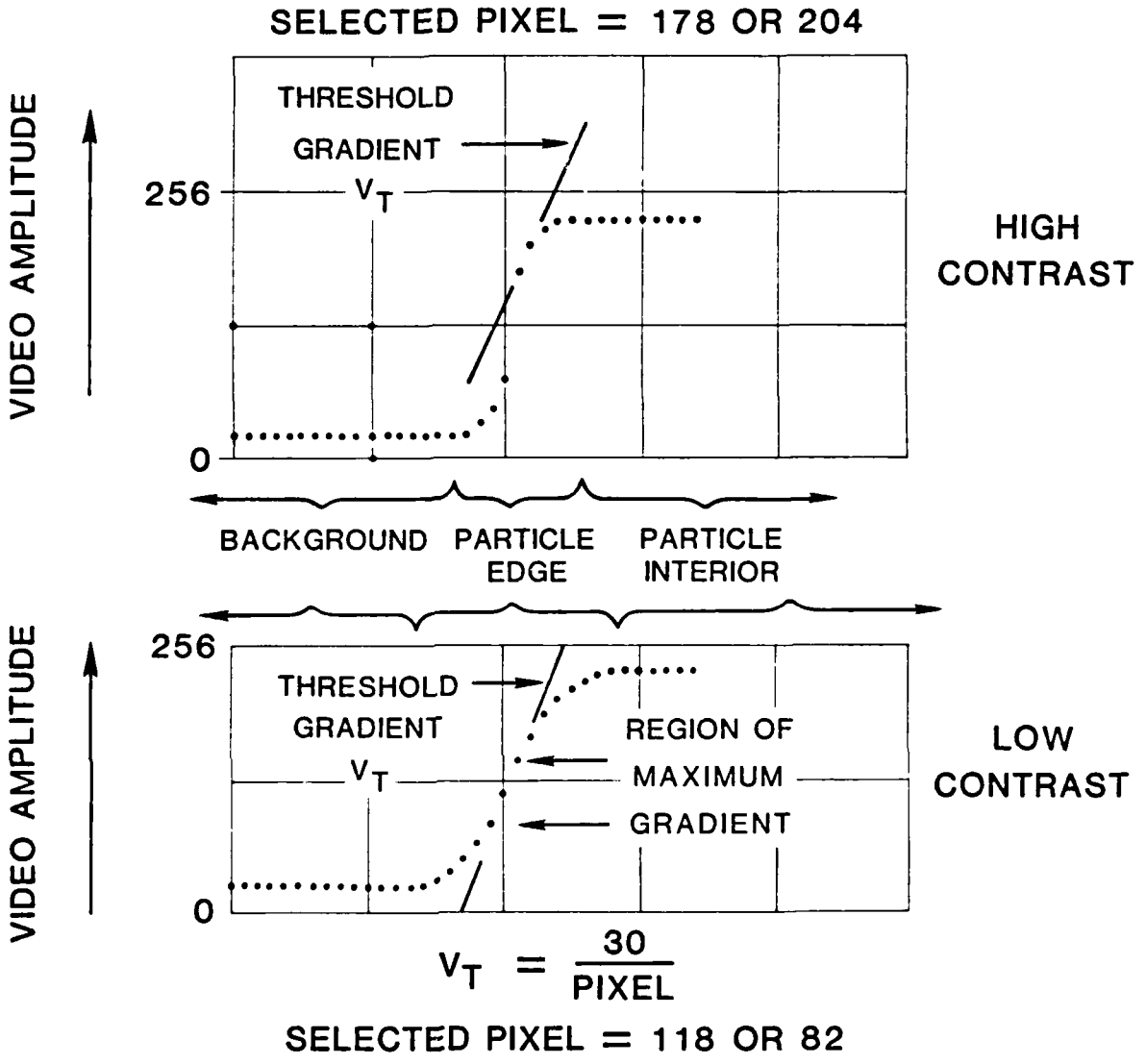


FIGURE 7 VIDEO AMPLITUDE ACROSS THE EDGE OF A HIGH CONTRAST (TOP) AND LOW CONTRAST (BOTTOM) PARTICLE

found about halfway between the intensities of the image and the background (see Fig. 7), cannot be exceeded without the algorithm "losing track" of the particle edge. The threshold intensity gradient value for the tracking program is generally selected to be smaller than the smallest normal edge gradient (bottom curve in Fig. 7) found along the particle edge. This insures that oblique approaches to the edge do not reduce the measured intensity gradient below that of the threshold. This reduced threshold value causes the tracking program for the high-contrast part of the particle (upper curve, Figure 7) to in effect underestimate the size of the particle for a white-on-black image and overestimate the size of a particle for a black-on-white image, especially for particles of varying contrast along the edges. For the white square on black background image addressed in Table 2, this resulted in particle size estimates that were ½ to 1½ pixels lower per edge transition (see upper curve in Figure 7), depending upon the video threshold intensity gradient selected, or a 1.2 to 3.6% underestimate of the length of each side. This underestimate would be offset to some extent by the radial error effect on the perimeter as described by Eq. (7).

## IV. PERFORMANCE EVALUATION

The performance of the scan and track algorithms was evaluated using white-on-black geometrical figures (square, equilateral triangle, and circle) of known size. The standards for comparison were accurate to within ½ to 1 pixel per side or to about ±2.5% for the small figures and ±1.25% for the large. The results of the comparisons are shown in Table 3. Digitization error appears to have produced a greater effect on accuracy of the small figures with complex shapes compared to the larger

ones. A digitization error of one pixel per edge can result in errors as large as ±3.6% for the small and ±2.0% for the large triangle measurements. However, this effect should approach zero as the shapes become larger and smoother.

Table 3. Perimeter and area measurement accuracies of the scanning and tracking algorithms for some standard geometrical shapes

| | | Track | | Scan | |
|---|---|---|---|---|---|
| | | Area | Perimeter | Area | Perimeter |
| Shape | Size (cm) | % Error | % Error | % Error | % Error |
| Square | 3.0 | 0.38 | -0.47 | +0.50 | +1.4 |
| Square | 2.0 | 0.98 | 0.17 | +2.89 | +3.2 |
| Triangle | 4.0 | -3.00 | -2.90 | -0.56 | 6.89 |
| Triangle | 2.2 | +3.98 | +1.83 | -0.80 | +4.23 |
| Circle | 4.0 | -0.90 | 0.62 | +3.14 | +14.45 |
| Circle | 2.2 | -0.88 | 2.97 | +0.66 | +9.36 |

% Difference

For the tracking program, most errors did not exceed the accuracy limits of the standard measurement. Digitization errors, together with the uncertainties in the standards, can account for the differences between the measured and "standard" sizes; inclusion of the potential of radial, corner-truncation, and threshold intensity/threshold intensity gradient errors insures that the maximum tracking error measured (3.98%) falls within potential error limits.

For the scan program, all of the areas measured were within expected error limits, although the triangle and circle perimeter errors were larger. The perimeter errors for the squares were quite low as the edges

of each square were aligned with the vertical and horizontal axes of the TV camera. Perimeters in the scan mode can be exaggerated by as much as $1 - \sqrt{2}/2$ for lines sloping 45° to the vertical. The largest manifestation of this "serrated edge" effect was found for the circle, with more than a +14% error.

## V. APPLICATION TO HOLOGRAMS

To demonstrate the application of the system and techniques to the analysis of in situ transmission holograms, they were utilized to re-examine holographic images of mica flakes collected during a settling experiment reported in (5). Because the mica flakes are very thin and tend to settle at some angle to the focal plane, only one side will be in sharp focus at a time. Therefore, a slightly defocused (lower contrast) image was analyzed (Figure 8). This lower contrast image is typical of the type collected from irregularly-shaped particles commonly found in seawater.

A comparison between the tracking and scanning algorithm data (Table 4) shows that the areas generated are within about 6% of each other for these mica holograms. The perimeter scanning algorithm serves best as an upward limit or check on the perimeter tracking algorithm. For example, the circular image of the third holographically recorded particle resulted in a perimeter that was 11% higher for the scanning than for the tracking algorithm. Since this was a circular particle, the scanning algorithm overestimated the perimeter by serrating the edge.

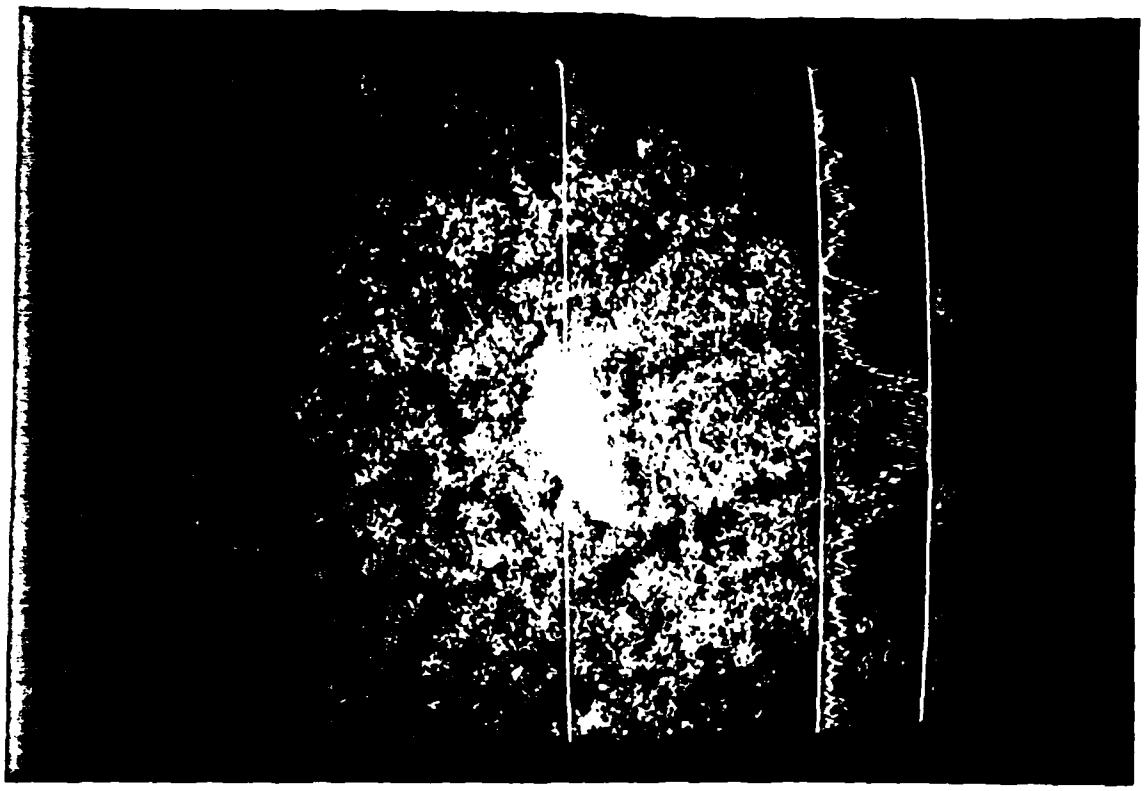

Figure 8. Photograph showing video display of reconstructed mica flake hologram. Two right-most bars are 0-256 video amplitude scale for all pixels along central bar.

Table 4. Holographic image analysis measurements of falling mica flakes using the scanning and tracking algorithms (magnification of 150X)

| ----------Scanning---------- | | | | --------Tracking--------- | | | |
|---|---|---|---|---|---|---|---|
| Sample | Area | Perim | Thresh | Area | Perim | Threshold Gradient | General Shape |
| 1 | 498 | 127 | 134 | 500 | 135 | 26 | Rectangular |
| 2 | 107 | 40 | 113 | 101 | 42 | 30 | Rectangular |
| 3 | 485 | 118 | 100 | 501 | 106 | 30 | Circular |

## VI. SUMMARY

The holographic microvelocimeter has proven to be an invaluable tool in studying the settling dynamics of particles both in the marine environment and in the laboratory. The data reduction of this tool has been semi-automated using a microcomputer to provide data base management and to control two phases of the analysis. In the first, a set of precision translation stages register different holographic frames and measure particle displacement between frames. The accuracies of this stage are on the order of ±0.0002 cm. Even greater accuracies in particle settling velocities can be achieved by adjusting the exposure interval.

The second microcomputer-controlled phase is the measurement of the size, shape and perimeter of the digitized video image of the hologram. Two techniques have been developed to measure the area and perimeter of an image. The first is a scanning algorithm which utilizes an absolute threshold of the video intensity of each pixel inside the video image. This is an extremely fast algorithm which is able to scan the area and perimeter in a single pass. It suffers in accuracy when dealing with lower contrast particles having a variable intensity in different sections, and with rounded particles since it tends to count a serrated

edge. A second technique has been developed to track the edge of an image and increment the area and perimeter utilizing an edge gradient between the background and image. Both algorithms have been tested with standard geometric images and with holographic images and are accurate to within 4-6%.

While this system has been developed to study particle settling dynamics, the techniques of image analysis could be applied to many pattern recognition and any digital image analysis problems. The edge coordinates from the tracking algorithm can be saved and further analysis of shape done using Fourier and Zernicke moments.

This effort was funded under Office of Naval Research contract N00014-75-C-0539 to the Marine Science Department, University of South Florida.

REFERENCES

1. Briones, R. A., L. O. Heflinger and R. F. Wuerker, App. Opt., 17-6, 944-950, (1978).
2. Heflinger, L. O., G. L. Stewart and C. R. Booth, App. Opt., 17-6, 951-954, (1978).
3. Carder, K. L., Opt. Eng., 18, 524-252, (1979).
4. Carder, K. L., and D. J. Meyers, SPIE, Ocean Optics, 6, 208, 151-158, (1979).
5. Doyle, L. J., K. L. Carder and R. G. Steward, J. of Sedimentary Petrology, (53), 2, (1983).
6. Carder, K. L., R. G. Steward and P. R. Betzer, J. of Geophys. Research 87, C8, 5681-5685, (1982).

7. Yakimovsky, Y., Fourth Int. Joint Conf. on Artificial Intelligence, (1974).

8. McKee, J. W., and J. K. Aggarwal, Pattern Recog., 7, 25-52, (1975).

9. Eccles, M. J., M. P. C. McQueen and D. Rosen, Pattern Recog., 9, 31-41, (1977).

10. Freeman, H., Pattern Recog. 10, 159-166, (1978).

11. Pavlidis, T., IEEE, PAMI, vol. 2, no. 4, (1980).

12. Teague, M. R., J. Opt. Soc. Am., 70-8, 920-930, (1980).

# APPENDIX THREE

Publication: Hydraulic Equivalence of Mica

Pre-publication draft: Journal of Sedimentary Petrology

# THE HYDRAULIC EQUIVALENCE OF MICA

by

Larry J. Doyle
Kendall L. Carder
Robert G. Steward

Department of Marine Science
University of South Florida
104 Seventh Avenue South
St. Petersburg, Florida 33701

ABSTRACT

Settling experiments performed on silt to fine sand sized mica flakes with a holographic micro-velocimeter revealed that mica is the hydraulic equivalent of quartz spheres having diameters a factor of 4 to 12 times smaller. Mica in the very fine to fine sand sizes has been traditionally used by sedimentologists to delineate areas of deposition or non-deposition and potential winnowing of fines, and is here found to be the hydraulic equivalent of silt sized particles but not of clay.

Experiments also showed that mica flakes tend to settle at orientations which are neither perpendicular nor parallel to the gravitational vector and to generally maintain their orientation throughout. Equations for the settling of a disc in Lerman and others (1974) and that developed by Komar and Reimers (1978) are shown to be mathematically similar for the coarse silt to fine sand ranges of discs and are adequate predictors of settling rates of mica flakes. A comparison of the hydraulic equivalency of quartz spheres to coarse silt through fine sand sized mica flakes is presented.

## INTRODUCTION

Because it cleaves into flaky particles, sand sized mica is a mineral group in which shape should obviously affect settling characteristics and, in fact, has often been considered to be the hydraulic equivalent of silt and clay. Neihesel (1965) noted the close association between sand sized mica and the clay fraction of Georgia estuaries, an association also recognized by Pamerancblum (1966) off Israel. Doyle and others (1968) used the abundance of mica in the 125-250 μm size fraction to delineate areas of the southeastern United States continental margin which might be undergoing winnowing or deposition of fines, a process which otherwise would be masked by the dominance of reworked Pleistocene sands. A similar approach was used by Adegobe and Stanley (1972) on the Niger Shelf. Doyle and others (1979) and Park and Pilkey (1981) discuss the significance of mica content to the depositional and erosional systems of the whole continental margin of the Eastern United States.

Despite its intuitive widespread use as a hydraulic analog of finer sized sediments, no quantitative evaluation of the sedimentologic characteristics of mica has yet been undertaken. The purpose of this paper is to determine as far as possible the hydraulic characteristics of mica flakes and how these characteristics compare with those predicted from settling equations in the literature.

## APPROACH

Our approach is to utilize a modified holographic micro-velocimeter developed and described by Carder (1978) and Carder and Meyers (1979).

Figure 1 shows the system used. Transmission holograms are simultaneously collected along the vertical and horizontal axes of a settling cuvette. A reference point in the cuvette is also recorded on each vertical and horizontal hologram to allow translation between the two axes. Sequential frames at accurately timed intervals (from 0.5 to 3.0 seconds depending on the particle size) record the settling velocity and orientation as well as particle size and shape. The images are reconstructed by placing the hologram back into the laser path and refocusing on particles in any of the infinite number of focal planes in the settling cuvette. This system offers the advantage of using actual sedimentary particles in the sand to clay size ranges, thus obviating any errors which may be inherent in scale modeling systems.

Mica samples were chosen from sediment cores from the Eastern United States continental slope (Doyle and others, 1979). Silt to fine sand sized mica flakes were added to a small quantity of filtered distilled water to obtain a slurry. A drop of slurry was picked up on a fine brush and the drop barely touched to the top of the miniscus of the distilled filtered water in the cuvette, thereby introducing mica flakes into the measuring apparatus. Other methods of sample introduction, including use of an eye dropper, were tried, but they tended to set up convection within the cuvette.

Resulting settling velocities were then compared with the theoretical settling rates generated from the equations of Lerman and others (1974) and Komar and Reimers (1978). In the calculations of settling rates a density for mica of 2.9 $g/cm^3$ was used, midway in the normal range for biotite and

muscovite. Examination of the mica by standard optical techniques showed that the mica fraction in the cores was composed of muscovite and a lesser amount of biotite. Finally, we compared the measured settling rates of the mica with those for quartz spheres.

## SHAPE AS A FACTOR OF GRAIN SETTLING

Shape has been recognized as an important factor in the analysis of sediments by hydraulic methods (principally settling tube) for over 100 years. Gibbs and others (1971), Lerman and others (1974), Komar and Reimers (1978) and Brezina (1979) have summarized the development of thinking concerning the hydraulic importance of shape and have contributed to the formulation of equations for settling velocity which take grain shape into account. In a series of recent articles Baba and Komar (1981 a and b) have begun to examine shape effects of various types of natural particles.

Lerman and others (1974) modified the equations for the settling of a disc of "no thickness" in the Stoke's range, developed by Lamb (1932), Payne and Pell (1960), and Brenner (1964) by adding a term for disc thickness. The resulting formulae for the two major orientations of fall are:

$$U = \frac{g(\rho_s - \rho)\, q_h r^2}{3.396\, \mu} \quad \text{(edgewise)} \qquad (1)$$

$$U = \frac{g(\rho_s - \rho)\, q_h r^2}{5.1\, \mu} \quad \text{(broadside)} \qquad (2)$$

Where: $U$ = settling speed

$r$ = disc radius

$h$ = thickness

$q_h$ = $h/r$

$\mu$ = dynamic viscosity of water

$\rho_s$ = particle density

$\rho$ = density of water

$g$ = acceleration due to gravity (981 $cm/sec^2$)

Komar and Reimers (1973) approached the effect of shape on settling velocity by scale modeling with pebbles in a glycerine settling medium, the results being equivalent to quartz sand and silt in water. They found experimentally that the Corey Shape Factor (CSF) introduced by Corey (1949), Malaika (1949), McNown and Malaika (1950), and McNown and others (1951) gave the best prediction of shape effects for the pebbles they used in their experiment. Based upon their experimental results, Komar and Reimers (1978) developed an empirical formula for settling velocity in the Stoke's range, taking into account shape effect:

$$U = \frac{1}{18\ \mu}\ \frac{1}{f(CFS)}\ (\rho_s - \rho)\ gD_n^2 \qquad (3)$$

Where: $D_n = (hD_iD_2)^{2/3}$

$D_i$ = intermediate axis particle diameter

$D_l$ = principal axis particle diameter

$CSF = h/\sqrt{D_iD_l}$

$h$ = small axis particle diameter

$f(CSF) = 0.946(CSF)^{-0.378}$ when $0.4 \leq CSF \leq 0.8$

$f(CSF) = 2.18 - 2.09(CSF)$ when $CSF \leq 0.4$

They further found that they could extend the range of the grain sizes following Stoke's settling to Reynolds numbers of up to 0.10 or for particles of up to 100 μm, and they were able to empirically extend their data to cover grain sizes up through pebbles.

For particles like mica where h is small relative to $D_i$ and $D_l$, CSF is $\leq 0.4$ and the general equation (3) becomes:

$$U = (1/18\ \mu)\ \frac{1}{[2.18 - 2.09\ (h/\sqrt{D_iD_l})]}\ (\rho_s - \rho)\ g(hD_iD_l)^{2/3} \qquad (4)$$

The particle thickness h may be expressed as a ratio with respect to D, i.e., D/100, D/50, D/25 .... $D/_\chi$ and therefore in the ranges in which we are working, the equations of Lerman and others (1973) and equation (3) are similar. For example, let $D_i = D_l = \overline{D}$, $\chi = \frac{\overline{D}}{h} = \frac{2r}{h}$, and $\eta_h = \frac{h}{r}$.

Then equation (4) becomes:

$$U = \frac{1}{18\mu} \frac{1}{(2.18 - 2.09 \frac{1}{\chi})} (\rho_s - \rho) g (\frac{\overline{D}}{\chi})^{2/3}$$

$$U = \frac{1}{(2.18 - 2.09 \frac{1}{\chi}) \chi^{2/3}} \underbrace{\frac{1}{18\mu} (\rho_s - \rho) g\overline{D}^2}_{\text{Stokes Formula}} \qquad (5)$$

Our measurements of h for mica flakes yielded a range of h ≈ 0.007D - 0.05 D. For $\chi = \overline{D}/h = \frac{1}{0.01} = 100$, and substituting in (5), we obtain:

$$U = 0.021 \frac{1}{18\mu} (\rho_s - \rho) g\overline{D}^2$$

Lerman's formulae are of the general form

$$U = \frac{g(\rho_s - \rho) q_h r^2}{c\mu}$$

where c = 3.396 to 5.1. Substituting as before we obtain

$$U = \frac{g(\rho_s - \rho) D^2}{2c\mu\chi}$$

Multiplying by 18/18 yields

$$U = \frac{18}{2c\chi} \underbrace{\frac{1}{18\mu} (\rho_s - \rho) gD^2}_{\text{Stokes Formula}}$$

For Lerman's formula to be equivalent to Komar and Reimers at $\chi = 100$ we can set

$$\frac{18}{2c\chi} = 0.021$$

$$c = \frac{18}{2(100)\ (0.021)}$$

$$c = 4.28$$

This value lies between Lerman's two values of 3.396 and 5.1 and therefore values derived from the two sets of formulae will be close to each other over the ranges we are examining.

Assuming $D_i = D_l = \bar{D}$ (where $\bar{D}$ is an average diameter) is an idealized case which all mica flakes do not meet. Any deviation from $D_i = D_l$ will obviously cause some deviation in the calculation of $\mu$. When $D_i = D_l$, the parameter $\chi = D/h$ becomes the shape parameter directly related to the Corey shape factor.

## THE HYDRAULIC EQUIVALENCY OF MICA

In our experiments mica flakes seldom settled either exactly broadside or edgewise. They usually assumed an orientation between the two extremes, neither perpendicular nor parallel to the gravitational vector which they maintained throughout. Stringham, et al (1969) also showed that particles settling at low Reynolds numbers maintain their initial orientation which need not be perpendicular to the settling direction.

Figure 2 shows the experimentally determined settling velocities of mica flakes plotted on the family of curves of Lerman and others (1974) and Komar and Reimers (1978) for thicknesses of D/200, D/50, D/20, and D/10. Komar and Reimers (1978) equation begins to diverge from those of Lerman (1974) only at thicknesses of D/20 and greater. The thickness/D ratios of 32 mica grains from a split of the slope sediment used for the settling velocity experiment were determined by scattering some quartz beach sand on an SEM stub and then sprinkling the mica-rich slope sample over it. Some of the mica flakes landed on edge and we were thus able to measure thickness to D ratios. Thicknesses ranged from 0.7% of D to 5% of D, with the average at 2%; and a standard deviation of 1.15%. Figure 2 also shows that most of the velocities of mica flakes which we measured fall within the envelope created by the theoretical curves. Scatter at the coarser end is probably mostly due to variation in thickness, symmetry (e.g., $D_i \neq D_i$) and in settling orientation, due to the fact that some particles in this size range are beginning to exceed the Stoke's low Reynolds number constraint on the Stokes equation.

At the coarser end of the scale, particles fall closer to Lerman and others (1974) equations than to Komar and Reimers (1978). Figure 3 shows the diameter of spherical quartz particles of density of 2.65 which would settle at rates of the variously sized mica flakes determined from Lerman and others (1974) equations for h = D/200, D/50 and D/20. Our experiments show that mica ranging in diameter from 62 μm to 250 μm, with a thickness of no more than 5% of the sieve diameter, is the hydraulic equivalent of 5 μm to 82 μm quartz spheres. Very fine, sand sized mica, then, is the hydraulic equivalent of silt sized quartz spheres while fine sand sized mica is the equivalent of silt to very fine sand sized spheres. Coarse silt size mica flakes are the equivalent of fine, and very fine quartz silts.

## CONCLUSIONS

1. The equations for determining settling velocity of a disc presented by Lerman and others (1974) and that developed by Komar and Reimers (1978) for particles where the Corey Shape Factor $\leq 0.4$ are similar for thicknesses of D/50 or less.

2. Experiments on fine sand to coarse silt sized mica flakes using a holographic micro-velocimeter showed that grains most often do not orient themselves perpendicular to the flow field as they settle but that they tend to settle at some orientation between broadside and edgewise.

3. Mica in the coarse silt, very fine sand, and fine sand sizes is the hydraulic equivalent of silt and very fine sand sized quartz spheres

according to the relationships shown in Figures 2 and 3.

Contrary to previous assumptions, mica in the coarse silt to fine sand sizes is not the hydraulic equivalent of clay.

ACKNOWLEDGMENTS

This research was partially supported under Office of Navel Research Contract No. N00014-75-C-0539. Gregg Brooks and Robert Byrne critically reviewed some of the manuscript. The authors wish to acknowledge the especially thorough review of Paul Komar who pointed out a more elegant comparison between Komar and Reimers and Lerman's equations than we had originally presented and which we have incorporated into this paper.

## REFERENCES CITED

Adegobe, O. S. and D. J. Stanley. 1972. Mica and shell as indicators of energy level and depositional regime on the Nigerian shelf. Mar. Geol. 13: M61-66.

Baba, J. and P. D. Komar. 1981. Settling velocities of irregular grains at low Reynolds numbers. Jour. Sed. Pet. 51: 121-128.

_____. 1981. Measurements and analysis of settling velocities of natural quartz sand grains. Jour. Sed. Pet. 51: 631-640.

Brenner, H. 1964. The Stokes' resistance of a slightly deformed sphere. Chem. Eng. Sci. 19: 519-539.

Brezina, J. 1979. Particle size and settling rate distributions of sand-sized materials. 2nd European Symposium on Particle Characterization, Nurnberg, September 24-26, 1979, 44 pp.

Carder, K. L. 1978. A holographic micro-velocimeter for use in studying ocean particle dynamics. SPIE Vol. 160 Ocean Optics V: 63-66.

_____ and D. J. Meyers. 1979. New optical techniques for particle studies in the bottom boundary layer. SPIE Vol. 208 Ocean Optics VI: 151-158.

Corey, A. T. 1949. Influence of shape on the fall velocity of sand grains. Unpublished M.S. Thesis, Colorado A&M College. 102 pp.

Doyle, L. J., W. J. Cleary and O. H. Pilkey. 1968. Mica: its use in determining shelf-depositional regimes. Mar. Geol. 6: 381-389.

Doyle, L. J., O. H. Pilkey, and C. C. Woo. 1979. Sedimentation on the Eastern United States continental slope. In Doyle and Pilkey (eds.), Geology of Continental Slopes, SEPM Spec. Pub. no. 27, p. 119-129.

Gibbs, R. J., M. D. Matthews, and D. A. Link. 1971. The relationship between sphere size and settling velocity. Jour. Sed. Pet. 41(1): 7-18.

Komar, P. D. and C. E. Reimers. 1978. Grain shape effects on settling rates. Jour. of Geol. 86: 193-209.

Lamb, H. 1932 (1945). Hydrodynamics, 6th Edition. Dover, New York.

Lerman, A., D. Lal, and M. F. Dacey. 1974. Stokes' settling and chemical reactivity of suspended particles in natural waters, p. 17-47. In R. J. Gibbs (ed.), Suspended solids in water, Plenum Press, New York.

Malaika, J. 1949. Effect of shape of particles on their settling velocity. Ph.D. Dissertation, State University of Iowa. 64 pp.

McNown, J. S. and J. Malaika. 1950. Effects of particle shape on settling velocity at low Reynolds numbers. Trans. Amer. Geophys. Union 31: M74-82.

_____, _____, and H. Pramanik. 1951. Particle shape and settling velocity. Proc. Intern. Assoc. Hydr. Res., 4th Meeting, Bombay, India, p. 511-522.

Neiheisel. J. 1965. Source and distribution of sediments at Brunswick Harbor and vicinity Georgia. U.S. Army Coastal Engineering Res. Center, Tech. Mem. 12: 21 pp.

Pamerancblum, M. 1966. The distribution of heavy minerals and their hydraulic equivalents in sediments of the Mediterranean continental shelf off Israel. Jour. Sed. Pet. 36: 162-174.

Payne, L. E. and W. H. Pell. 1960. The Stokes' flow problem for a class of axially symmetric bodies. Jour. Fluid Mech. 7: 529-549.

Park, Y. A. and O. H. Pilkey. 1981. Detrital mica: environmental significance of roundness and grain surface textures. Jour. Sed. Pet. 51: 113-120.

Stringham, G. E., D. B. Simons and H. P. Guy. 1969. The behavior of large particles falling in quiescent liquids. U.S. Geological Survey Professional Paper 562-C, 36 pp.

## FIGURE CAPTIONS

Figure 1. Holographic micro-velocimeter set up used to measure the settling velocity of the mica flakes.

Figure 2. Lerman and others (1974) equations for the settling of discs both broadside and edgewise plotted along with that of Komar and Reimers (1978) for thickness of D/200, D/50, D/20, D/10. Note that the equations yield values which are very close to each other at thicknesses of D/50 or less, thicknesses most prevalent for mica flakes. X's are values of mica flakes we measured.

Figure 3. The hydraulic equivalency of mica to quartz spheres. Mica sizes are coarse silt to fine sand and thicknesses are D/200, D/50, D/20.

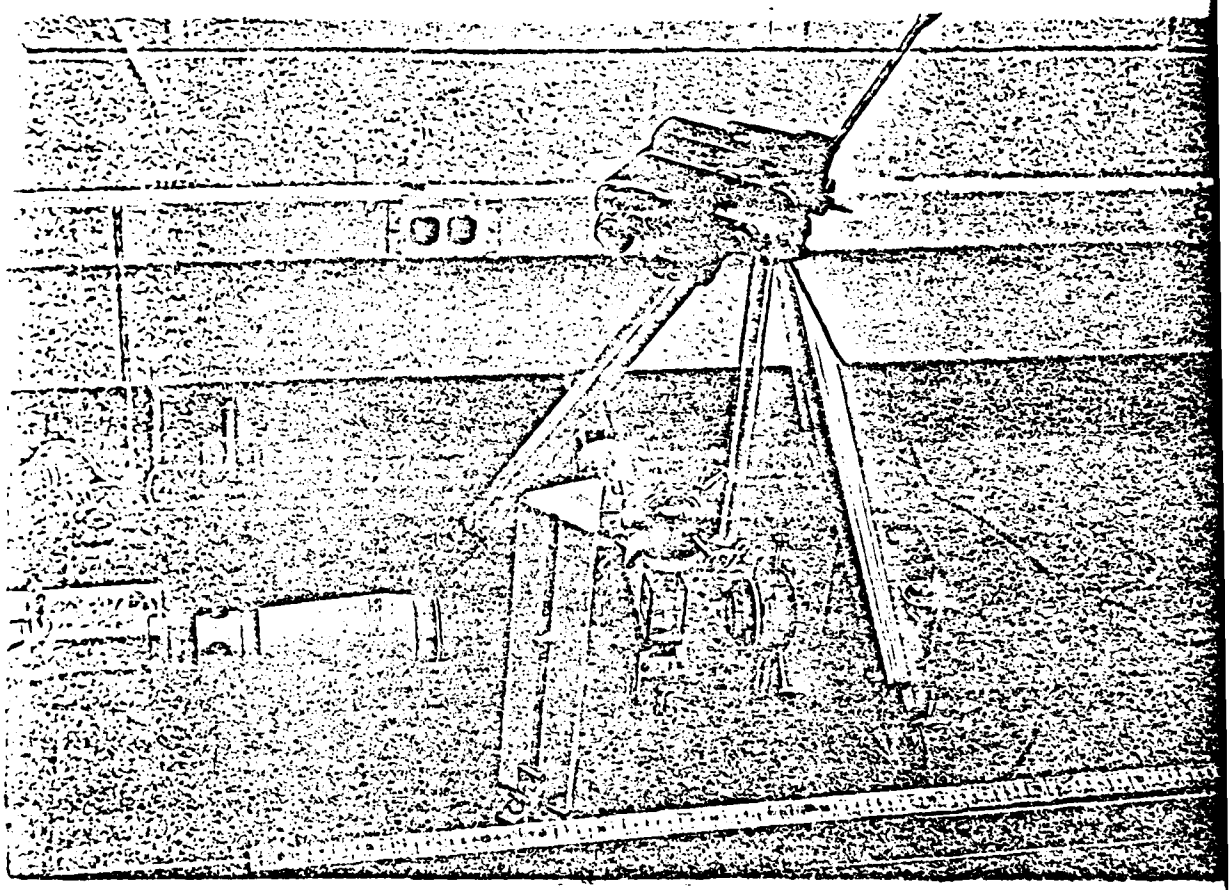

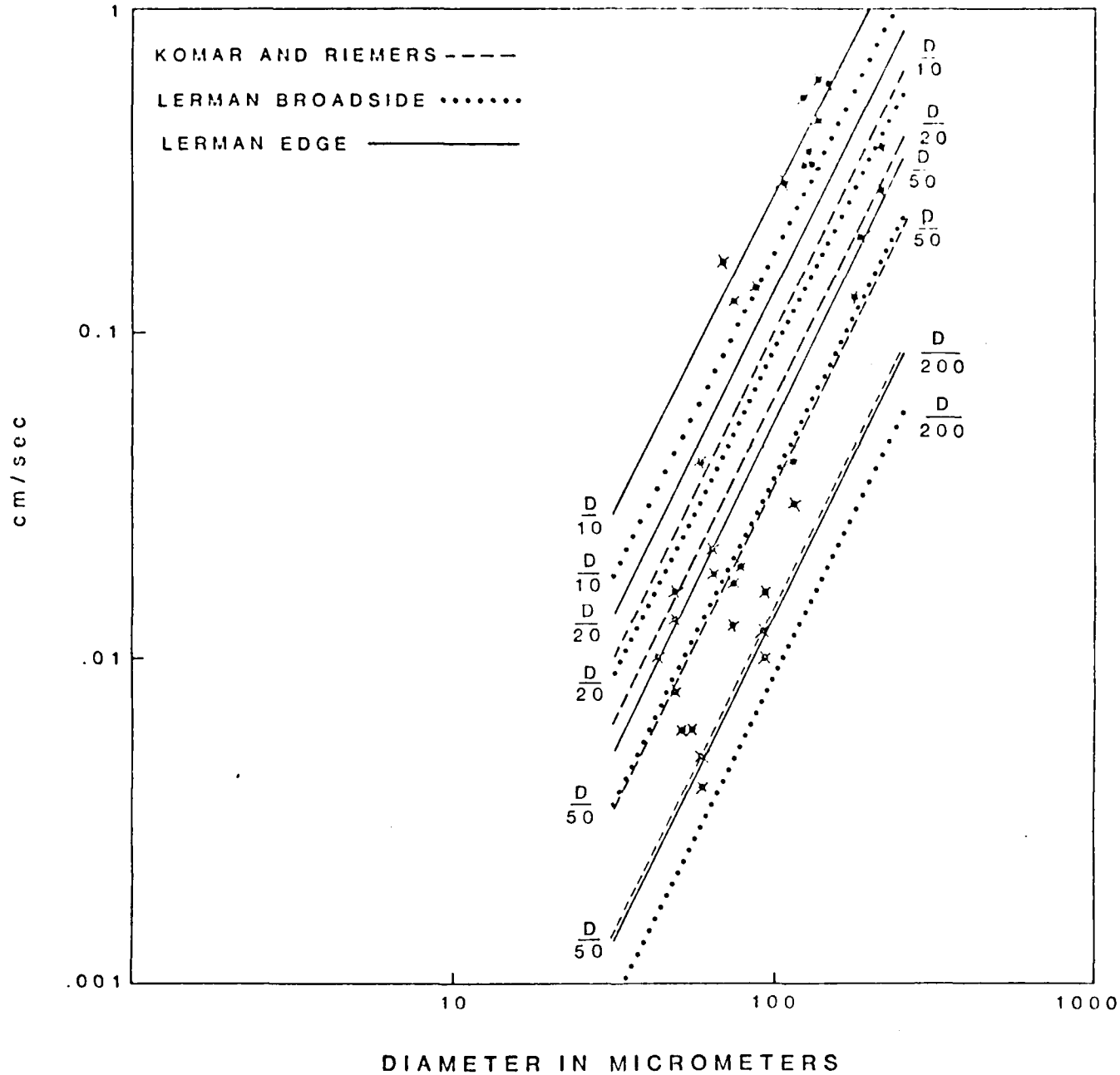
KOMAR AND RIEMERS
LERMAN BROADSIDE
LERMAN EDGE
1
0.1
.01
.001
cm/sec
10
100
1000
DIAMETER IN MICROMETERS
D/10
D/20
D/50
D/200

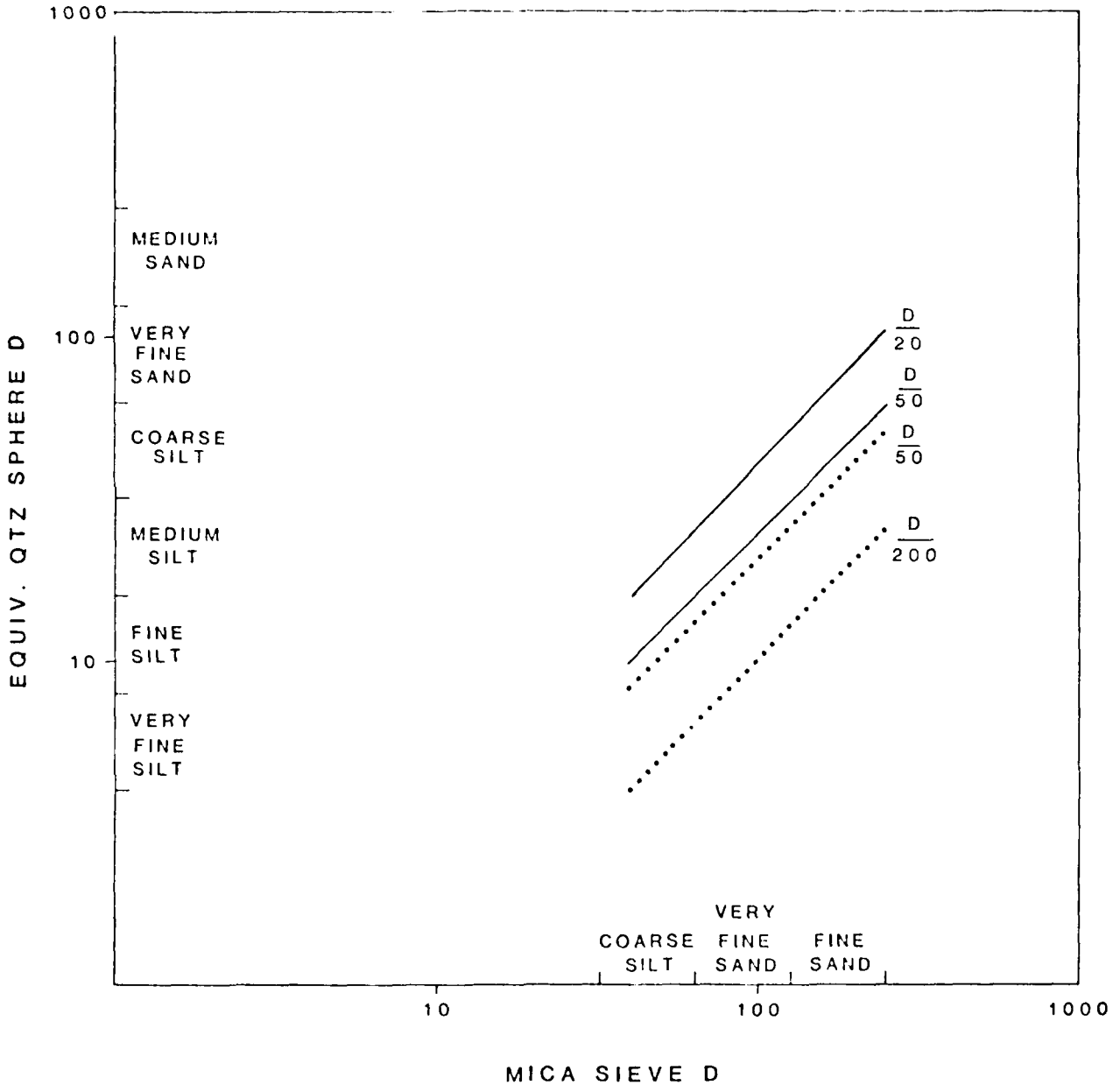
1000
100
10
EQUIV. QTZ SPHERE D
MEDIUM SAND
VERY FINE SAND
COARSE SILT
MEDIUM SILT
FINE SILT
VERY FINE SILT
D/20
D/50
D/50
D/200
COARSE SILT
VERY FINE SAND
FINE SAND
10
100
1000
MICA SIEVE D

APPENDIX FOUR

JOURNAL OF GEOPHYSICAL RESEARCH, VOL. 87, NO. C8, PAGES 5681–5685, JULY 20, 1982

# In Situ Holographic Measurements of the Sizes and Settling Rates of Oceanic Particulates

KENDALL L. CARDER,[1] ROBERT G. STEWARD, AND PETER R. BETZER

*Department of Marine Science, University of South Florida, St. Petersburg, Florida 33701*

A free-floating sediment trap equipped with a holographic particle velocimeter (HPV) was deployed for 14.4 hours at a depth of 30 m in the western North Atlantic Ocean. The system recorded the in situ sizes, shapes, orientations, and settling rates of microscopic particles moving through the laser beam. The primary data reduction revealed particles from the system's lower limit of resolution, 15 micrometers in diameter, to 250 micrometers in diameter with settling velocities ranging from 0.0190 to 0.2302 cm s (16–198 m day). Individual particle densities, calculated from a modified Stokes equation, ranged from 1.37 to 5.10 g ml. The presence of high density particles was independently corroborated through individual particle analysis of the trapped material with a computer-controlled, scanning electron microscope equipped with an energy dispersive X-ray analyzer. In the future, in situ holographic systems might be used to further our understanding of primary productivity, sediment erosion deposition, and particle aggregation disruption dissolution.

## INTRODUCTION

Size, shape, and density are key variables controlling the settling dynamics and fate of marine particulate matter. The classical method of determining size and shape is to collect suspended particulate matter with a device such as a Niskin bottle [*Gordon*, 1970] or sediment trap and then concentrate the particles onto a membrane filter or in a settling chamber for microscopic analysis. The universal problem with this approach is determining the degree to which the size distribution and shapes have been altered by the collection and concentration sequences. *Fournier* [1978] and *Trent et al.* [1978] have shown that sample handling can cause particle disruption. *Bishop and Edmond* [1976] and *Bishop* [1977] have used a high volume in situ pump to isolate microscopic oceanic suspended material, but even with this well-engineered system there is a possibility that friable material will not maintain its integrity through the separation process. There is considerable advantage in using passive in situ systems to characterize settling particles, as the above uncertainties are obviated.

## PURPOSE

A holographic particle velocimeter (HPV) has been developed in our laboratory that measures size, shape, and settling velocity of individual particles [*Carder*, 1979; *Carder and Meyers*, 1979]. The laboratory version of this device has been modified for use in a free-floating sediment trap for in situ studies. The purpose of this report is to describe the holographic device and present some results from what are believed to be the first in situ settling measurements of individual, microscopic, and oceanic particles.

## THEORY

The technique is an application of far-field or Fraunhoffer holography [*Thompson et al.*, 1967]. The in-line hologram is a record of the interference between the far-field diffraction patterns scattered by the particle and the collinear background [*Cartwright et al.*, 1980; *Thompson et al.*, 1967]. Each hologram provides a permanent record of the three dimensional position and geometric cross section of all particles in the laser-illuminated sample volume (3.27 ml) (Figure 1).

The laboratory HPV was modified three ways for use at sea. First, the spatial filter was removed since its critical alignment might not have withstood the stresses associated with deployment and recovery of the sediment trap array. Second, the imaging lens was changed from 50 to 72 mm focal length. Finally, the 1 mW HeNe laser was upgraded to 2 mW. The last two modifications were effected to optimize the device for faster settling particles. That is, with reduced magnification a larger sample field was recorded and with increased laser intensity a shutter speed fast enough to stop particle motion on film was achieved. To dampen all motion other than that due to gravitational settling, the sample volume was isolated in a 30-cm tall settling chamber (Figure 1). The 4.5 × 4.5 cm square chamber contained two sets of flow dampers, one 5 cm long and the other 10 cm. Each of the sets consisted of about 50 juxtaposed cylinders, each 0.5 cm in diameter.

The in situ HPV was remotely controlled with a digital timer programed to trigger exposures at 7, 7.5, 9.0, and 13.5 s after starting the laser. The time between exposures, the number of exposures sequence, and the number of sequences hour were programable variables. With the present film pack, the system can collect up to 250 exposures.

## EXPERIMENT

The HPV-equipped sediment trap collected for 14.4 hours starting from 1900 June 19, 1980, at a site (26 N, 96 W) about 60 nautical miles east of the Bahamas. The components depicted in Figure 1 were mounted in the main cylinder (46 cm in diameter) of the trap itself. The trap was located at 30 m depth on a free-floating array composed of four parts connected by polyethylene-sheathed, steel cable (Figure 2). In ascending order, these were (1) the sediment trap with stainless steel protective cage, (2) a set of three subsurface floats starting 5 m above the trap, (3) a set of three surface floats, and (4) a surface marker buoy equipped with a strobe light and radar reflector. To dampen wave-induced vertical motion, multiple strands of shock cord (1.0 cm diameter) were strung between each of the floats.

NOAA scuba divers were unable to detect any motion or

[1] Now on sabbatical at Office of Space and Terrestrial Applications, NASA, Washington, D.C. 20546.



Paper number 2C0391
0148-0227/82/002C-0391$5.00

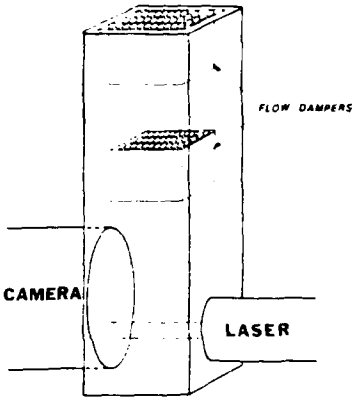


Fig. 1. An unscaled schematic diagram of the in situ holographic particle velocimeter (HPV) components that were housed in the sediment trap. The square settling tube was open only at the top and had two sets of flow dampers to minimize water motion in the sampling path.

harmonic vibrations in the array just prior to its recovery. Neither was any trap-induced vertical motion detected with the holographic records. That is, the variation in settling velocity per particle was less than that due to the precision of successive frame registration (± 2 μm). This work was conducted under moderate sea conditions (wave heights of 0.5–1 m and winds less than 10 knots). Additional testing of this array is required to learn if it can minimize vertical motion of the trap under severe surface conditions.

## METHODS

Upon recovery of the trap, the holographic film was developed, and the particulate matter from the bottom chamber of the trap was concentrated onto pre-tared, 0.45 μm pore diameter, membrane filters. To determine the total mass flux m$^{-2}$ day, the filters were weighed at our shore-based laboratory. In addition, portions of the pads were analyzed by a computer-controlled, scanning electron microscope equipped with an energy dispersive X-ray analyzer at the State University of New York Syracuse (D. L. Johnson).

The holographic data were also analyzed at our shore-based facilities. Data reduction was performed manually by reconstructing the holographic images onto a white screen at 200 × magnification and measuring the particle dimensions and displacement between frame with a vernier micrometer (± 5 μm). The density of each particle was calculated based on the settling velocity and volume estimated from the two-dimensional image.

The accuracy and precision of the data reduction techniques were tested in two laboratory settling experiments using the same holographic components as deployed in the field. The experiments were conducted with presized (20–45 μm) calcite and sphalerite grains. Two methods of estimating the particle volume were compared. The first used the average of several measured dimensions from the projected cross-sectional image as the spherical equivalent diameter in the standard Stokes settling equation for spheres [*Lerman et al.*, 1974]. The second used the appropriate measured dimensions of the particle as the major and minor axes of a spheroid. These axes were each used as the rotational axis to approximate oblate and prolate spheroids. By assuming the polar axis was either parallel to or perpendicular to the gravitational axis, two densities each were calculated by using equations in *Lerman et al.* [1974].

Compared with the published values for each mineral [*Hurlbut*, 1971], the spherical approximation gave the most consistent density: 2.49 ± 0.22 calculated versus 2.72 g ml published for calcite and 3.66 ± 0.10 calculated versus 4.0 ± 0.10 g published for sphalerite. In both cases, the spherically derived densities were within 10% of the published values. Pycnometer determinations on the same samples gave 2.63 ± 0.22 g ml for calcite and 4.15 ± 0.22 for sphalerite. Occasionally, individual spheroidally derived densities were much closer to the published values, but the variation in the measurements was quite high (as much as 300%) reflecting the inability to measure the third dimension with a single laser system. The spherically derived densities with a potential error of about 10% seem adequate for this initial attempt at quantifying these properties in situ.

## RESULTS

The primary data on each hologram is a particle size distribution of all the particles in the sample volume. Figure 3 is included as an example of such data. The 30 particles depicted in this figure represent all particles in excess of 15 μm that were recorded and reconstructed from a single hologram. At present, it is not feasible to integrate such a small time increment to get an estimate of mass flux. Under developement is a semi-automated data reduction system that will facilitate the generation of a sufficient amount of optical data to permit estimation of the mass flux. Through gravimetric analysis of the collected material, the mass flux at 30 m was estimated to be 149 mg m$^{-2}$ day.

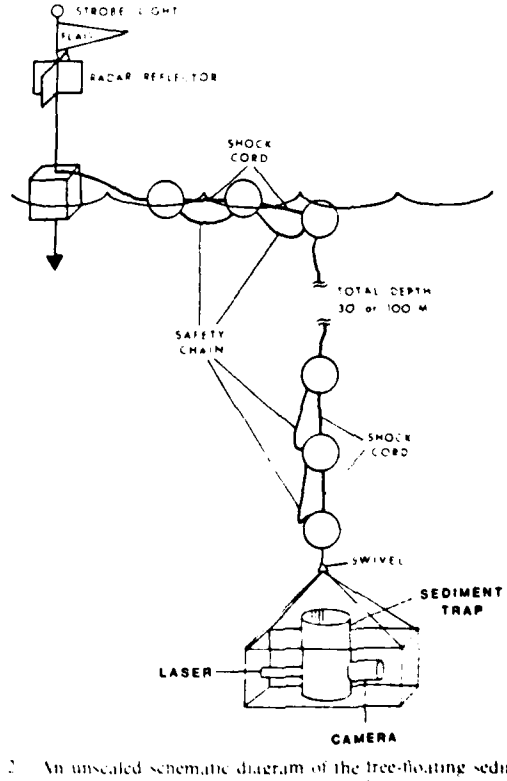


Fig. 2. An unscaled schematic diagram of the free-floating sediment trap array containing the HPV.

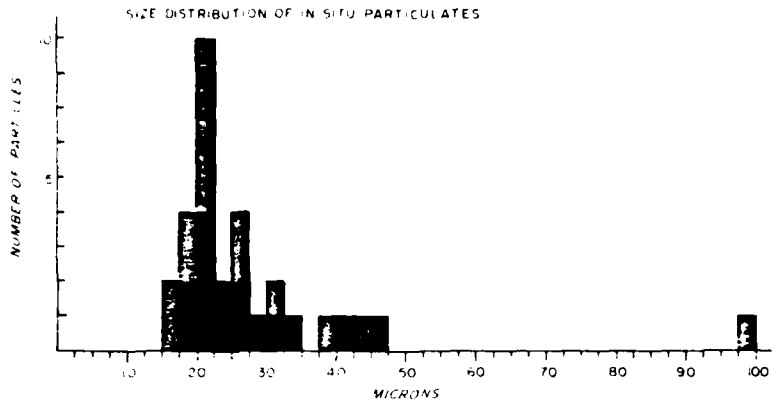


Fig. 3. A mean diameter frequency histogram of particles larger than 15 microns from a single in situ hologram of a 3.27 ml volume of water measured on June 19, 1980, in the western Atlantic Ocean.

The termination of the size distribution at 15 μm diameter was dictated by the resolution of the in situ system as it lacked a spatial filter and had lower magnification. SEM EDXA analysis of the trapped material revealed that 93% of the sample mass was contributed by particles whose diameter exceeded 16 μm. While there would be obvious advantages in extending the resolution of the system to smaller sizes, the present configuration accounted for the bulk of particles which contributed significantly to the mass flux at this oceanic site.

Some of the faster settling particles were selected to show the range of sizes, settling velocities, and densities found during this in situ experiment (Table 1). The velocities ranged from 0.0190 to 0.2300 cm/s or daily excursions from 16 to 199 m. Density calculations for these same materials ranged from 1.37 to 5.10 g/ml. Figures 4*a*–4*c* are photographs of the reconstructed holographic images of three particles from Table 1 having densities of 4.10, 2.90, and 1.37 g/ml, respectively. Figure 4*d* was from a deployment of the HPV-sediment trap to 100 m near the same site 2 days later. This thin-walled sphere, tentatively labeled an invertebrate egg case, was included as an example of one of the most unusual particles recorded during the experiment.

## Discussion

The results show that it is possible to capture in situ the holographic images of microscopic marine particles and use them to measure their individual sizes, shapes, settling velocities, and orientations. As far as we can determine, these are the first in situ measurements of these variables. Although there are many possible improvements, the success of this experiment should spark the application of this technique to a variety of fundamental oceanographic research problems including primary productivity, sediment erosion deposition, and particle aggregation disruption dissolution. A distinct advantage of the system described herein is the ease with which it can be altered to study selected particle size and density ranges. Magnification can be controlled by the imaging lens, and the exposure frequency can be programed to capture either slowly or rapidly settling particles.

One of the more interesting aspects of this study was the density approximations for some of the particles noted at this location. Three of the 11 listed in Table 1 had densities in excess of 4.0 g/ml, considerably higher than one would predict from a knowledge of typical oceanic suspended particulate matter that includes carbonates, clay, amorphous silica, quartz, and organics. As this is a new technique, independent verification of these results was sought by using a scanning electron microscope equipped with an energy dispersive X-ray analyzer and image analysis system. This measured particle sizes and collected X-ray data for 21 elements on a particle-by-particle basis from the trapped material on a portion of the filter pad.

Of the 872 particles examined, 39 (4%) were titanium-rich, 98 (11%) were iron-rich, and another 87 (10%) exhibited an X-ray

TABLE 1. Individual Suspended Particulate Size and Settling Velocity From a Holographic Particle Velocimeter-Sediment Trap Deployed During the Night of June 19, 1980

| Part Number | Maximum, $\mu m^{-1}$ | Minimum, $\mu m^{-1}$ | Average Diameter, $\mu m^{-1}$ | Settling Velocity, cm/s | Spherical-Equivalent Density, g/ml |
|---|---|---|---|---|---|
| 1 | 30 | 16 | 23 | 0.1096 | 4.10 |
| 2 | 28 | 12 | 20 | 0.0776 | 4.16 |
| 3 | 21 | 18 | 20 | 0.1010 | 5.10 |
| 4 | 40 | 29 | 34 | 0.0404 | 1.59 |
| 5 | 29 | 09 | 19 | 0.0570 | 3.52 |
| 6 | 31 | 17 | 24 | 0.0670 | 2.90 |
| 7 | 22 | 12 | 17 | 0.0212 | 2.21 |
| 8 | 24 | 23 | 24 | 0.0660 | 2.99 |
| 9 | 23 | 19 | 21 | 0.0193 | 1.79 |
| 10 | 41 | 10 | 26 | 0.0486 | 2.19 |
| 11 | 119 | 87 | 103 | 0.2302 | 1.37 |

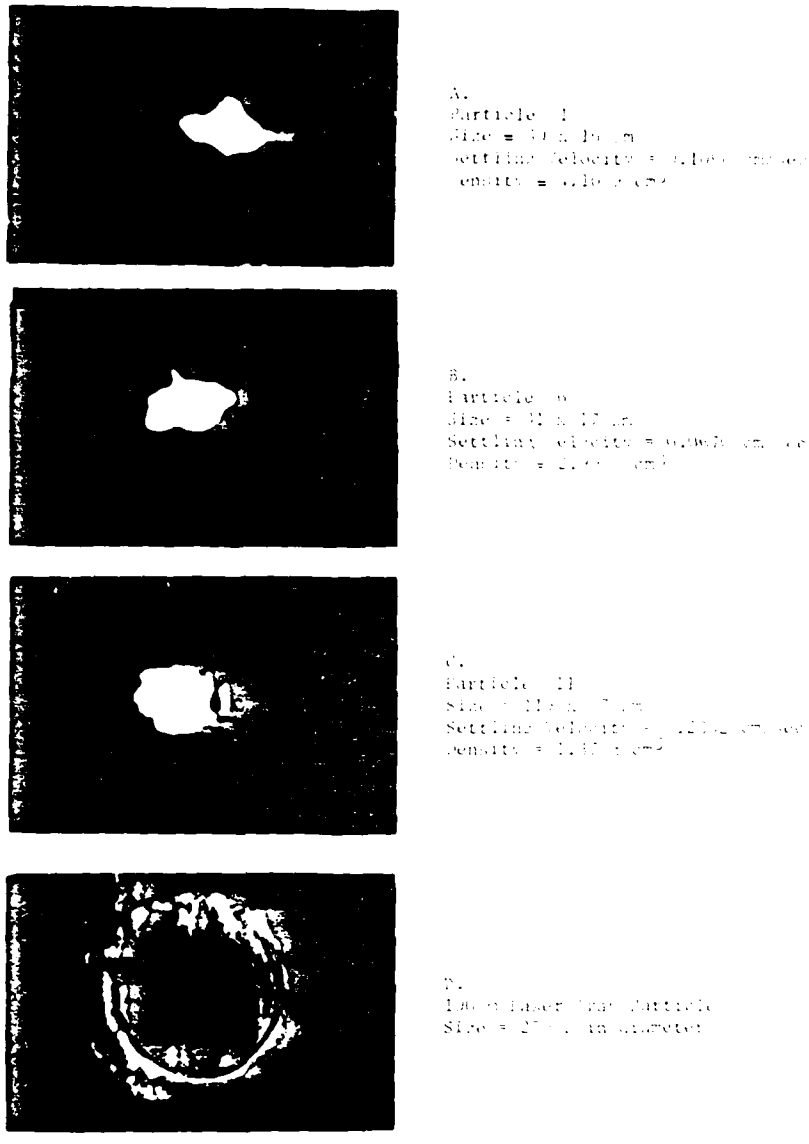

Fig. 4. Photographs of the reconstructed holographic images of three particles listed in Table 1 and one large spherical particle collected during a later experiment at the same site. All particles are oriented with the gravitational vector pointing toward the bottom of the page.

spectrum totally (greater than 95%) made up of iron. Thus, 25% (by number) of the particles were dominated by elements normally associated with high density minerals, (e.g., rutile, ilmenite, and hematite). Furthermore, the elemental distributions of these particles were distinct from the metallic structural components of the sediment trap (the stainless-steel cage and galvanized chain). Although, we cannot completely rule out contamination, the above evidence suggests that we captured high density materials settling through the upper layers of the ocean from sources other than the trap or ship. As three eruptions of Mt. St. Helens volcano occurred within a month of the cruise (the last within 2 days of the sampling), we cannot rule out the possibility that it provided some eolian inputs to these samples.

In addition, the particle-by-particle data were examined to see whether the dimensions of the high density particles noted holographically were consistent with those measured by the SEM EDXA system. Several titanium and iron-rich particles were found microscopically to have dimensions essentially coincident (within 2 $\mu$m each of the major and minor axes) with the high density particles reported in Table 1. Thus, not only do the compositional characteristics that, when translated to oxides found in sediments ($TiO_2$, $FeTiO_3$, $FeO$) match the holographically determined densities, but the actual dimensions of the high density particles recorded by the laser are the same as several recorded by the scanning electron microscope. On the basis of this corroboration and the results of our own laboratory calibrations, the density approximations made with the in situ HPV are reasonably accurate.

The calibration experiments demonstrated the importance to the spheroidal settling equation of the proper settling orientation and of the proper rotation of a two-dimensional image to

calculations of a three-dimensional volume. The HPV simultaneously records the actual settling direction and orientation, plus the cross-sectional shape of each particle in the sample field. However, this single laser system does not allow definition of an axis of rotation needed to calculate particle volumes (mass). Despite this limitation, the spherical equivalent densities determined for two standard materials were within 10% of accepted values. Thus, it should provide similar accuracies for most compact particles (e.g., dimensions varying by less than a factor of 2).

On the basis of shape, size, settling velocity, particle 11 (Table 1 and Figure 4c) has been tentatively labeled as a fecal pellet. The estimated density, 1.37 g ml, is consistent with wet, compact organic matter. Despite its low density, the size of this particle was large enough to give it the highest settling velocity measured (0.230 cm s). Such a speed is close to the lower end of the range reported for fecal material from the equatorial Atlantic [*Bishop et al.*, 1977]. On the basis of this estimated rate of descent, the particle would have moved though the euphotic zone in less than a day. This underscores the potential that in situ systems have in addressing biological removal processes that may exert primary control over mass flux in both shallow and deep ocean waters [*Lerman et al.*, 1977; *Smayda*, 1971; *Wiebe et al.*, 1976; *Bishop et al.*, 1977; *Fowler and Small*, 1972; *Honjo and Roman*, 1978; *Knauer et al.*, 1979; *Schrader*, 1971].

Our experience with the holographic system indicates that it is especially well suited for analysis of inorganic materials. Primarily, this results from their being more refractive than similarly sized organic material. As a result, inorganic material such as quartz grains and clay particles have high contrast diffraction patterns that provide a sharper holographic image.

The utility of this and similar devices will be greatly extended with the addition of a rugged spatial filter collimator that will improve the contrast of the recorded diffraction patterns. In laboratory tests, such an optical arrangement with higher magnification and spatial filtering has allowed us to record and reconstruct mineral grains as small as 2 $\mu$m in diameter. Such a change to the system will also be an advantage in studies of organic-rich material since these are characterized by lower contrast diffraction patterns. In addition, the manual image reduction technique could be automated with a computer-based image analysis and precision frame registration system. The great advantage here is the speed and accuracy with which the data from large numbers of holograms could be processed. With these and other changes, passive in situ optical systems may help increase our understanding of a number of fundamental oceanic processes.

*Acknowledgements.* The captain and crew of the NOAA vessel R.V. *Researcher* helped make this work possible as did George Harvey of the Atlantic Oceanographic and Meteorological Laboratory. We especially thank Donald Atwood for his kind invitation to participate on this cruise. This work was supported under Office of Naval Research contract N00014-75-C-0539.

## REFERENCES

Bishop, J. K. B., The chemistry, biology, and vertical flux of oceanic particulate matter, Sc.D. thesis, Mass. Instit. of Technol., Woods Hole Oceanogr. Instit., 1977.

Bishop, J. K. B., and J. M. Edmond, A new large volume filtration system for the sampling of oceanic particulate matter, *J. Mar. Res.*, *34*, 181–198, 1976.

Bishop, J. K. B., J. M. Edmond, D. R. Ketten, M. P. Bacon, and W. B. Silker, The chemistry, biology, and vertical flux of particulate matter from the upper 400 m of the equatorial Atlantic Ocean, *Deep Sea Res.*, *24*, 511–548, 1977.

Carder, K. L., Holographic microvelocimeter for use in studying ocean particle dynamics, *Opt. Eng.*, *18*, 524–525, 1979.

Carder, K. L., and D. J. Meyers, New optical techniques for particle studies in the bottom boundary layer, *Soc. Photo. Opt. Instrum. Eng. Ocean Opt.*, *6*, 208, 151–158, 1979.

Cartwright, S. L., P. Dunn, and B. J. Thompson, Particle sizing using far-field holography: New developements., *Opt. Eng.*, *19*, 727–735, 1980.

Fournier, R. O., Membrane filtering, in *Phytoplankton Manual*, edited by A. Sournia, pp. 108–112, UNESCO, Paris, 1978.

Fowler, S. W., and L. F. Small, Sinking rates of euphausid fecal pellets, *Limnol. Oceanogr.*, *17*, 293–296, 1972.

Gordon, D. C., Jr., A microscopic study of organic particles in the North Atlantic Ocean, *Deep Sea Res.*, *17*, 175–186, 1970.

Honjo, S., and R. R. Roman, Marine copepod fecal pellets: production, preservation, and sedimentation, *J. Geophys. Res.*, *56*, 45–57, 1978.

Hurlbut, C. S., Jr., *Dana's Manual of Mineralogy*, 18th ed., John Wiley, New York, 1971.

Knauer, G., J. H. Martin, and K. W. Bruland, Fluxes of particulate carbon, nitrogen, and phosphorus in the upper water column of the northeast Pacific, *Deep Sea Res.*, *26*, 97–108, 1979.

Lerman, A., K. L. Carder, and P. R. Betzer, Elimination of fine suspensoids in the oceanic water column, *Earth Planet. Sci. Lett.*, *37*, 61–70, 1977.

Lerman, A., D. Lal, and M. F. Dacey, Stokes settling and chemical reactivity of suspended particles in natural water, in *Suspended Solids in Water*, edited by R. J. Gibbs, Plenum, New York, 1974.

Schrader, H. J., Fecal pellets: Role in sedimentation of pelagic diatoms, *Science*, *174*, 55–57, 1971.

Smayda, T. J., Normal and accelerated sinking of phytoplankton in the sea, *Mar. Geol.*, *11*, 105–122, 1971.

Thompson, B. J., J. H. Ward, and W. R. Zinky, Application of hologram techniques for particle size analysis, *Appl. Opt.*, *6*, 519–526, 1967.

Trent, J. D., A. L. Shanks, and M. W. Silver, In situ and laboratory measurements on macroscopic aggregates in Monterey Bay, California, *Limnol. Oceanogr.*, *23*, 626–635, 1978.

Wiebe, P. H., S. H. Boyd, and C. Winget, Particulate matter sinking to the deep-sea floor at 2000 m in the Tongue of the Ocean, Bahamas with a description of a new sediment trap, *J. Mar. Res.*, *34*, 341–354, 1976.

(Received December 14, 1981;
accepted March 8, 1982.)

APPENDIX FIVE

Deep Sea Research, Vol. 29, No. 8A, pp. 953 - 965, 1982.
Printed in Great Britain.

0198-0149/82/080953-13 $03.00/0


# Sediment resuspension by coastal waters: a potential mechanism for nutrient re-cycling on the ocean's margins

KENT A. FANNING, KENDALL L. CARDER and PETER R. BETZER

(*Received* 21 *November* 1980; *in revised form* 18 *September* 1981; *accepted* 15 *November* 1981)

**Abstract**—Nutrient profiles from the continental shelf of the northeastern Gulf of Mexico indicated considerable near bottom enrichment in silica and nitrate above coarse sediments east of the Mississippi delta. In contrast, near bottom waters of the carbonate-rich West Florida Shelf showed no such enrichments. Storm related suspension apparently produced the enrichments because, in near bottom waters south of Mobile Bay, silica, nitrate plus nitrite, and suspended load increased substantially as a winter storm front passed. Also, laboratory simulation of resuspension by stirring the supernatant seawater over a clay rich core produced similar increases in silica and nitrate plus nitrite, with ammonia being the apparent precursor to the nitrate and nitrite. Most of the nutrient increase appeared to come from previously deposited sediments in the early stages of resuspension. Using the ratios of nutrients released to sediments resuspended, calculations indicate that resuspension of as little as 1 mm of shelf sediment could intermittently augment overlying productivity by as much as 100 to 200%. Thus, resuspension may accelerate nutrient recycling on continental margins.

## INTRODUCTION

AS PART of a survey of the continental shelf of the eastern Gulf of Mexico during mid-May 1974, stations were occupied in two adjacent regions, the northeastern gulf shelf from the Mississippi delta to Cape San Blas (29°42′N, 85°24′W) and the West Florida Shelf from Cape San Blas south to Tampa Bay. At each station (Table 1), water depth was 70 m or less, and nutrients and salinities were determined for surface, mid-depth, and near-bottom waters. The resultant profiles indicated the two regions to be different in an important respect (Figs 1a, b). Near-bottom waters of the northeastern gulf shelf were considerably richer in silica and nitrate than those of the West Florida Shelf even though the near-bottom salinity profiles for the two regions were virtually identical. The empty dashed zones in Fig. 1b show where equivalent enrichments would plot if they also occurred in the West-Florida-Shelf profiles. But enrichments were only found on the northeastern gulf shelf, and those for stations near the Mississippi delta tended to be the highest for either or both silica and nitrate (Table 1, Fig. 1a). There were also slight increases in near-bottom phosphate on the northeastern gulf shelf compared to the West Florida Shelf.

The enrichments on the northeastern gulf shelf might have resulted from four processes: (a) transport of nutrient rich river water from the southern United States, (b) upwelling of deeper offshore waters, (c) more intense near bottom regeneration of inorganic nutrients on the

* Department of Marine Science, University of South Florida, 140 Seventh Avenue South, St. Petersburg, FL 33701, U.S.A.

*Table 1. Station locations for survey of the eastern continental shelf of the Gulf of Mexico, 15–18 May, 1974*

| Station | Latitude (N) | Longitude (W) | Shelf section |
|---|---|---|---|
| 10 | 29°36 | 87°25 | NE gulf shelf |
| 11 | 29°41 | 87°39.5 | NE gulf shelf |
| 12 | 29°46 | 87°54 | NE gulf shelf |
| 13* | 29°57 | 88°14 | NE gulf shelf |
| 14* | 29°56.5 | 88°23.5 | NE gulf shelf |
| 15* | 29°56 | 88°33 | NE gulf shelf |
| A5* | 29°17 | 88°26 | NE gulf shelf |
| A6* | 29°20 | 88°45 | NE gulf shelf |
| C3 | 29°57 | 87°10 | NE gulf shelf |
| C4* | 29°33 | 88°13 | NE gulf shelf |
| M7 | 29°43 | 86°01 | NE gulf shelf |
| M8 | 29°44 | 86°14 | NE gulf shelf |
| M9 | 29°52 | 86°15.5 | NE gulf shelf |
| C2 | 29°28 | 85°49.5 | NE gulf shelf |
| M1 | 27°45 | 83°28 | West Florida Shelf |
| M2 | 27°52 | 83°34 | West Florida Shelf |
| M3 | 27°56 | 83°43 | West Florida Shelf |
| M4 | 28°21 | 84°24 | West Florida Shelf |
| M5 | 28°29 | 84°21 | West Florida Shelf |
| M6 | 28°43 | 84°20 | West Florida Shelf |
| C1 | 29°13 | 84°02.5 | West Florida Shelf |

* Close to Mississippi delta.

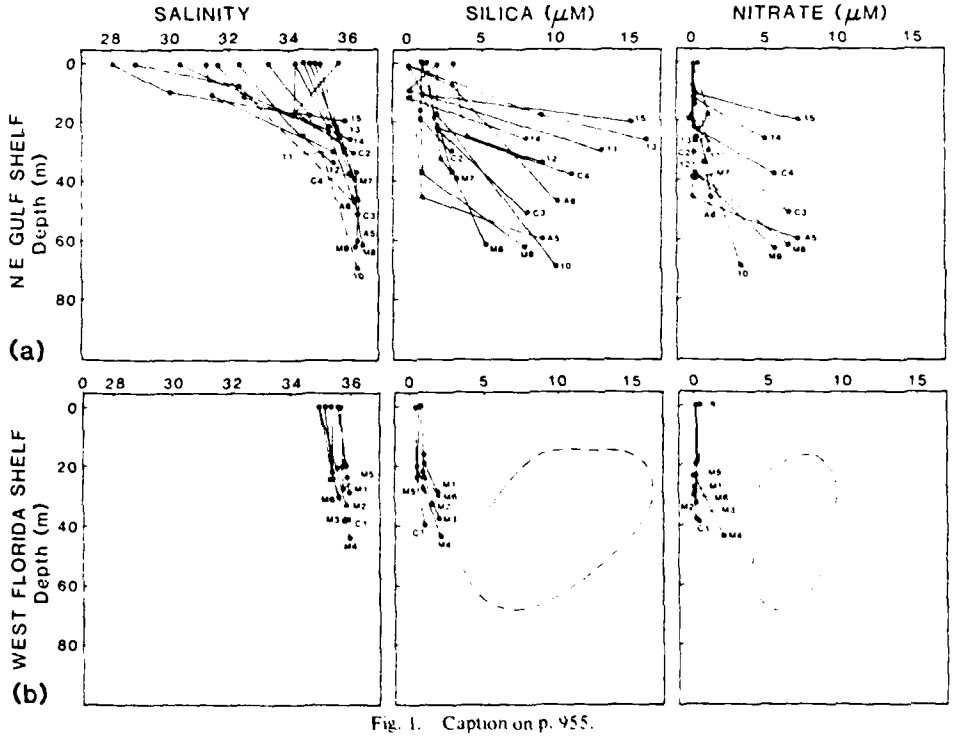


Fig. 1. Caption on p. 955.

northeastern gulf shelf, or (d) an injection from bottom sediments. Transport of river water was probably not responsible because, at around $36 \times 10^{-3}$, the near-bottom salinities were too high. Upwelling was also unlikely. Nutrient–salinity plots for an offshore station at 28°N, 87°W (G. BERBERIAN and D. ATWOOD, personal communication) indicated that the near-bottom waters at Stas 11, 13, and 15 had much higher silica concentrations (13 to 16 μM) than could be produced by the upwelling and mixing of deeper water. Also, if upwelling had provided most of the nutrients, then enrichments in silica and nitrate should have occurred at all stations having upwelled water. But near-bottom waters at Stas 11 to 13 were enriched in silica but not in nitrate, while near-bottom waters at Stas 14 and 15 were enriched in silica *and* nitrate (Fig. 1a). Thus, the pattern of near-bottom enrichment was not consistent with upwelling as the major source of increased nutrient concentrations. There is no reason to expect that near-bottom nutrient remineralization on the northeastern gulf shelf was more intense than on the West Florida Shelf, so that means of enrichment was also improbable.

Thus, much of the near-bottom enrichment on the northeastern gulf shelf appears to have been caused by sediment–water interaction, with turbulent resuspension of shelf sediments being a reasonable possibility. Because such a process could be important to nutrient recycling on continental margins, we conducted two related studies: (1) observation of nutrient increase and sediment resuspension during the passage of a storm front on the northeastern gulf shelf and (2) measurement of releases of silica, phosphate, and nitrogenous nutrients during a laboratory simulation of sediment resuspension.

## METHODS

Salinity was determined with a Beckman salinometer or a Guildline Autosal conductometric salinometer standardized against standard seawater. Dissolved ammonia was determined automatically with a Technicon AutoAnalyzer II® using the method of GRASSHOFF and JOHANNSEN (1972). Silica, phosphate, nitrate, and nitrite were determined by the automatic techniques discussed by FANNING and MAYNARD (1978). The beam attenuation coefficient due to particles suspended in seawater, $c_p(m^{-1})$, was measured with a Hydroproducts® 906-912 transmissometer. A particle-free value of $c_p$ is zero. Suspended particle loads were determined gravimetrically on Nuclepore membranes (BETZER, CARDER and EGGIMANN, 1974). Oxygen concentrations were measured by Winkler titration.

## NUTRIENT INJECTION BY STORMS

Storm-generated resuspension and nutrient release were observed SSE of Mobile Bay at Sta. 2639 (29°53'N, 88°12'W), water depth 30 m. For a 5-day period (20 to 25 February, 1978), the station was occupied at anchor, with transmissometry profiles taken every 2 h and near-bottom water samples taken daily for determination of nutrients and suspended loads. Water samples for nutrients were immediately filtered and frozen for later analysis, and the filter pads were weighed to get suspended loads. Salinity samples were taken every 2 h.

A winter storm front passed by between 21 and 22 February (Fig. 2). About 0100 on 21

Fig. 1. Profiles of nutrients and salinity from the northeastern Gulf of Mexico and West Florida shelves in May 1974. Station numbers from Table 1 are shown next to the bottom-most samples of the stations. The dashed profiles indicate stations where insufficient sampling at intermediate depths introduced some uncertainty in salinity distributions. The dashed regions are explained in the text.

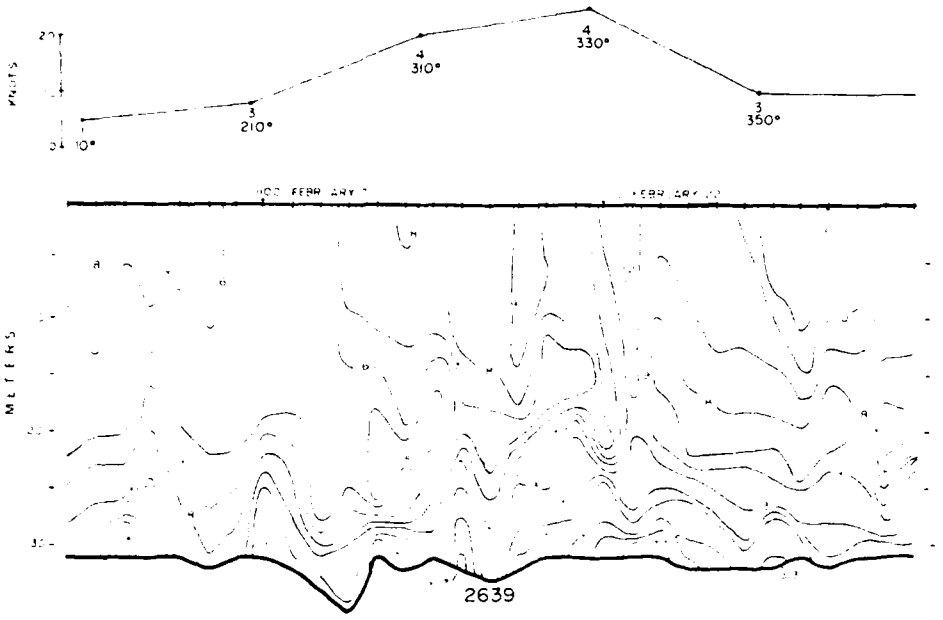


Fig. 2. Variation in physical parameters during passage of a 1978 winter storm front at Sta. 2639, SSE of Mobile Bay (29°53'N, 88°12'W). Top: wind speed, wind direction, sea state. Bottom: vertical profile of beam attenuation coefficient of the transmissometer ($c_p$) ($m^{-1}$).

February the sea state was 3, and the wind speed began to shift from 8 kn out of the southwest toward much higher speeds coming more out of the north. The maximum speed occurred about 24 h later, 23 kn out of the northwest at 0100 on 22 February. By that time the sea state had reached 4. About 30 h after it started the storm passed, the wind returned to about 8 kn, and the sea state dropped to 3. In the last half of the storm's passage, the turbidity of the water column began to increase. Near-bottom values of the beam attenuation coefficient of the transmissometer ($c_p$) rose from 1.1 to 2.7 $m^{-1}$ around 0300 on 22 February and finally to more than 3.3 $m^{-1}$. About the time of the highest wind speed, the surface value of $c_p$ also reached a maximum.

The storm's passage was also reflected in the relationship between nutrient concentrations and suspended load in near-bottom waters (Fig. 3). Both suspended load and concentrations of silica and nitrate plus nitrite decreased between 20 and 21 February (see Discussion). But the onset of the storm was followed by corresponding increases in suspended load and in concentrations of both silica and nitrate plus nitrite. Suspended load increased 7-fold, and each nutrient concentration more than doubled. The bottom half of the water column had salinities of 34.5 to 35.5 $\times 10^{-3}$ on 20 and 21 February, and the water that moved in at the storm's height on 22 February was slightly more saline (35.5 to 36.1 $\times 10^{-3}$) as well as being richer in suspended matter and nutrients. The salinity range is within the range to be expected along the northwest Florida continental shelf (see salinity profiles for the upper 30 m in Fig. 1a).

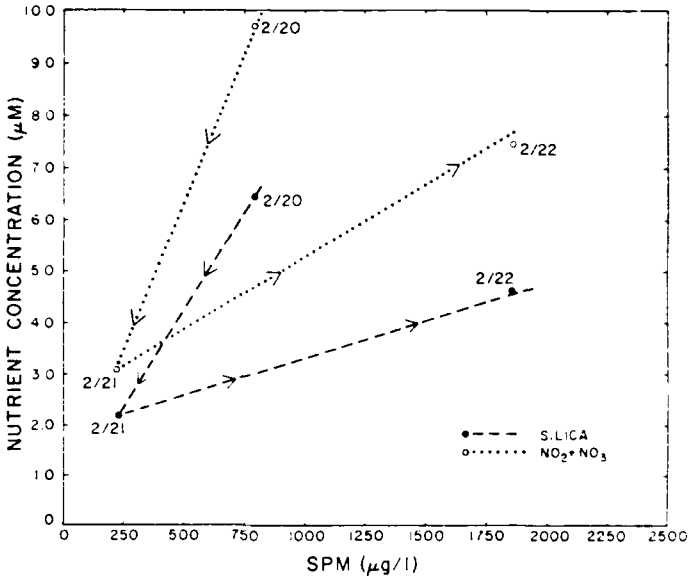


Fig. 3. Variation of silica and nitrate plus nitrite with suspended load in near-bottom waters at a station SSE of Mobile Bay (Sta. 2639, 29°53'N, 88°12'W). A storm front passed the spot between 21 and 22 February, 1978. Arrows mark the time course of the changes.

The near-bottom suspended load during the storm was higher than those from other seasons. The same station was occupied during summer (five determinations in July 1976) and fall (five determinations in November 1978) by BETZER, PEACOCK and JOLLEY (1978). Their samples were taken 5 m above bottom with a 30-l Niskin bottle, and their averages for summer and fall were 170 (±103) and 380 (±228) μg $l^{-1}$, respectively, both of which are much smaller than the 1850 μg $l^{-1}$ during the storm of 22 February (Fig. 3). BETZER *et al.* (1978) also made five determinations of near-bottom suspended load at the station in February 1978 independently of the data in Fig. 3, and their average was 1070 (±910) μg $l^{-1}$, which is also higher than the fall and summer averages. The standard deviation for the winter sampling is 4 to 8 times those for other seasons. Such a large scatter is consistent with the suggestion that winter storms produce increases in suspended load by resuspension and transport.

The coincidence of a storm passage with marked increases in suspended matter and dissolved nutrients is unmistakable and strongly suggests the changes were related. Resuspension could produce dissolved silica in two ways, the mixing of pore waters into bottom water and the solution of silicate particles during and after resuspension. Marine pore waters contain much higher concentrations of silica than bottom waters, and release of silica from stirred sediment has been demonstrated (FANNING and SCHINK, 1969; FANNING and PILSON, 1971). Nitrate–nitrite enrichments could have occurred through the intermediate of ammonia. In shallow-water reducing sediment, interstitial ammonia concentrations can be several millimolar while the overlying water column has much less ammonia (MATISOFF, BRICKER, HOLDREN and KAERK, 1975). Ammonia may also be sorbed to deposited sediment

(ROSENFELD, 1979). Resuspension of a few millimeters of reducing sediment could cause a temporary increase in ammonia in a shallow water column, and subsequent oxidation could then produce nitrate and nitrite.

The suspended matter associated with the suspended-load maximum on 22 February (Fig. 3) contained a considerable fraction of clay—about 50%. This conclusion was reached from its aluminum content (6.3%) and its Si : Al ratio (3.4 : 1). Such a low Si : Al ratio means that much of the suspended silica was associated with aluminum in aluminosilicates. The estimate of 50% clay was made using a mass conversion ratio of 8 units clay to 1 unit aluminum, based on mineralogic determinations on the suspended matter. Thus, the suspended matter near the bottom during and after the storm not only had greatly enhanced concentration but also had a composition consistent with an origin in a clay-rich substrate.

Recent work indicates that the bottom under Sta. 2639 has many sand-sized particles (DOYLE and SPARKS, 1980). However, just to the west the sand content decreases markedly as fine-grained pro-delta facies of the Mississippi River are encountered. Thus, the resuspension and nutrient increases observed at the station may have originated in the west and been carried to Sta. 2639 as the storm moved eastward.

## STIRRING EXPERIMENT

To investigate nutrient release by resuspension under more controlled conditions, we conducted a laboratory resuspension of deposited sediment. Because the sediment in the water column at Sta. 2639 contained considerable amounts of aluminosilicates, the deposit to be artificially resuspended had to be clay-rich and could not come from beneath Sta. 2639 (see above). We lacked cores from the Mississippi delta, but, on cruise 78-R-2 of the R.V. *Researcher*, we were able to obtain clay-rich sediment from the continental margin north of Venezuela. Those deposits derive from the Orinoco river and are typical clay-bearing deltaic muds. By gently lowering a weight stand with two core liners attached 13 cm apart, two cores were taken simultaneously in 103 m of water at 11°00′N, 62°01′W. The cores, G.C. 17 and G.C. 18, were 6.7 cm in diameter and were sealed in nitrogen-filled plastic bags and refrigerated to retard bacterial activity until opened and processed.

Core G.C. 17 was used to characterize the sediment. At room temperature (22°C), it was sliced in a nitrogen atmosphere and the slices squeezed to remove pore waters, which had high concentrations of interstitial silica (200 to 300 μM) and phosphate (4 to 9 μM). Most of the sediment was reducing; the top centimeter had 15 μM nitrate, but the rest had much less than 5 μM nitrate. The sediment was brownish on top and greenish below 5 cm. Results for G.C. 17 were assumed to apply for G.C. 18 as well because the two were collected so close together.

Core G.C. 18 was used for the resuspension experiment at 22°C, approximately the *in situ* temperature (19°C). The old supernatant seawater was carefully removed, and 1 l of low-nutrient surface seawater (salinity: $36.57 \times 10^{-3}$) was put over the sediment. The seawater was very slowly added through capillary tubing so that it trickled gently down the liner wall above the sediment until the water column over the sediment was 28 cm high. The emplacement took 3 to 4 h. The seawater was allowed to stand for 30 min and then sampled. A 6 cm wide Teflon paddle was placed about 10 cm above the sediment–water interface and, over the next 20 h, was rotated to resuspend the sediment. The rotation was slow at first, with the outer edge of the paddle having a tangential velocity of 9 cm $s^{-1}$. At intervals, rotation speed was increased, and samples of the suspension were taken for the determination of suspended load and dissolved components (Table 2).

*Table 2. Stirring speeds, suspended loads, and nutrient concentrations during the resuspension experiment on Core G.C. 18 from the Venezuelan continental shelf* (11°N, 62°01'W). *Supernatant seawater was initially nutrient-poor with* 36.57 × $10^{-3}$ *salinity*

| Elapsed time (min) | Tangential velocity of paddle's outer edge (cm $s^{-1}$) | Volume of supernatant seawater (ml) | Suspended load (mg $l^{-1}$) | Dissolved nutrient concentration (μM) | | | | |
|---|---|---|---|---|---|---|---|---|
| | | | | $NO_3^-$ | $NO_2^-$ | $NH_4$ | $PO_4^{3-}$ | $Si(OH)_4$ |
| 0 | 0 | 1,000 | 21 | 0.29 | 0.13 | 4.05 | 0.44 | 5.0 |
| 10 | 9 | 970 | 23 | 0.17 | 0.15 | 3.72 | 0.46 | 6.1 |
| 17 | 9 | 955 | 32 | 0.14 | 0.14 | 3.84 | 0.46 | 5.8 |
| 25* | 24 | 940 | 167 | 0.20 | 0.14 | 4.11 | 0.55 | 7.7 |
| 30 | 24 | 925 | 550 | 0.25 | 0.15 | — | 0.57 | 8.3 |
| Extensive erosion begins | | | | | | | | |
| 35* | 38 | 910 | 2,309 | 0.25 | 0.19 | 3.67 | 0.87 | 13.9 |
| 40 | 38 | 895 | 3,518 | 0.38 | 0.21 | 3.99 | 1.69 | 17.4 |
| 60* | 53 | 880 | 6,726 | 0.48 | 0.29 | 6.91 | 1.79 | 30.4 |
| 80 | 53 | 865 | 5,859 | 0.67 | 0.38 | 7.00 | 2.01 | 36.4 |
| 129* | 68 | 850 | 18,795 | 0.89 | 0.26 | — | 2.37 | 69.0 |
| 140 | 68 | 835 | 18,202 | 0.94 | 0.29 | 6.80 | 2.29 | 68.4 |
| 193 | 68 | 820 | 22,943 | 1.37 | 0.26 | — | 2.40 | 87.7 |
| 204 | 68 | 805 | 19,890 | 1.16 | 0.33 | 4.84 | 2.61 | 85.6 |
| 1172 | 68 | 790 | 47,137 | 8.32 | 0.20 | 2.57 | 2.44 | 106.4 |
| Seawater before emplacement | | — | — | 0 | 0.09 | 0 | 0.23 | 0.2 |

* Times when the rotation speed was increased.

Erosion of the sediment was slight for the first 30 min. Then the stirring speed was increased to 38 cm $s^{-1}$ (Table 2, Fig. 4), and the suspended load increased rapidly with stirring rate until, between 190 and 200 min, it reached 20 g $l^{-1}$. Stirring was continued for another 16 h, and ultimately about 40 g of sediment were eroded. The area of the sediment–water interface was 35.3 $cm^2$, so between 1 and 2 cm of sediment had been resuspended, assuming a surface sediment porosity of 60 to 80% and a dry particle density of 2.7 g $cm^{-3}$.

Nutrient release seemed to be in three stages (Table 2, Fig. 4), but the first stage was the most unexpected and perhaps the most significant. It occurred during the emplacement operation before any stirring was begun. The seawater trickling down the core-liner wall had almost no nutrients (Table 2); yet, after emplacement and 30 min of waiting, all nutrient concentrations had increased. The ammonia increase was from undetectable to 4.5 μM and silica increased 25 fold. Thus, a release of nutrients is shown at zero stirring time in Table 2 and Fig. 4, with the initial release of nitrogenous nutrients being nearly half of the final release observed. Diffusion across the sediment–water interface did not provide all of the release observed during emplacement. Again assuming 60 to 80% porosity in the sediment, the increases in silica and phosphate would have required all the interstitial silica and phosphate in the upper 5 to 10 mm of sediment, and, during the 3 to 4 h emplacement period, diffusive exchange could not have occurred over more than 1 to 2 mm. Thus, the initial release came partly from a small amount of sediment resuspended during the emplacement. No release was anticipated, so the suspended matter in the seawater was not determined before emplacement, and how much of the 21 mg $l^{-1}$ suspended matter before stirring (Table 2) was due to the emplacement is unknown. Thus, the nutrient release per gram of emplacement-resuspended sediment is difficult to ascertain. Assuming that the emplacement water initially had no suspended matter, we can estimate minimum release ratios (Table 3).

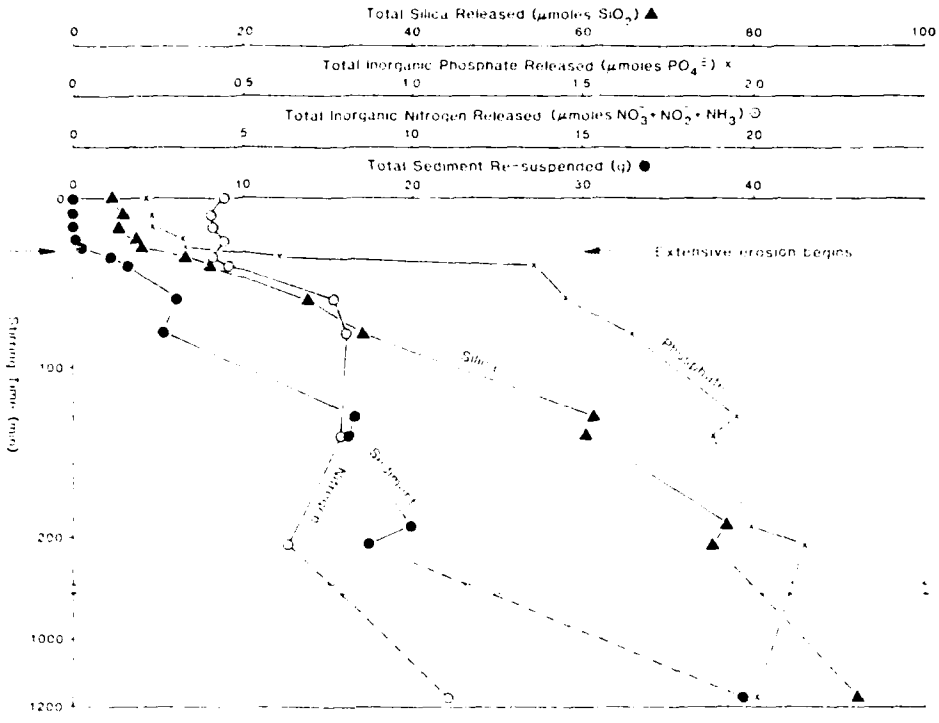


Fig. 4. The time course of the release of silica, inorganic phosphate, inorganic nitrogen, and suspended matter during laboratory resuspension of sediment from the Venezuelan continental shelf (11°00'N, 62°01'W).

*Table 3. Release ratios of nutrients during a laboratory resuspension experiment on core GC 18 from the Venezuelan continental shelf and from changes during passage of a storm front south of Mobile Bay, Alabama at Sta. 2639*

| | Release ratios (μg at. nutrient $g^{-1}$ resuspended sediment) | | | |
|---|---|---|---|---|
| | $\Sigma N(NO_3 + NO_2 + NH_3)$ | $PO_4$ | P | Silicon |
| Stirring experiment (gentle emplacement) | ≥210 | ≥10 | | ≥230 |
| Stirring experiment (extensive erosion) | 0.94 | 0.18 | | 3.8 |
| Sta. 2639 | 2840 | -- | | 1480 |

The second stage of nutrient release came after 30 min of stirring when the stirring speed was increased to 38 cm $s^{-1}$ and extensive erosion began (Table 2, Fig. 4). All nutrient concentrations increased rapidly during the resuspension, and the relative increases in phosphate and silica were higher than that of suspended matter (Fig. 4). Ratios of nutrient released per gram of eroded sediment were calculated for the period of 35 to 60 min stirring time when the erosion was most rapid (Table 3). The release ratios are roughly two orders of magnitude less than those for the first stage.

AD-A131 290 OPTICAL MEANS OF MEASURING PARTICLE-SEA INTERACTIONS IN THE CARIBBEAN SEA..(U) UNIVERSITY OF SOUTH FLORIDA ST PETERSBURG MARINE SCIENCE INST.. K L CARDER ET AL. 2/2

UNCLASSIFIED APR 83 N00014-75-C-0539 F/G 8/3 NL

END

DATE FILMED

DTIC

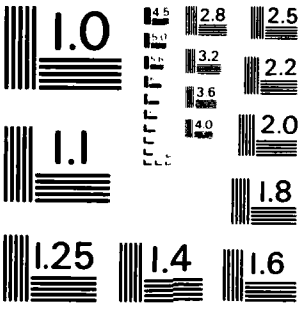

The third stage of nutrient release was between 3 and 19.5 h of stirring and was weaker than the other two. Silica and nitrogenous nutrients were released slightly and phosphate may have even decreased, however the total amount of resuspended sediment nearly doubled (Fig. 4). The implication is that most of the releasable nutrients are in the upper few millimeters of sediment.

During the three stages, release of nitrite and nitrate appeared to be related to that of ammonia (Table 2). The first major change was the appearance of ammonia. As erosion commenced and continued, ammonia concentrations remained fairly constant and then rose to about 7 μM after 1 h of stirring. Meanwhile, nitrate concentrations increased slightly and then, after the first hour, began to increase as the ammonia concentrations began to fall. After 3 to 19 h of stirring, nitrate became the principal nitrogen compound. The pattern of ammonia release followed by increasing nitrate concentration resembles the classic description of the regeneration of nutrients from phytoplankton populations—ammonification followed by nitrification (RICHARDS, 1965; HARVEY, 1955). Oxygen concentrations measured at 3.2 and 19.5 h stirring time were 4.0 and 4.4 ml (STP) $l^{-1}$, respectively. Thus, ample oxygen was present to oxidize ammonia and bacterial substrate was ample.

The flux of nitrogenous compounds during stirring can be compared with fluxes estimated for other nearshore sediments (Table 4). The rate used for the experiment was that from when erosion was extensive between 35 and 60 min. The flux in the experiment is much higher than the other estimates, which are either for long time periods (BILLEN, 1978) or for benthic chambers that prevent resuspension (NIXON, OVIATT and HALE, 1976). In contrast, a resuspension flux associated with erosion is for a single, dramatic, and fairly infrequent event.

*Table 4. Estimated fluxes of inorganic forms of combined nitrogen from various areas of the continental margin under different conditions*

| Sediment location | Sediment condition during release | Fluxes of $NH_3 + NO_3^- + NO_2^-$ (μg-at. N $m^{-2}$ $min^{-1}$) |
|---|---|---|
| Venezuelan shelf (water depth, 100 m) | Artificially eroded | 41.4 |
| North Sea | | |
| coastal* | Natural | 2.8 |
| offshore* | Natural | 1.5 |
| whole area* | Natural | 2.0 |
| Narragansett Bay† | Under benthic chamber | 1.3–1.7 |

* BILLEN (1978), long term average.
† NIXON *et al.* (1976), averaged over 1 year.

If the interstitial concentrations of core G.C. 17 represent those of the stirred core, the pore waters released during stirring had about 250 μM $SiO_2$ and 5 μM $PO_4^{3-}$. Assuming a sediment of 60 to 80% porosity and a dry density of 2.7 g $cm^{-3}$, the amounts of interstitial silica and phosphate available were:

$$8.3 \times 10^{-6} \text{ to } 2.2 \times 10^{-5} \text{ g } SiO_2 \text{ per g solid}$$

and

$$2.6 \times 10^{-7} \text{ to } 7.0 \times 10^{-7} \text{ g } PO_4^{3-} \text{ per g solid.}$$

But the data in Table 3 show that, during rapid erosion, the release ratios of silica and phosphate were:

$$2.3 \times 10^{-4} \text{ g } SiO_2 \text{ per g resuspended solid}$$

and

$$1.7 \times 10^{-5} \text{ g } PO_4^{3-} \text{ per g resuspended solid.}$$

Thus, during the second stage, the interstitial waters appeared to contribute only a small fraction of the total silica and phosphate released. The implication is that the upper few millimeters of continental-margin sediment may contain a considerable reservoir of nutrients attached to the deposited particles and releasable by resuspension.

## DISCUSSION

The information presented suggests that resuspension of continental margin sediment is important in fertilizing nearshore waters. Near-bottom nutrient enrichment along the northeastern margin of the Gulf of Mexico can be explained by such a process as can storm-related changes in nutrients and suspended load south of Mobile Bay, Alabama. Further, a laboratory study of deltaic sediment from the Orinoco demonstrated substantial nutrient release from rather gentle disturbances.

The question of the true importance of resuspension as a fertilizing mechanism arises. However, we wish to emphasize that resuspension is at best a mechanism for recycling nutrients between water column and sea bed. Any nutrients released by resuspension could only have reached the sea bed by the sinking of some form of organic matter from the water column. The ultimate source of most oceanic nutrients is land runoff. However, resuspension could play a role in sustaining high productivity on some continental margins by accelerating nutrient turnover.

For the Gulf of Mexico, considerations of the importance of resuspension to nutrient recycling involve calculations of potential production from riverine nutrients, storm intensity and the distribution of fine-grained sediment, and near-bottom er .chment.

According to work of the U.S. GEOLOGICAL SURVEY (1980), during 1977 to 1979 the Mississippi River contained an average of 8.25 μg-at. $P\ l^{-1}$ in both dissolved and particulate form and an average of 164 μg-at. $N\ l^{-1}$ as ammonia, nitrite, nitrate, and dissolved and particulate organic nitrogen. We will consider that all forms of nitrogen and phosphorus can be used by phytoplankton and that all of the river runoff to the gulf from the United States has the average concentrations obtained for the Mississippi. The Mississippi River runoff is $1.54 \times 10^{12}\ l\ d^{-1}$ (HOLEMAN, 1968) and the runoff from other United States rivers is $0.41 \times 10^{12}\ l\ d^{-1}$ (EL-SAYED *et al.*, 1972), making a total runoff from the United States to the gulf of $2 \times 10^{12}\ l\ d^{-1}$. The area of the United States gulf shelf is $3.34 \times 10^{11}\ m^2$ (MANHEIM, 1980). Therefore, if we assume the Redfield ratios apply (106 C : 16 N : 1 P; RICHARDS, 1965), the United States rivers could sustain an average shelf productivity along the gulf coast of 63 mg C $m^{-2}$ based on the total riverine phosphorus or 78 mg C $m^{-2}\ d^{-1}$ based on total riverine nitrogen. Yet the measured productivities along the United States gulf coast are 2 to 3 times higher: 100 to 200 mg C $m^{-2}\ d^{-1}$ (EL-SAYED *et al.*, 1972). It is possible that the phytoplankton of the United States gulf coast photosynthesize more atoms of carbon per atom of phosphorus or nitrogen than the Redfield ratios predict, but the higher shelf productivities may come from recycled nutrients. The possibility appears more likely because

all of the riverine nitrogen and phosphorus used in the above estimate may not be usable by phytoplankton; sediment resuspension could provide the additional source of nutrients.

An estimate suggests the potential enhancement of primary production by resuspension along the gulf shelf with storms playing a major role. If 1 mm of shelf sediment is resuspended, and the sediment had 80% porosity and 2.7 g $cm^{-3}$ dry density, its resuspension would introduce 540 g of solid material per square meter of water column. If resuspension of shelf sediment from the gulf shelf releases approximately the same quantities of nitrogen and phosphorus as occurred during the experiment, we can multiply the 540 g $m^{-2}$ by the release ratios in Table 3 and the Redfield ratios to predict the potential enhancement in production. The appropriate Redfield ratios are: 0.0795 mg C (μg-at. N)$^{-1}$ and 1.272 mg C (μg-at. P)$^{-1}$. From Table 3, release ratios for the emplacement stage predict enhancements ranging from more than 6900 to more than 9000 mg C $m^{-2}$; the ratios for the extensive-erosion stage predict enhancement of 40 to 120 mg C $m^{-2}$. So resuspension of 1 mm of sediment could raise primary production considerably, especially if the phytoplankton fix more carbon than predicted by the Redfield ratios (GOLDMAN, MCCARTHY and PEAVEY, 1979). Further, there are many storms to resuspend sediment in the Gulf of Mexico. Fine-grained resuspendable sediment covers approximately 200,000 $km^2$ of shelf from Mobile Bay (DOYLE and SPARKS, 1980) to Mexico (SHIDLER, 1977), and much of it is under 50 m of water or less. Intense storm fronts cross the area from northwest to southeast an average of four times a month (HENRY, 1979); during the hurricane season, an average of four tropical cyclones and hurricanes run ashore across this sediment (SIMPSON and LAWRENCE, 1971). Each storm takes 1 to 2 days to pass a given point on the shelf, implying that the nutrients could be introduced fast enough to be important to rates of productivity.

There are published references to the importance of recycled nitrogenous compounds from the sea bed. HO and BARRETT (1977) concluded that ammonia enrichments in near-bottom waters of Caminada and Barataria bays near the Mississippi delta in March and May of 1973 were produced when waves agitated sediments. NIXON (1981) presented budgets that show that ammonia emitted from benthic communities is an important part of the nutrient balances in coastal waters.

Our work on resuspension has some puzzling features. During the storm passage at Sta. 2639 south of Mobile Bay (Fig. 3), suspended sediment increased 1620 μg $l^{-1}$, silica rose 2.4 μM, and nitrate–nitrite rose 4.6 μM throughout the bottom 15 m of the water column. The release ratios as calculated from these field data are considerably larger than observed in the stirring experiment (Table 3). The sediment resuspended during the first stage of the stirring experiment could only be estimated as a maximum. If less were actually resuspended during the emplacement, the release ratios for the first stage would have been higher, more in agreement with ratios from Sta. 2639. The high fraction of clay minerals in suspension at Sta. 2639 suggests that the suspended matter may have originated elsewhere, perhaps to the west. During transit to Sta. 2639, some of the suspended matter may have settled, but any nutrients present were dissolved and may not have vanished from the water column as quickly. The ratio of released nutrient concentrations to resuspended sediment loads would appear to have increased during transit and would have been higher at Sta. 2639 than immediately after a resuspension event, either *in situ* or in the laboratory. Another puzzling feature of our work is the data from 20 February (Fig. 3). On that day, the water at Sta. 2639 had nutrient concentrations higher than those during the storm's passage and yet much lower suspended loads. Again, the explanation may be the sinking of resuspended sediment away from the soluble nutrients. In winter, storms pass that area every 2 to 4 days. Water

may have been carried in before 20 February with high nutrient concentrations and suspended loads and then remained, allowing the suspended matter to settle while the nutrient concentrations remained fairly high. However, without more data we can only speculate about events prior to 20 February.

## CONCLUSIONS

Evidence from nutrient profiles on the northern rim of the Gulf of Mexico, from increases in nutrients and suspended matter during a winter storm, and from laboratory resuspension studies on fine-grained shelf sediment strongly suggest nutrient release during the resuspension of sediments.

The results from a laboratory release experiment on stirred sediment can be used in evaluating the potential impact of resuspension by normalizing the nutrient release to the sediment release during stirring, giving a release ratio (Table 3). Application of those ratios show that as little as 1 mm of resuspended shelf sediment could, with subsequent mixing into the euphotic zone, significantly fertilize the overlying waters. The effect is an enhancement in nutrient recycling on continental shelves, thus providing a reasonable explanation of why shelf productivities could be higher than predicted from fluxes of river nutrients.

The potential release of recycled nutrients from resuspended sediment should be included in studies of nutrient balances along continental margins.

*Acknowledgements*—The authors thank KEN HADDAD, VALENTINE I. MAYNARD HENSELY, and ROBERT G. STEWARD for assistance with the analyses and interpretation of the data. The authors also are very grateful to A.O.M.L. of the National Oceanic and Atmospheric Administration for permission to use some of their nutrient data from the Gulf of Mexico (G. BERBERIAN and D. ATWOOD) and for shiptime on the R.V. *Researcher*. Financial assistance for the work from the following sources is gratefully appreciated: U.S. Bureau of Land Management Contracts MAFLA 08559 CT4 11 and AA550 CT7 34; National Science Foundation Grants GA 41200, OCE 74 01480 A02, and OCE 76 82416; Office of Naval Research Contract N00014-75 C 0539.

## REFERENCES

BETZER P. R., K. L. CARDER and D. W. EGGIMANN (1974) Light scattering and suspended particulate matter on a transect of the Atlantic Ocean at 11°N. In: *Suspended solids in water*, R. J. GIBBS, editor, Plenum Press, New York, pp. 295–314.

BETZER P. R., M. A. B. PEACOCK and R. R. JOLLEY (1978) Trace metals in suspended matter and zooplankton of the northeastern Gulf of Mexico MAFLA survey. Report to Dames and Moore Contract AA500 CT7 34, 50pp. (Unpublished document.)

BILLEN G. (1978) A budget of nitrogen recycling in North Sea sediments off the Belgian Coast. *Estuarine and Coastal Marine Science*, **7**, 127–146.

DOYLE L. J. and T. N. SPARKS (1980) Sediments of the Mississippi, Alabama, and Florida (MAFLA) continental shelf. *Journal of Sedimentary Petrology*, **50**, 905–916.

EL SAYED S. Z., W. M. SACKETT, L. M. JEFFREY, A. D. FREDERICKS, R. P. SAUNDERS, R. S. CONGER, G. A. FRYXELL, K. A. STEIDINGER and S. A. EARLE (1972) *Serial atlas of the marine environment*. Folio 22. Chemistry, Primary Productivity and Benthic Algae of the Gulf of Mexico. American Geographic Society, New York, unpaged.

FANNING K. A. and D. R. SCHINK (1969) Interaction of marine sediments with dissolved silica. *Limnology and Oceanography*, **14**, 59–68.

FANNING K. A. and M. E. Q. PILSON (1971) Interstitial silica and pH in marine sediments: some effects of sampling procedures. *Science*, **173**, 1228–1231.

FANNING K. A. and V. I. MAYNARD (1978) Dissolved boron and nutrients in the mixing plumes of major tropical rivers. *Netherlands Journal of Sea Research*, **12**, 345–354.

GOLDMAN J. C., J. J. MCCARTHY and D. G. PEAVEY (1979) Growth rate influence on the chemical composition of phytoplankton in oceanic waters. *Nature*, **274**, 210–215.

GRASSHOFF K. and J. JOHANNSEN (1972) A new sensitive and direct method for the automatic determination of ammonia in seawater. *Journal du Conseil, Conseil permanent International pour l'Exploration de la Mer*, **34**, 516–521.

HARVEY H. W. (1955) *The chemistry and fertility of sea waters*. Cambridge University Press, Cambridge, 224 pp.

HENRY W. K. (1979) Some aspects of the fate of cold fronts in the Gulf of Mexico. *Monthly Weather Review*, **107**, 1078–1082.

HO C. L. and B. B. BARRETT (1977) Distribution of nutrients in Louisiana's coastal waters influenced by the Mississippi River. *Estuarine and Coastal Marine Science*, **5**, 173–195.

HOLEMAN J. N. (1968) The sediment yield of major rivers of the world. *Water Resource Research*, **4**, 737–747.

MANHEIM F. T. (1980) Personal communication from Program Feasibility Document, OCS Hard Mineral Leasing Mining Policy, Phase II Task Force, U.S. Department of the Interior, unpublished report, 1979.

MATISOFF G., O. P. BRICKER III, G. R. HOLDREN JR. and P. KAERK (1975) Spatial and temporal variations in the interstitial water chemistry of Chesapeake Bay sediments. In: *Marine chemistry in the coastal environment*, T. M. CHURCH, editor, American Chemical Society Symposium Series **18**, Washington, DC, pp. 343–363.

NIXON S. W. (1981) Remineralization and nutrient cycling in coastal marine ecosystems. In: *Estuaries and nutrients*, B. NEILSON and L. E. CRONIN, editors, Humana Press, pp. 111–138.

NIXON S. W., C. A. OVIATT and S. S. HALE (1976) Nitrogen regeneration and the metabolism of coastal marine bottom communities. In: *The role of terrestrial and aquatic organisms in decomposition processes*, J. M. ANDERSON and A. MACFADYED, editors, Proceedings of the 17th Symposium, British Ecology Society, Blackwell Scientific Publishers, pp. 269–283.

RICHARDS F. A. (1965) Anoxic basins and fjords. In: *Chemical oceanography* (1st edition), Vol. I, J. P. RILEY and G. SKIRROW, editors, Academic Press, London, p. 624.

ROSENFELD J. K. (1979) Ammonium adsorption in nearshore anoxic sediments. *Limnology and Oceanography*, **24**, 356–364.

SHIDLER G. L. (1977) Late Holocene sedimentary provinces, south Texas outer continental shelf. *American Association of Petroleum Geologists Bulletin*, **61**, 708–722.

SIMPSON R. H. and M. B. LAWRENCE (1971) Atlantic hurricane frequencies along the U.S. coastline. N.O.A.A. Technical Memorandum MWS TM SR-58, U.S. National Oceanic and Atmospheric Administration, Southern Region Headquarters, Scientific Series Division, Fort Worth, Texas.

U.S. GEOLOGICAL SURVEY (1980) Water Quality Data Reports for 1977–78 and 1978–79, Mississippi River mile 76, Belle Chasse, LA.


DATE:
ILMF